NASA CONTRACTOR REPORT

NASA CR-1238
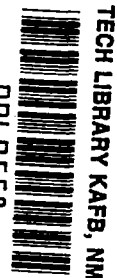
MEASUREMENT OF PILOT DESCRIBING FUNCTIONS IN SINGLE-CONTROLLER MULTILOOP TASKS

by Robert L. Stapleford, Samuel J. Craig,
and Jean A. Tennant

Prepared by
SYSTEMS TECHNOLOGY, INC.
Hawthorne, Calif.
for Ames Research Center

NATIONAL AERONAUTICS AND SPACE ADMINISTRATION • WASHINGTON, D. C. • JANUARY 1969

NASA CR-1238

MEASUREMENT OF PILOT DESCRIBING FUNCTIONS IN

SINGLE-CONTROLLER MULTILOOP TASKS

By Robert L. Stapleford, Samuel J. Craig,
and Jean A. Tennant

Distribution of this report is provided in the interest of
information exchange.   Responsibility for the contents
resides in the author or organization that prepared it.

Issued by Originator as Technical Report No. 167-1

FOREWORD

SUMMARY

This report deals with the problems of measuring pilot describing functions in multiloop tasks with one controller, i.e., where the pilot is controlling two, or more, response variables with a single manipulator. Both direct and implicit measurement techniques were considered and tested experimentally. The experimental task used was attitude and altitude control with elevator of an aircraft in a simulated landing approach.

The experimental results show that the measurement of multiloop describing functions is feasible although the techniques are considerably more complex than those required for single-loop compensatory tasks. However, there are certain fundamental limitations on the accuracy of some of the results. These are discussed in detail in the report. The experimental data also provide a spot check on the existing multiloop pilot model. The results support the current model and, in particular, show that the inner-loop (attitude) closure is quite similar to that for single-loop attitude tracking.

CONTENTS

FIGURES

ix

TABLES

SYMBOLS

A   Gain of adjustment loop in Crossover Model Parameter Tracker

D_i Denominator term in data-reduction equation for Y_θ, see Eqs. B-14, B-24, or B-30; $i = 1-3$

e   Tracking experiment error

e^* Model tracking error

G   Total loop transfer function

h   Altitude

H_g h/w_g transfer function

H_δ h/δ_e transfer function

i   Input

j $\sqrt{-1}$

K_h Low frequency gain of Y_h

K_θ Low frequency gain of Y_θ

M_q Pitching acceleration due to pitch rate, $q = \dot{\theta}$

M_w Pitching acceleration due to velocity perturbation along Z axis, w

$M_{\dot{w}}$ Pitching acceleration due to linear acceleration along Z axis, $\dot{w}$

M_{δ_e} Pitching acceleration due to elevator deflection, δ_e

n   Pilot remnant

N_i Numerator term in data-reduction equation for Y_θ, see Eqs. B-13, B-23, or B-29; $i = 1-3$

N_x^y Numerator of y/x transfer function, where $y = \theta$ or h, $x = \delta_e$ or w_g

$N_{\delta_e w_g}^{\theta\,h}$ Coupling numerator for θ/δ_e and h/w_g

q   Pitch rate, $\dot{\theta}$

s   Laplace operator, $s = \sigma + j\omega$

T_h Time constant of lag term in Y_h

T_I Time constant of lag term in Y_θ

T_L Time constant of lead term in Y_θ

U_o Aircraft steady-state velocity

w Velocity perturbation along Z axis

w_g Vertical gust velocity

Y_h Pilot transfer function in altitude loop

Y_θ Pilot transfer function in attitude loop

Z_w Acceleration along Z axis due to velocity perturbation along Z axis, w

Z_{δ_e} Acceleration along Z axis due to elevator deflection, δ_e

α Low-frequency phase approximation parameter

δ_e Elevator deflection

Δ Denominator of aircraft transfer functions

ϵ Model matching error, $e - e^*$

ζ Damping ratio of second-order mode; particularized by subscript

θ Pitch angle

Θ_g θ/w_g transfer function

Θ_δ θ/δ_e transfer function

ρ_a^2 Relative correlated output

σ Real part of s

τ Transport lag

Φ_{xy} Cross spectra between x and y

ω Imaginary part of s

ω Undamped natural frequency of second-order mode particularized by subscript

ω_c Crossover frequency

SECTION I

INTRODUCTION

The quasi-linear pilot model has proven to be an invaluable engineering tool in the analysis of manual control of a wide variety of vehicles. While the model for single-loop compensatory tracking is well developed, see Ref. 1, expansion and refinement of the model in other areas are the subjects of current research activities. This report deals with one such expansion effort, multiloop* control situations.

The only previous data on multiloop pilot describing functions is that presented in Ref. 2. The task used in that experiment was essentially attitude (bank angle) tracking of a command input with a second feedback (yaw rate) to stabilize a secondary mode (a dynamically unstable dutch roll). This is an example of one potential function of an inner loop, to suppress subsidiary modes or degrees of freedom.

Another, and perhaps more important function, is to provide equalization for outer loops. For example, direct control of altitude with elevator is quite difficult because of the lags involved. One solution is to add a pitch altitude inner loop as the pitch response leads the altitude response. The research reported here deals with control situations of this second type, i.e., where the function of the inner loop is to act as equalization for outer loops and there is more than one feedback to a single controller.

This program had two specific objectives. The first was to investigate techniques for measuring pilot describing functions in multiloop tasks of this type. The second objective was to spot check and, if necessary, revise the existing multiloop pilot model, Ref. 3. The model is currently based on a rational extension of the single-loop data and that of Ref. 2. To date, the strongest justification for this model has been that it has been successful in several applications. Experimental verification for even one typical task would greatly increase our confidence in it.

---

*As used here, the term multiloop refers to two or more interacting control loops.

1

Section II of this report discusses the selection of a representative task and set of vehicle dynamics for the experiment. An analysis of two techniques for measuring the multiloop describing functions is presented in Section III. An outline of the data reduction procedure used is also included. Section IV describes each of the elements in the experimental setup. The experimental results are discussed in Section V. This discussion includes:

1. The effects of changes in the inputs.

2. The results of the on-line performance measures.

3. Verification of the direct measurement technique from analysis of data for an analog pilot.

4. The describing-function measurements for the human pilot.

5. The remnant data.

The major findings of this study are summarized in Section VI and miscellaneous detailed developments are presented in four appendices.

SECTION II

CONFIGURATION SELECTION

Several requirements guided the selection of the configuration and control task used in these multiloop experiments. Each of the requirements is discussed in this section. However, before reviewing the specifics, the selection of a familiar and realistic piloting situation may be properly cited as an initial underlying consideration. The realism was somewhat restricted by the simplified display and simulator equipment available, but by limiting the task to an IFR flight situation the face validity of the simulator was enhanced. A longitudinal control task was selected to insure subject familiarity and because the resulting pilot describing function data could have broad application to the handling qualities problems of larger present-day aircraft.

The fundamental requirements established for selecting the control task are listed below:

1. The task must provide a multiloop single-controller problem for the pilot.

2. The dynamic properties of the controlled element should be such that pilot compensation and control structure may be determined. More specifically, since the pilot may operate in either a parallel manner or series manner in the multiloop situation, the pilot should be required to generate lead in the inner loop. This constraint provides the means for identifying parallel or series closures; see Section III.

3. The pilot should operate in a compensatory manner with reasonably tight loop closures.

Of the above selection criteria, the critical requirement for the control task is that the pilot adapt a multiloop control structure. Attitude and altitude control with the elevator is a suitable multiloop piloting task. In fact, from the analyses performed in Ref. 4, this technique is the best method of control for a number of familiar longitudinal flight situations. Also, the pilot is forced into a multiloop control structure to obtain satisfactory altitude control.

3

Both a supersonic transport at cruise and a jet transport in landing approach were considered. The landing approach task was selected in preference to one associated with the supersonic transport at cruise. The principal reasons were:

1. Landing is a precision task in which a tight closure of the altitude loop is required.

2. A realistic, random appearing disturbance over a broad frequency range may be used if the input signal is assumed to represent both gust disturbances and ILS beam noise.

3. A supersonic transport at cruise has very low gust responses. Unrealistically large gusts would be required to provide inputs of adequate magnitude for measuring pilot describing functions.

4. A simulated ILS approach is a much more familiar task to the available subjects, commercial transport pilots.

Having selected the approach task, it was then necessary to select a specific set of vehicle dynamics. According to the analyses of Ref. 4, the requirement for pilot lead in the attitude loop could be satisfied by choosing a configuration with a low short-period frequency, roughly 1 rad/sec or less. The short-period characteristics of the Boeing 707 aircraft are in this category, and the use of 707 dynamics had two other advantages:

1. The test subjects were familiar with the dynamics of this aircraft, so the training required would be minimized.

2. The approach characteristics of the 707 are typical of several current aircraft.

Consequently, a simplified approximation to the longitudinal dynamics of the 707 in landing approach was selected for the controlled element; see Appendix A for details. A brief preliminary experiment verified the adequacy of the simplified dynamics and the CRT display.

4

SECTION III

DATA REDUCTION TECHNIQUES

In this section the data reduction techniques used to directly and implicitly measure the pilot describing functions will be discussed. With the _direct_ _measurements_, both the attitude and altitude describing functions can be determined from a single run with two inputs. Two inputs are required because the number of measurable describing functions equals the number of uncorrelated system inputs multiplied by the number of pilot controls or outputs. For the particular task used here, the two describing functions were measured directly by using the two inputs, θ_c and h_c, with one pilot output, elevator.

With the _implicit_ _measurements_, two runs, each with a single input, are used. One run is a single-loop attitude-tracking task with a θ_c input. An attitude-loop describing function is computed from this run. The second run is multiloop tracking (attitude and altitude) with only the h_c input. From this run the altitude describing function is computed by assuming that the attitude describing function is the same as it was in the single-loop run. Details of both the direct and implicit computations will be discussed later in this section.

A major objective of this program was to compare the direct and implicit measurements. This comparison should indicate:

1. Any changes in the pilot's inner-loop characteristics due to the addition of the outer loop.

2. Any effects of adding the second input to the multiloop tracking task.

3. Relative merits of the two measurement techniques.

The results of this comparison are discussed in Section V. The remainder of this section describes the details of the data reduction for the two measurement schemes.

The basic technique used in both measurement schemes is to compute the cross-spectra between the inputs and various other parameters. The

5

cross-spectral approach is necessary to remove the effects of the pilot's remnant. Before the relationships between the pilot describing functions and the cross-spectra can be determined, we must decide on the form of the pilot model we wish to use. For this particular task there are two possible forms which are referred to as series and parallel closures; see Fig. 1. In the series model the pilot makes altitude corrections by mentally biasing his attitude reference up or down an appropriate amount. In the parallel model these are separate, direct altitude and attitude feedbacks to the elevator.

Series closures are more consistent with pilot comments on how they fly so this model was the one selected. However, either model could be used to match experimental results. The ultimate choice should be the form which produces the simpler model. To illustrate this point, consider two hypothetical cases. In the first case the series model results in a pure gain Y_h and a Y_θ which has a lead term. It would be simpler to keep the series model than to use a parallel model with identical lead terms in both loops. On the other hand, the series model might have a lag in Y_h equal to a lead in Y_θ. Then a parallel model would be simpler in that the outer loop would be a pure gain. As discussed in Section V, the series model is the simpler one for the data obtained in these experiments.

The relationships between the pilot describing functions and the various cross-spectra are derived in Appendix B. For θ_c and h_c inputs the expression for Y_θ can be written as

$$Y_\theta = \frac{N_1}{D_1} \tag{1}$$

where N_1 and D_1 can be expressed in the following ways:

$$N_1 = \begin{cases} \dfrac{\Phi_{\theta_c \delta_e}}{\Phi_{\theta_c \theta_c}} & \text{(2a)} \\[3ex] \dfrac{\Phi_{\theta_c \theta}}{\Theta_\delta \Phi_{\theta_c \theta_c}} & \text{(2b)} \\[3ex] \dfrac{\Phi_{\theta_c h}}{H_\delta \Phi_{\theta_c \theta_c}} & \text{(2c)} \end{cases}$$
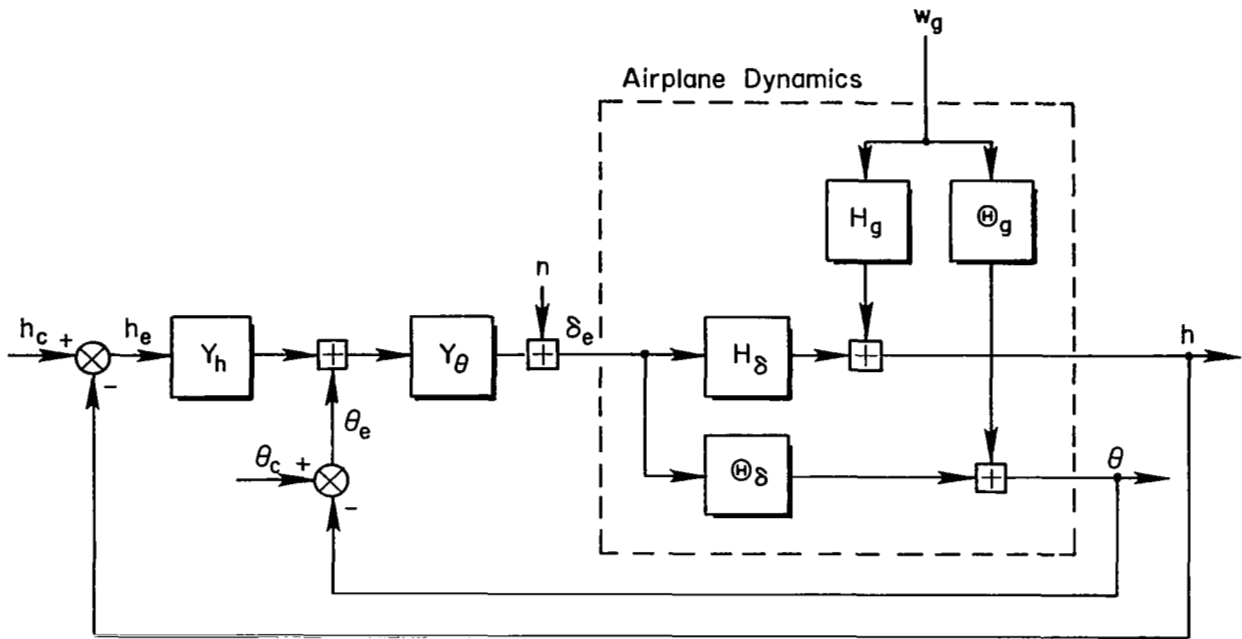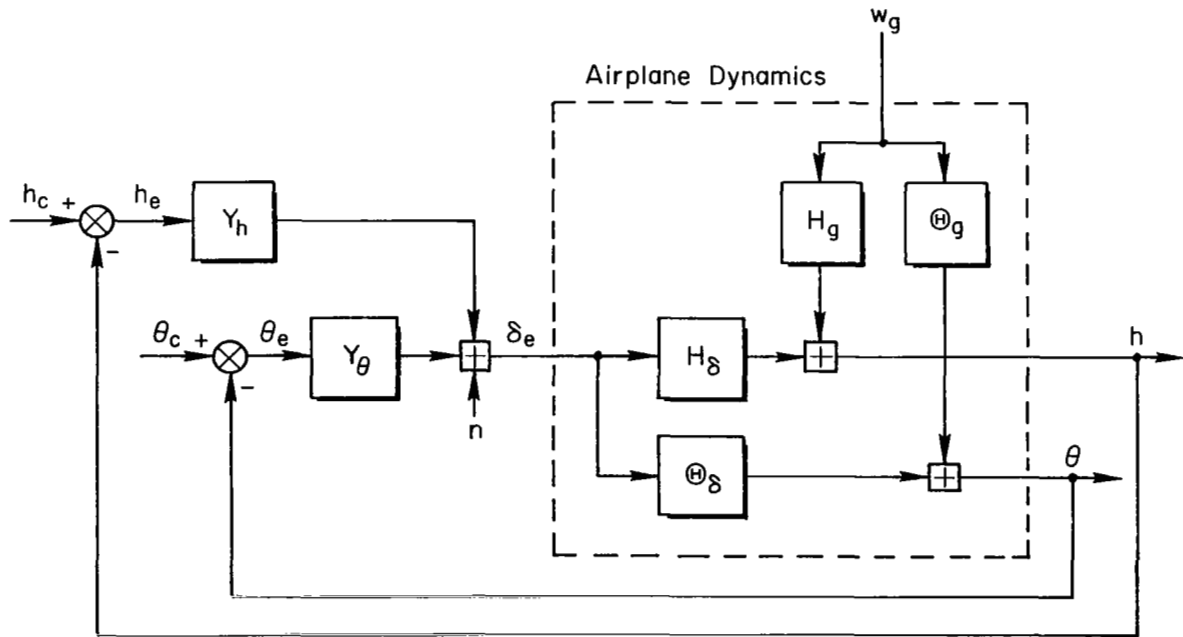
a) Series Closures

b) Parallel Closures

Figure 1. Multiloop Models for Series and Parallel Closures

7

$$D_1 = \begin{cases} \dfrac{\Phi_{\theta_c \theta_e}}{\Phi_{\theta_c \theta_c}} - \dfrac{\Phi_{h_c h}}{\Phi_{h_c h_c}} & (3a) \\[3ex] \dfrac{\Phi_{h_c h_e}}{\Phi_{h_c h_c}} - \dfrac{\Phi_{\theta_c \theta}}{\Phi_{\theta_c \theta_c}} & (3b) \end{cases}$$

The various cross-spectral ratios in Eqs. 2 and 3 can be interpreted as measured closed-loop responses, e.g., $\Phi_{\theta_c \delta_e}/\Phi_{\theta_c \theta_c}$ is the measured closed-loop response of δ_e to a θ_c input. The characteristics of these ratios were investigated prior to the experiments by computing the various input/output relationships for a predicted set of pilot dynamics. The results are shown as a series of Bode plots in Appendix C.

Examination of Fig. C-6 shows that the δ_e ratio $(\Phi_{\theta_c \delta_e}/\Phi_{\theta_c \theta_c})$ has its greatest magnitude at higher frequencies of interest (above 3 rad/sec). At low frequencies the response is very small. Consequently, Eq. 2a should be adequate at high frequencies, but at low frequencies measurement errors may be quite large because of the low signal levels. Fortunately, the other two ratios have complementary characteristics. Figure C-3 shows that the θ-response is largest in the midfrequency band and from Fig. C-5 we see that the h-response is greatest at low frequencies. Thus by using Eq. 2a at high, 2b at mid, and 2c at low frequencies we should be able to minimize measurement errors. In effect, we take advantage of the signal conditioning due to the vehicle dynamics to maintain a good signal/noise ratio at all frequencies.

The above discussion has shown that the numerator (N_1) of Y_θ presents no measurement problems. Unfortunately, the same is not true of the denominator (D_1). Either expression for D_1, Eq. 3, involves the difference of two terms, and at low frequency the difference is relatively very small. Thus small errors in measuring the cross-spectral ratios can produce very large errors in D_1. Other expressions for D_1 can be derived but they also involve the relatively small difference of two or more terms. There is no known way to avoid this problem. It even exists with a gust and θ_c or h_c inputs. The net result is to place a lower limit on the frequency range for which good measurements of the inner-loop describing function can be made.

The problem does not exist at the higher frequencies. Then the error ratio ($\Phi_{\theta_c\theta_e}/\Phi_{\theta_c\theta_c}$ or $\Phi_{h_ch_e}/\Phi_{h_ch_c}$) approaches unity and the second term becomes small.

For the series model, the altitude-loop describing function, Y_h, can be written in the simple forms

$$Y_h = \begin{cases} \dfrac{\Phi_{h_c\delta_e}/\Phi_{h_ch_c}}{\Phi_{\theta_c\delta_e}/\Phi_{\theta_c\theta_c}} & \text{(4a)} \\[2em] \dfrac{\Phi_{h_c\theta}/\Phi_{h_ch_c}}{\Phi_{\theta_c\theta}/\Phi_{\theta_c\theta_c}} & \text{(4b)} \\[2em] \dfrac{\Phi_{h_ch}/\Phi_{h_ch_c}}{\Phi_{\theta_ch}/\Phi_{\theta_c\theta_c}} & \text{(4c)} \end{cases}$$

As with the Y_θ numerator, we can take advantage of the signal conditioning provided by the vehicle dynamics to improve the signal/noise ratio. This can be done by using Eq. 4a at high, 4b at mid, and 4c at low frequencies. Thus we have a simple, yet accurate, method of measuring the outer-loop describing function at all frequencies of interest.

The implicit measurement techniques are quite different from the direct ones described above. The attitude-loop describing function is measured from the single-loop tracking results with a θ_c input. The describing function expressions are

$$Y_\theta = \begin{cases} \dfrac{\Phi_{\theta_c\delta_e}}{\Phi_{\theta_c\theta_e}} & \text{(5a)} \\[2em] \dfrac{\Phi_{\theta_c\theta}}{\Theta_\delta\Phi_{\theta_c\theta_e}} & \text{(5b)} \end{cases}$$

Equation 5a is used at high frequencies and Eq. 5b is used at the lower frequencies where the δ_e response is small. However, the accuracy at the

9

lowest frequencies will still be rather poor because of the low signal levels of the attitude error, θ_e.

The outer-loop describing function is determined from the multiloop tracking with only a h_c input by assuming that Y_θ is the same as in the single-loop case. The basic equation for this case is

$$\Phi_{h_c\delta_e} = -Y_\theta\Phi_{h_c\theta} + Y_hY_\theta\Phi_{h_ch_e} \tag{6}$$

or

$$Y_h = \frac{\Phi_{h_c\delta_e} + Y_\theta\Phi_{h_c\theta}}{Y_\theta\Phi_{h_ch_e}}$$

$$= \frac{\Phi_{h_c\delta_e}}{Y_\theta\Phi_{h_ch_e}}(1 + Y_\theta\Theta_\delta) \tag{7}$$

Equation 7 could also be written as

$$Y_h = \frac{\Phi_{h_c\theta}}{\Phi_{h_ch_e}}\left(1 + \frac{1}{Y_\theta\Theta_\delta}\right) \tag{8}$$

Signal/noise ratios are maximized by using Eq. 7 at high and Eq. 8 at low frequencies. There are, however, two problems in computing Y_h. At low frequencies the h_e response is small so the measurement variability will increase. The second problem occurs near the inner-loop crossover frequency. If the inner loop is closed with a small phase margin, then $Y_\theta\Theta_\delta \doteq -1$ in the region of the θ-loop crossover. Consequently, the sum $1 + Y_\theta\Theta_\delta$ will be quite sensitive to variations in Y_θ.

Having described the relationships between various cross-spectra and the measured describing functions, the procedure used to compute the cross-spectra will now be outlined. This procedure consisted of three steps:

1. Continuous analog recordings were made on an FM recorder.

2. Four minutes of data for each run were converted to digital form at a sampling rate of 20 samples/sec.

3. A large-scale digital computer was used to compute the cross-spectra. Computations were done using the BOMM Program, Ref. 5.

Because the inputs were the sums of sine waves, the cross-spectra were actually evaluated by Fourier transforms, e.g., $\Phi_{\theta_c \delta_e} / \Phi_{\theta_c \theta_c}$ equals the Fourier transform of δ_e divided by Fourier transform of θ_c. Furthermore, these spectra exist only at the input frequencies. Precise determination of the input frequencies was obtained by Fourier transforming the inputs for a band of frequencies centered about the estimated values. From each band the frequency which gave the maximum magnitude of the input Fourier transform was selected. Fourier transforms of the remaining parameters at these selected frequencies were then computed.

One additional step was then required before the describing function equations presented earlier could be solved. As the two inputs had to be uncorrelated, they had no common frequencies. Consequently, the θ_c spectra could be computed only at one set of frequencies and the h_c spectra at another set. To obtain data at common frequencies it was necessary to plot the individual spectra and interpolate. This problem could have been eliminated by using two independent random noise generators. However, with random inputs the variability in the measured cross-spectra is increased because the input power is spread out over a frequency band instead of being concentrated at a few frequencies. Whether the higher variability would produce larger describing function errors than those resulting from the interpolation errors is unknown.

11

SECTION IV

EXPERIMENTAL SETUP

A flow chart of the overall experimental setup is shown in Fig. 2. Each of the items shown in the figure is briefly described below.

The vehicle equations of motion were mechanized on an analog computer. The linearized short-period-approximation equations given in Appendix A were used.

The display was a CRT. The two displayed quantities were attitude error, $\theta_e = \theta_c - \theta$, and altitude error, $h_e = h_c - h$. An "inside out" attitude display was used with a moving horizontal line representing the horizon; see Fig. 3. Altitude error was represented by moving dot with an upward displacement of the dot if the aircraft were too high. The attitude display was scaled at 20 deg/in. and altitude at 80 ft/in.

Two subjects were used in the experiments. Both were commercial jet-transport pilots. Subject A had logged 2,300 hr of flying time and Subject B had 2,100 hr.

The manipulator was a conventional-aircraft-type center stick with a force gradient of approximately 7.5 lb/in., measured at the grip. The control sensitivity was varied until the subject felt it was nearly optimum. Both subjects used control sensitivities of 15 deg/sec^2/in.

The inputs used were the sums of sine waves. Ten sine waves were produced by a series of motor-driven resolvers. Five more sine waves were produced with oscillator circuits on the analog computer. These were combined into two inputs, one with eight components and the other with seven. The nominal frequencies for the eight-component input are given below. This produced a random-appearing input with a bandwidth of about 1 rad/sec and with a high frequency shelf. This combination was used either as an attitude input, θ_c, or as a gust input, w_g.
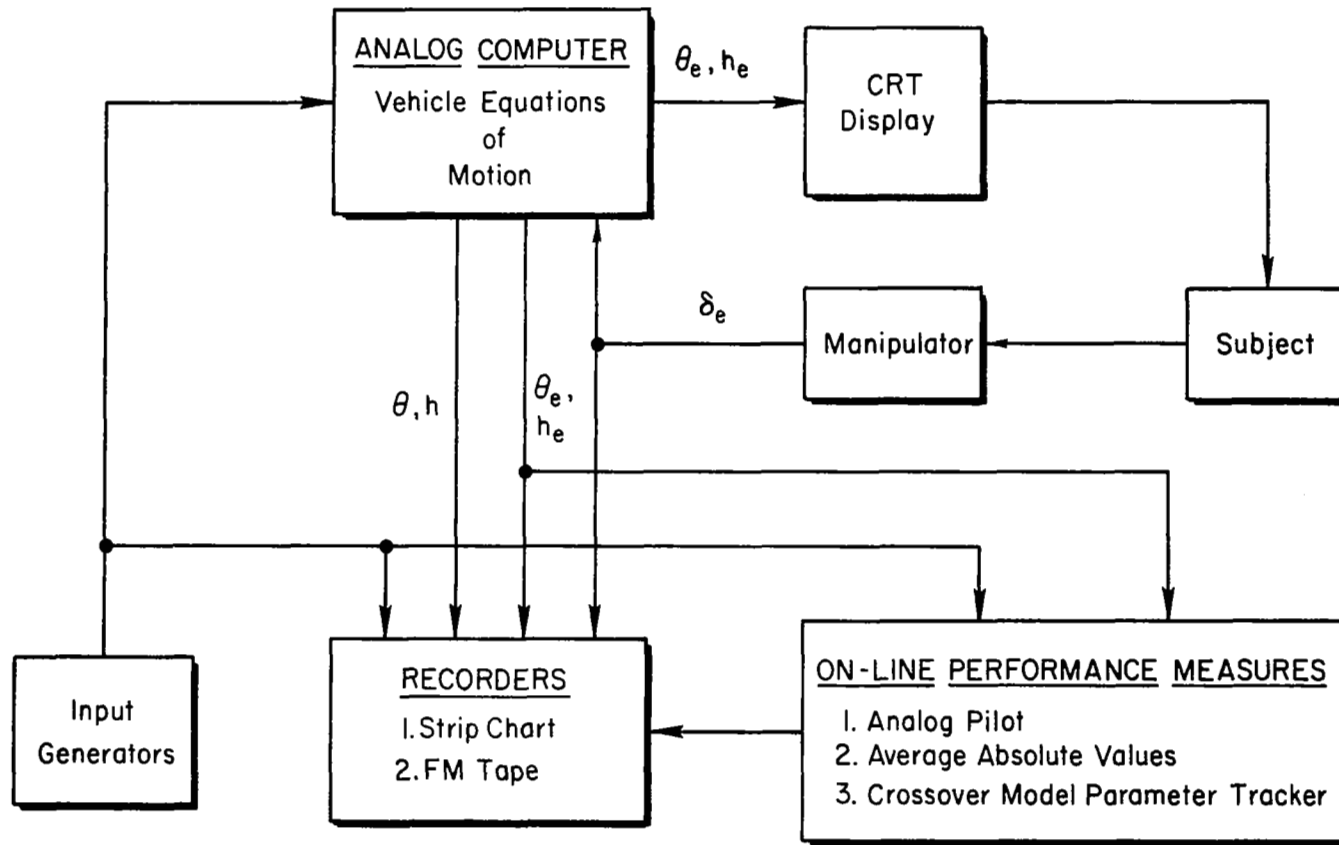
Figure 2. Flow Chart for Experimental Setup
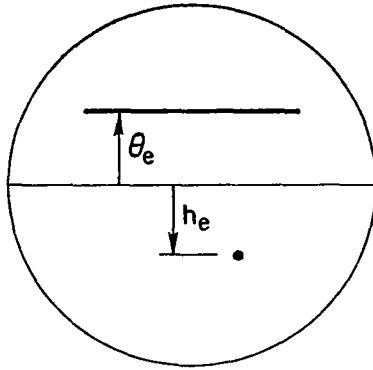
Figure 3. CRT Display

Number of Cycles in 4 Minutes	Frequency (rad/sec)	Relative Magnitude
6	0.157	1
11	0.288	1
20	0.524	1
37	0.969	1
67	1.75	0.1
124	3.25	0.1
229	6.00	0.1
425	11.1	0.1

The nominal frequencies for the 7-component input are given below. This input was also random-appearing with a high-frequency shelf, but the bandwidth was somewhat lower. This combination was used as the altitude input, h_c.

Number of Cycles in 4 Minutes	Frequency (rad/sec)	Relative Magnitude
8	0.209	1
14	0.367	1
26	0.681	1
49	1.28	0.1
91	2.38	0.1
169	4.42	0.1
312	8.17	0.1

14

Two types of recorders were used. An 8-channel strip chart recorder was used to visually monitor the experiments. The parameters which were recorded were the input (s), θ, θ_e, h, h_e, δ_e, and the analog pilot output. Sample time histories are shown in Section V.

The other recorder was a 7-channel FM magnetic tape recorder. Those runs which were to be used for describing function and other data analyses were tape recorded. The seven recorded parameters were θ_c, θ, θ_e, h_c, h, h_e, and δ_e.

Three types of on-line performance measures were used to monitor the subject's performance, especially during training. The most useful device was the analog pilot. This predicted model of the pilot's characteristics was mechanized on the analog computer. When a real pilot was flying the simulator, the inputs to the analog pilot were the same as those displayed to the subject, θ_e and h_e. However, the analog pilot output was not fed back into the vehicle equations of motion; it was merely put on the strip-chart recorder for comparison with the subject's output. Some runs were made without a real pilot, but with the analog-pilot output being fed back into the vehicle equations. These runs were used to check the other on-line performance measures and the describing function calculations.

The analog-pilot output was

$$\delta_e = Y_\theta(\theta_e + Y_h h_e) \tag{9}$$

where[*]

$$Y_\theta = K_\theta \frac{(T_L s + 1)}{(T_I s + 1)} \frac{\left(-\frac{\tau s}{2} + 1\right)}{\left(\frac{\tau s}{2} + 1\right)} \tag{10}$$

$$Y_h = K_h \tag{11}$$

---

[*]The form of Y_θ is slightly different from that used in Appendix C to compute the predicted closed-loop dynamics.

15

The nominal values of the parameters were

$$K_\theta = 1 \text{ sec}^{-2}$$

$$T_L = 2 \text{ sec}$$

$$T_I = 0.1 \text{ sec}$$

$$\tau = 0.3 \text{ sec}$$

$$K_h = 0.344 \text{ deg/ft}$$

After the pilot training had been completed, a brief attempt was made to improve the match between the real and analog-pilot outputs by adjusting these parameters. No combination which was superior to those given above was found.

The second type of on-line performance measure was the average absolute values of the displayed parameters, θ_e and h_e. These averages were taken over 100 sec intervals.

The third performance measure was the Crossover Model Parameter Tracker. This device, which is described in Appendix D, provided an on-line continuous estimate of the pilot's crossover frequency in the outer control loop.

16

SECTION V

RESULTS

A major reason for the success of the experimental part of the present program may be attributed to the comprehensive training program conducted prior to the main data-taking efforts. The primary objective of this training was to allow each subject to reach a stabilized level of closed-loop tracking performance. In addition, the effects of input type and magnitude were investigated; see Subsection A.

Approximately ten hours of simulator flight time were required before each subject reached a stable performance level. A visual comparison of the analog pilot and the test subject performances proved invaluable as a direct cross check on training process. Typical before and after performance is shown in Fig. 4. The most noticeable difference between these two states is shown in the subject's output (stick motion). Prior to obtaining the trained state, his output is hesitant and relatively small, and is charac-terized by the apparent lack of coordination between displayed error signals and stick motion. The output control signals are also unlike the "linear" analog pilot and may be concluded to exhibit a nonlinear behavior. These characteristics are in direct contrast with the after-training state shown in the adjacent traces. Here the analog and human pilot outputs appear to be synchronized except for the small-amplitude high-frequency component.

In the remainder of this section the major experimental results which were obtained are discussed. For convenience, this discussion has been subdivided into the following five topics:

        A.   Effects of Input Type and Magnitude
        B.   On-Line Performance Measures
        C.   Analog Pilot Describing Functions
        D.   Human Pilot Describing Functions
        E.   Remnant Data

A. EFFECTS OF INPUT TYPE AND MAGNITUDE

During the training sessions the input type (θ_c, h_c, w_g, or combinations of these) and magnitude were varied. The pilots preferred that the command signals approximate the aircraft response to a vertical gust. In the opinions

Gust Input
σ_{wg} = 8.4 fps RMS
Pilot "A"

Trained Subject "B"
During Data Runs
θ_c = 2 deg rms , h_c = 8 ft rms

Initial Sessions

After Training

δ_e

(deg/sec²)

20

0

-20

(δ_e) Analog
Pilot

(deg/sec²)

20

0

-20
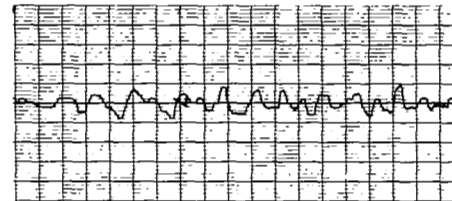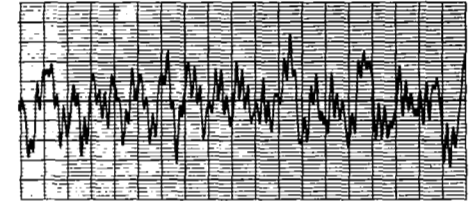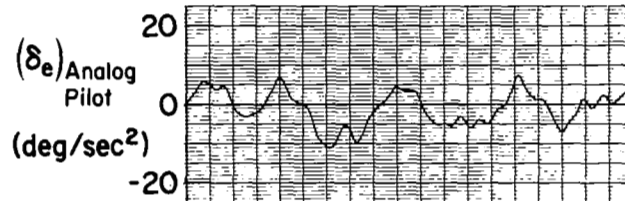
10 sec

Figure 4. Typical Stick Input Time Histories Showing the Effects of Training on Subjects

of the test subjects, they could fly the simulator regardless of the input signal characteristics, but the ILS task was more realistic and their control reactions and impressions were closer to an actual flight situation when the vertical gust inputs were used.

However, a gust input is not a good input for measuring describing functions. The dynamics of the aircraft severely attenuate the response parameters at high frequencies; see Appendix C. Thus the high-frequency measurements would suffer from very poor signal/noise ratios. A secondary and relatively minor disadvantage of using a gust input (and θ_c or h_c) is that the relationships between the measured cross spectra and pilot describing functions become somewhat more complex; see Appendix B.

As a result, it was decided to use command-type inputs for the data runs but to scale the two inputs (θ_c and h_c) to approximate a gust disturbance. Except at extremely low frequencies (much less than 0.1 rad/sec), the open-loop attitude and altitude responses of the simulated vehicle to a gust are proportional to each other in a ratio of approximately 4 ft/deg. The command inputs were set to have bandwidths roughly equal to the short-period frequency and with rms magnitudes in the ratio 4 ft of h_c per degree of θ_c. This provided a fairly realistic approximation to the gust disturbance except for the high-frequency components due to the input shelves. The high-frequency perturbations in the altitude display were particularly disturbing to the subjects. After being told the high-frequency altitude perturbations were due to ILS beam noise, the subjects again considered the simulation satisfactory.

The selection of the input magnitude was a compromise between realism and signal levels. Realism puts an upper bound on the input magnitude, while large inputs are desirable to provide good signal levels to minimize the effects of pilot remnant. At one point in the training session a variety of gust magnitudes were simulated. The pertinent pilot comments are summarized in Table I. The largest reasonable gust level was 8.5 ft/sec.[*] The command input levels finally selected (θ_c, 2 deg rms; h_c, 8 ft rms) closely approximate that magnitude gust disturbance. Although other combinations

_____

[*]See Ref. 8 for data on probability distributions of gust intensity. According to Ref. 8, rms intensities of 8.5 ft/sec or greater have a probability of roughly 0.03.

TABLE I

EVALUATION OF GUST MAGNITUDE

RMS GUST MAGNITUDE (FT/SEC)	PILOT COMMENTS
0	Reasonably smooth IFR flight. No gusts.
2.8	Reasonable control for IFR flight. Light gusty condition.
5.7	Moderate gust. Reasonably good performance considering disturbance.
8.5	Large gust. Unusual for IFR flight. Positive control of vehicle.
11.4	Very large gust. Poor performance. Doubt if landing possible. ±80 ft excursions.
14.2	Largely out of control relative to scope.

of inputs and a variety of magnitudes were tested, the final selection of input type and magnitude was based on the considerations given above. The resultant experimental plan is indicated in Table II.

TABLE II

EXPERIMENTAL PLAN

TASK	SUBJECT	INPUTS		REPLICATIONS
		θ_c (deg rms)	h_c (ft rms)	
Multiloop (θ and h)	A	2	8	3
		—	8	3
Single-loop (θ)	A	2	—	3
Multiloop (θ and h)	B	2	8	3
		—	8	3
Single-loop (θ)	B	2	—	3

B. ON-LINE PERFORMANCE MEASURES

The on-line performance measures provide valuable clues about the pilots' dynamic characteristics, especially when compared with the analog pilot results. A sample time history for the multiloop task with the analog pilot closing the loops is shown in Fig. 5a. This can be compared directly with Figs. 5b and 5c which show time histories with the real pilots in the loop. Also included in Figs. 5b and 5c are the outputs of the analog pilot which were not fed back into the vehicle equations of motion but merely recorded for comparison purposes.

Examination of the figures indicates that the dominant difference between the analog and human pilots is at relatively high frequencies. The outputs of the real pilots have considerably less high-frequency content. The similarities between the analog and human pilots is also shown in the measured average absolute values and crossover frequencies, summarized in Table III. Considering all these data together, it is clear that the measured describing functions for the human subjects should not be drastically different from those of the analog pilot in the regions of inner- and outer-loop crossovers. However, at higher frequencies the describing functions for the real pilots should have considerable amplitude attenuation.

TABLE III

AVERAGE ON-LINE PERFORMANCE MEASURES

TASK	SUBJECT	AVERAGE ABSOLUTE VALUES		CROSSOVER FREQUENCY (RAD/SEC)
		θ_e (deg)	h_e (ft)	
Multiloop θ_c and h_c Inputs	Analog Pilot	3.3	9.7	0.9
	A	3.8	9.7	0.9
	B	3.8	8.3	0.9
Multiloop h_c Input	A	2.3	5.9	0.9
	B	2.3	5.8	0.8
Single-Loop θ_c Input	A	0.7		
	B	0.6		

Sample time histories for the multiloop task with only the h_c input are given in Figs. 5d and 5e, and the performance measures are listed in Table III. With the elimination of the θ_c input, the pilot's output and the vehicle responses are significantly reduced in magnitude. From the predicted loop closures of Appendix C, the average θ_e and h_e responses should be roughly 0.6 of the values with both inputs.* This agrees quite well with the measured average absolute values shown in Table III. Thus we would expect the pilot characteristics with one input (h_c) to be quite similar to those obtained with both inputs and to differ significantly from the analog pilot characteristics only at higher frequencies.

Sample time histories for the single-loop task (θ_c input) are shown in Figs. 5f and 5g. The most significant feature of these responses is that the pilot's output is considerably more bimodal or like a square wave. This is particularly pronounced with Subject B.

C. ANALOG PILOT DESCRIBING FUNCTIONS

The analog pilot was used to check the direct measurement technique. To separate the describing function errors due to the errors in measuring the cross spectra from those due to the errors in interpolating between input frequencies, two sets of calculations were made. One set used the measured cross-spectral ratios for those runs during which the vehicle was being controlled by the analog pilot. The other set used computed values of the cross-spectral ratios at input frequencies.

The calculated cross-spectral ratios were plotted and interpolations were made between input frequencies. The direct measurement expressions of Section III were then applied in computing the Y_θ and Y_h describing functions presented in Figs. 6 and 7. In general, the errors due to interpolation indicated by these results are relatively small. The Y_h calculation confirms the pure gain outer loop using either of the indicated cross-spectral ratios. However, the calculated Y_h derived from the δ_e ratios has somewhat less variation; i.e., interpolation of the δ_e ratios was more accurate than for θ ratios.

---

*The factor of 0.6 is determined by combining the predicted contributions of the sine wave component of the θ_c and h_c inputs to the θ_e and h_e responses.
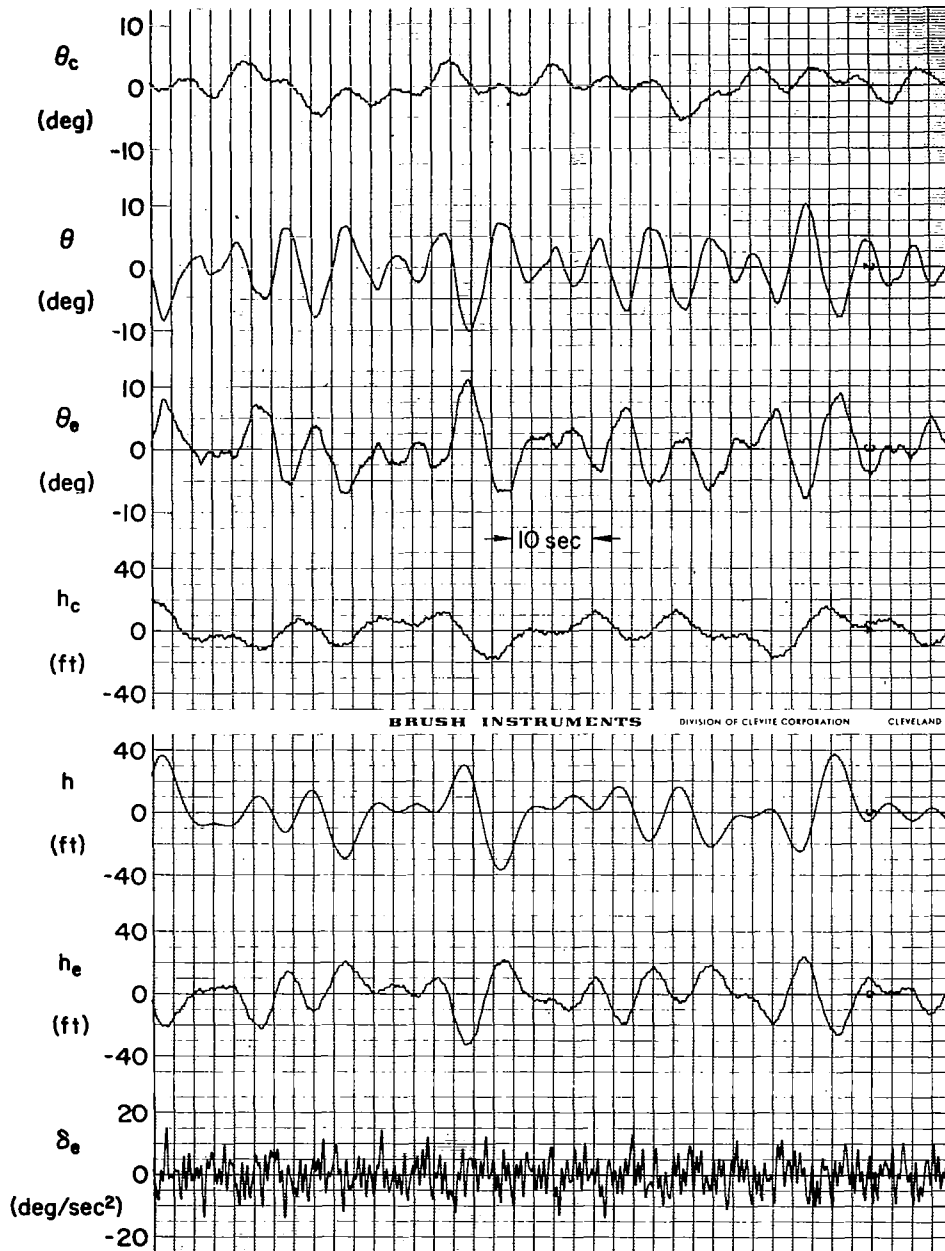
(a) Multiloop, θ_c and h_c Inputs, Analog Pilot

Figure 5. Sample Time Histories
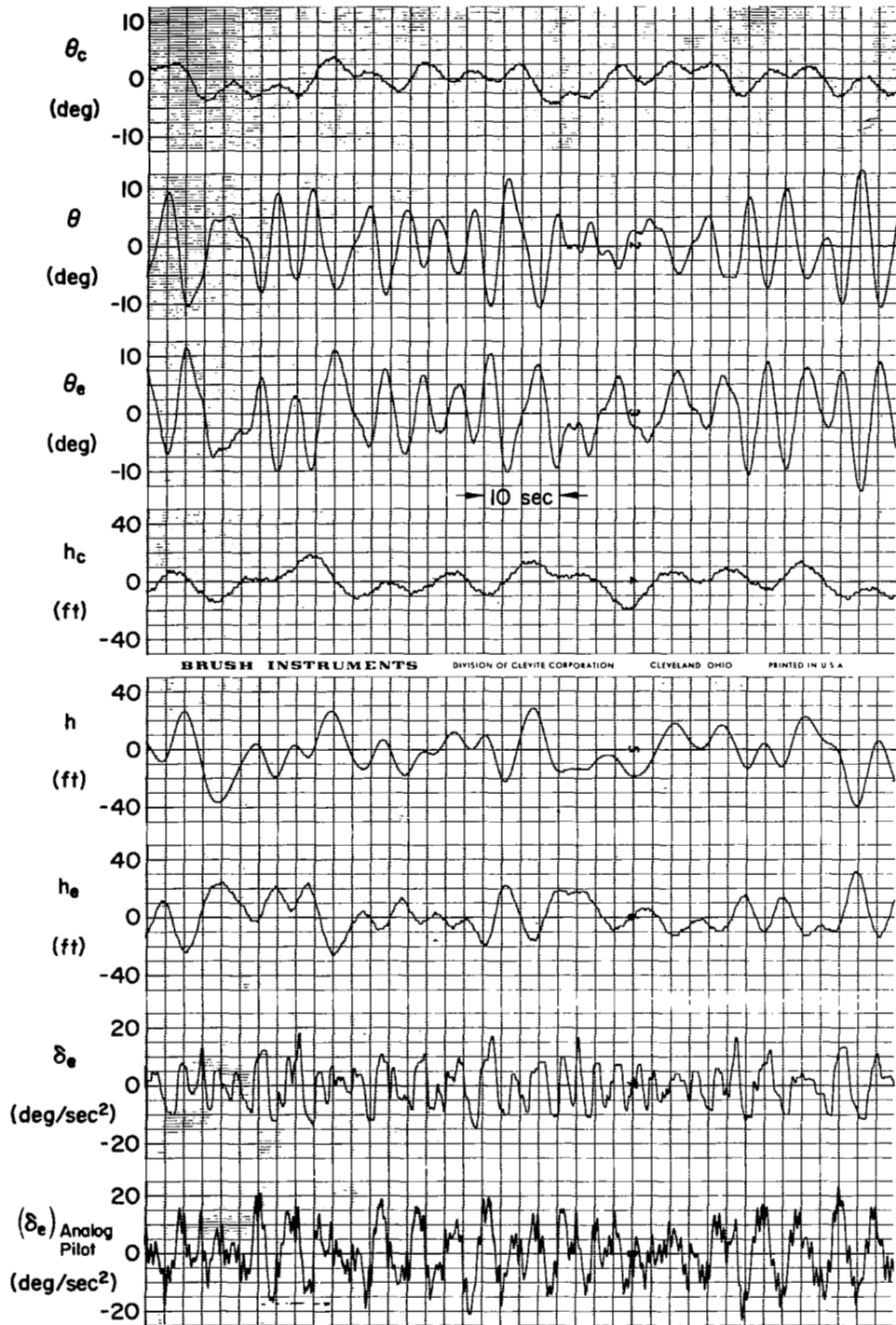
(b) Multiloop, θ_c and h_c Inputs, Subject A

Figure 5. Continued
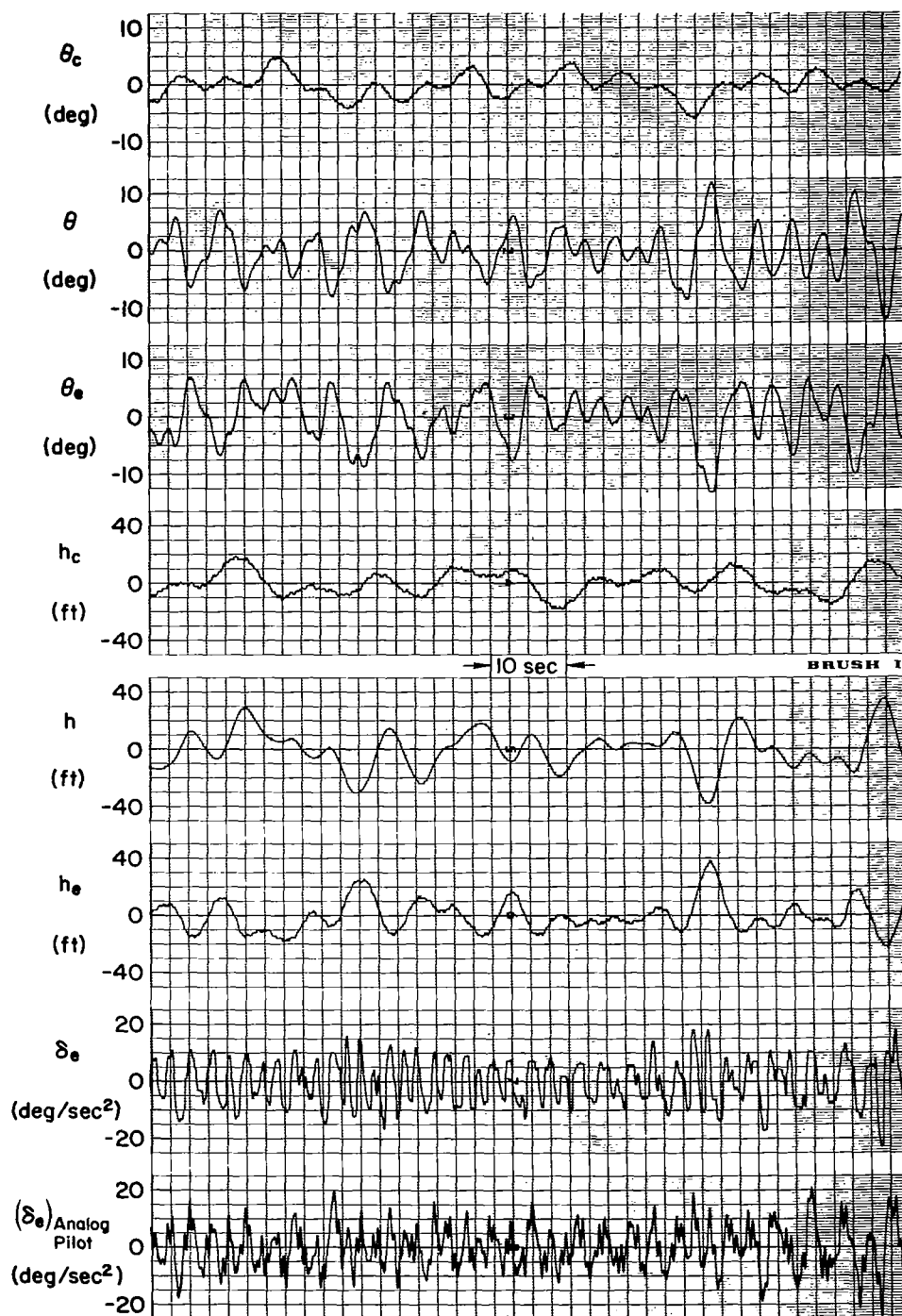
(c) Multiloop, θ_c and h_c Inputs, Subject B

Figure 5. Continued

25
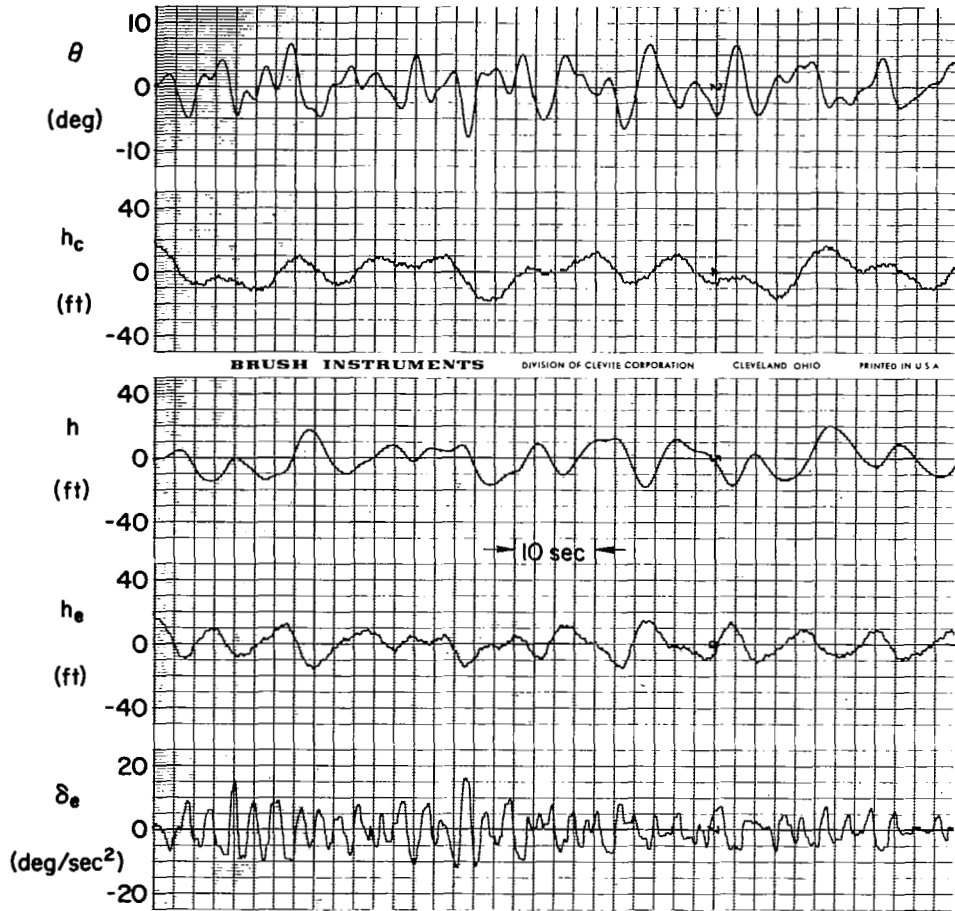
(d) Multiloop, h_c Input, Subject A

Figure 5. Continued

(e) Multiloop, h_c Input, Subject B

Figure 5. Continued

(f) Single Loop, θ_c Input, Subject A

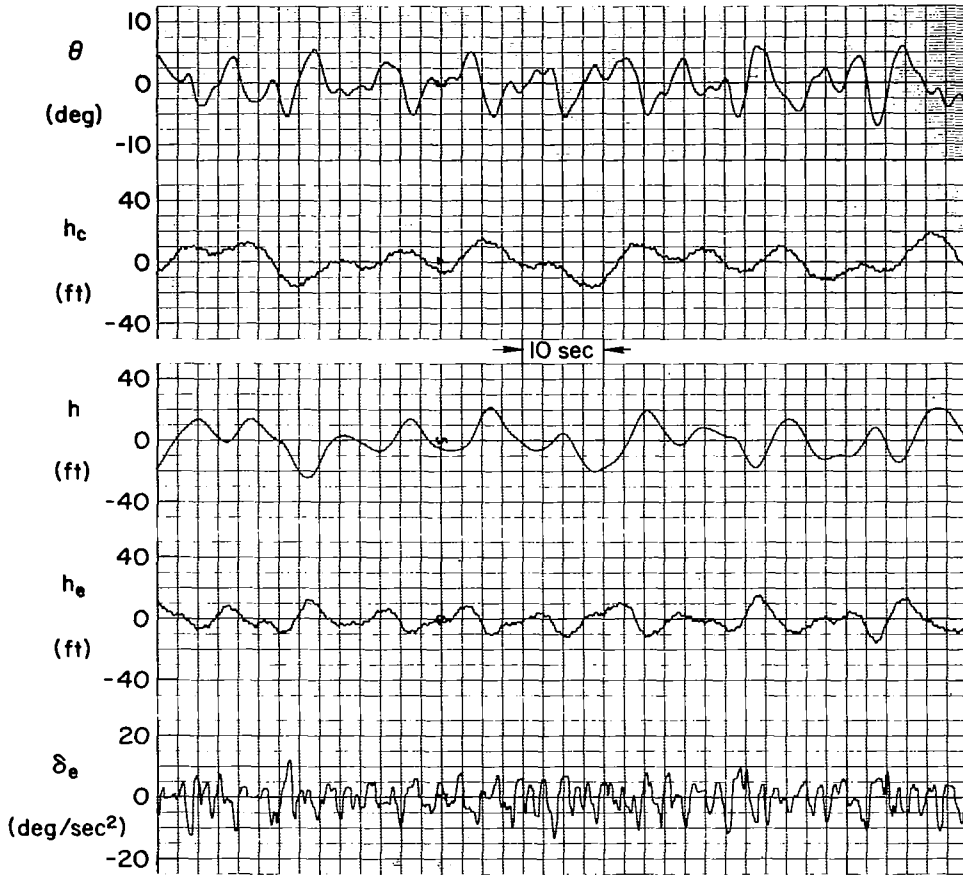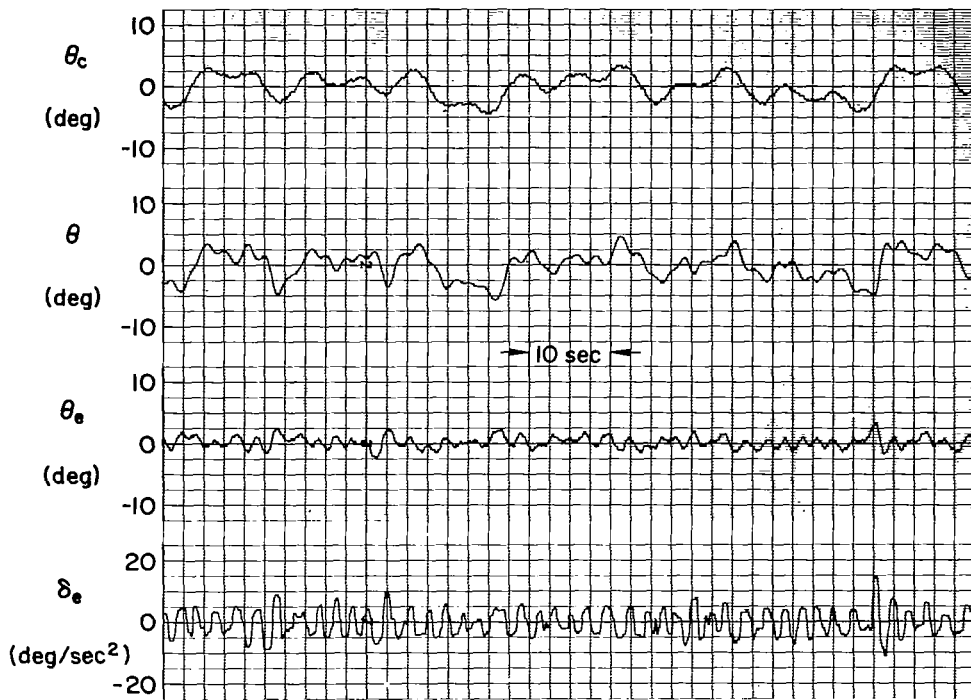Figure 5. Continued

(g) Single Loop, θ_c Input, Subject B
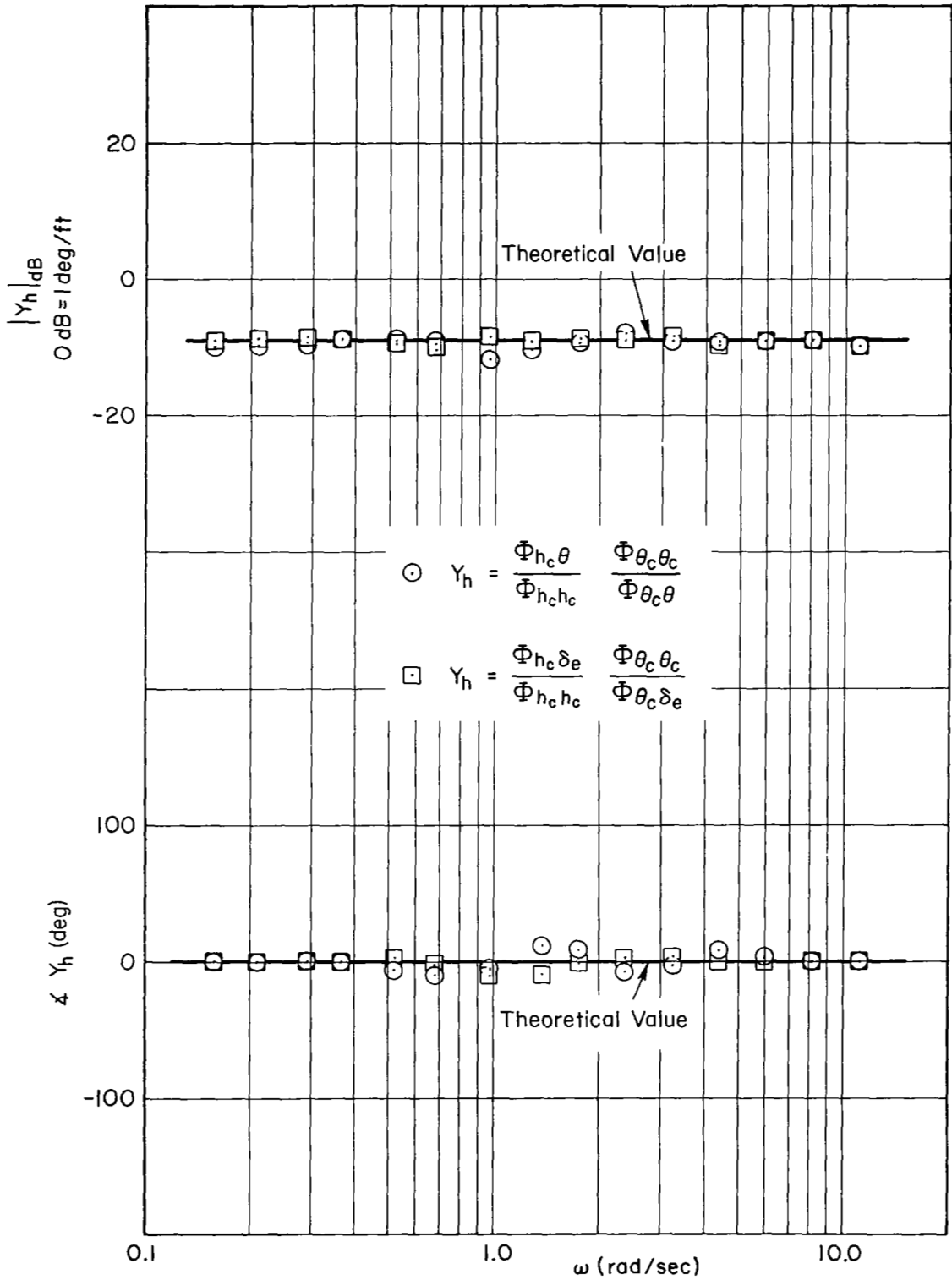
Figure 5. Concluded

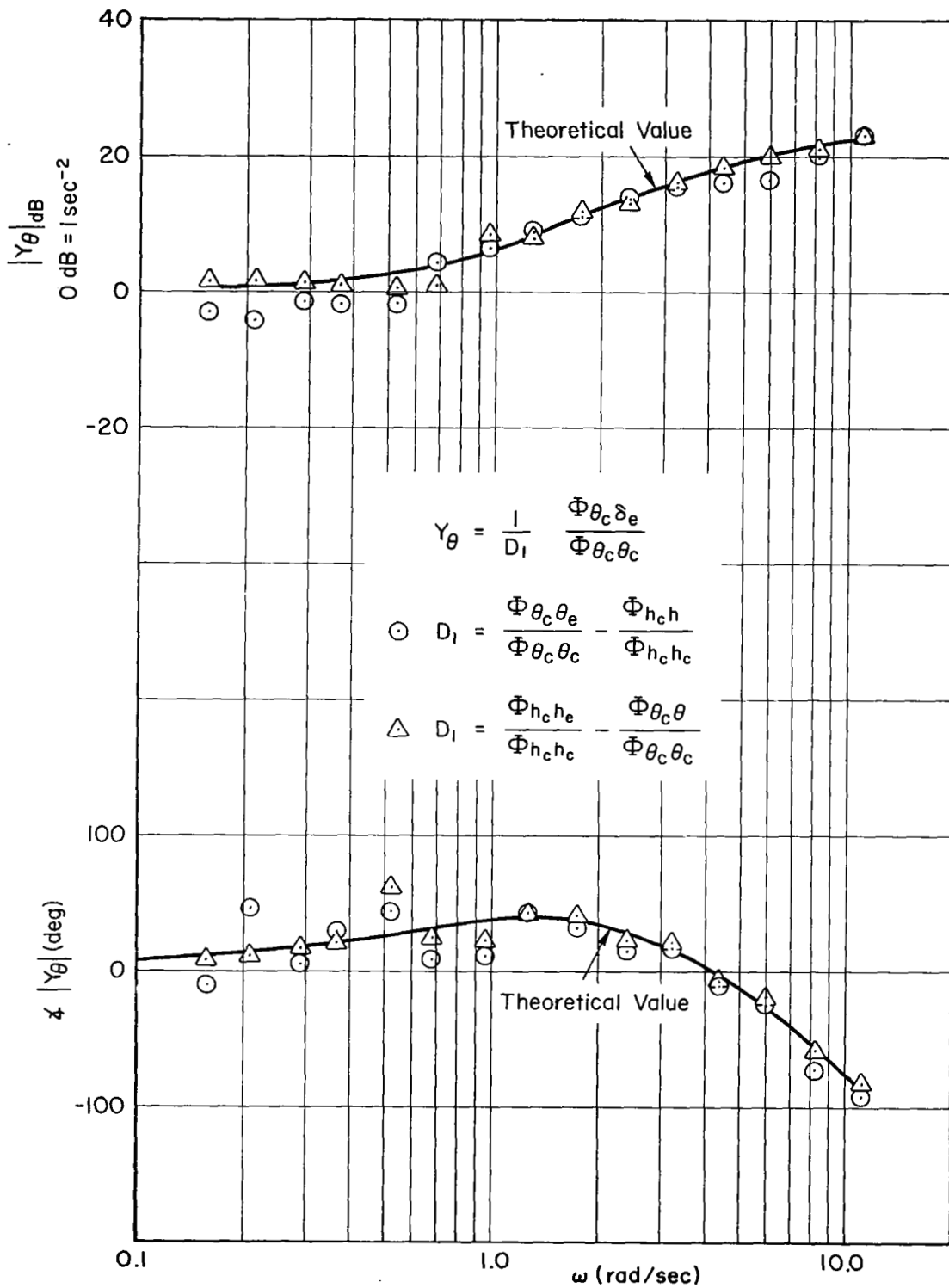Figure 6. Calculated Analog Pilot Describing Function, Y_h

Figure 7. Calculated Analog Pilot Describing Function, Y_θ

The most significant result of this exercise was a clear indication of the difficulty in computing the inner-loop describing function, Y_θ, at low frequencies. From Fig. 7 we note that appreciable scatter exists at all frequencies below 1 rad/sec in both the amplitude and phase calculations. Some improvement is obtained by using $\left(\Phi_{h_c h_e}/\Phi_{h_c h_c}\right) - \left(\Phi_{\theta_c \theta}/\Phi_{\theta_c \theta_c}\right)$ for the denominator calculation. This aspect may be concluded based on the more consistent trend evident in the amplitude plot and the smaller scatter in the phase angle plot. This result was anticipated because the difference at low frequencies of the $\left(\Phi_{h_c h_e}/\Phi_{h_c h_c}\right) - \left(\Phi_{\theta_c \theta}/\Phi_{\theta_c \theta_c}\right)$ expression is a larger fraction of either term than for the terms in the corresponding expression, $\left(\Phi_{\theta_c \theta_e}/\Phi_{\theta_c \theta_c}\right) - \left(\Phi_{h_c h}/\Phi_{h_c h_c}\right)$. However, the measured values of of the cross-spectral ratios in the first expression should be less accurate than those of the second expression because of lower signal levels. Thus one form of the denominator should have lower measurement errors and the other lower interpolation errors.

While the Y_h discussed above has a consistent trend throughout the frequency range, some evidence of the interpolation errors is present. For example, part of the variability in both Y_h and Y_θ describing functions is due to the interpolation of the calculated cross spectra between the h_c input frequencies in the region of 1 rad/sec. An examination of the calculated h_c cross spectra in Figs. 8 and 9 shows that accurate interpolation is sometimes difficult because of the sharp variations in amplitude and phase between the calculated data points. It should be noted also that the closed-loop modes resulting from the closures using the analog pilot describing function are well damped so that the variations shown in Figs. 8 and 9 are not necessarily an extreme. Also, the rapid changes in the closed-loop cross spectra may result from the presence of lightly damped zeros as well as poles. Thus, because the numerator (zeros) differs for each cross spectra, the problem of interpolation will generally be less critical for some ratios than others.

An important aid to the interpolating process is obtained by judicial selection and comparison of cross spectra from different command inputs. For example, the relatively smooth, continuous trend of the $\Phi_{h_c h_e}/\Phi_{h_c h_c}$ (Fig. 8) represents an obvious interpolation between input frequencies,

while the peaked interpolation near 1 rad/sec shown for the $\Phi_{h_c\theta}/\Phi_{h_c h_c}$ ratio (Fig. 9) requires some justification. In support of this interpolation, consider the calculated $\Phi_{\theta_c\theta}/\Phi_{\theta_c\theta_c}$ cross-spectral ratio of Fig. 10. This θ_c spectrum is defined for different input frequencies. (For experimental data, the frequency separation is required because two uncorrelated inputs are needed to reduce the data.) The intermediate value of the θ_c ratio provides a data point in the critical region. Since Y_h is given by $\left(\Phi_{h_c\theta}/\Phi_{h_c h_c}\right)\big/\left(\Phi_{\theta_c\theta}/\Phi_{\theta_c\theta_c}\right)$, the peaked interpolation of $\Phi_{h_c\theta}/\Phi_{h_c h_c}$ is necessary to avoid an unrealistic peak in Y_h. The Y_h describing function is also estimated from the alternate δ_e ratios as indicated in Fig. 6. The iterative procedure implied by the foregoing does ease the interpolation task involved, and this approach provides a direct cross check of the cross spectral data.

The theoretical cross-spectral data analyzed in the foregoing are a basis for comparison and evaluation of errors in the measured data. The measured cross-spectral ratios for the analog pilot[*] are shown for selective responses in Figs. 11, 12, 13, and 14. These data are shown for two data runs which are identified by the symbols. In general, the magnitudes and trend of these results are in close agreement with the theoretical cross-spectral ratios. The only significant differences are restricted to the low-frequency regions. These measured data are also repeatable over the entire frequency range except for the low-frequency extreme. In general, the small variance in the data does not influence the fairing of the curves, and therefore the interpolating task is no more complex than that for the theoretical data considered in previous paragraphs.

The variance in the data due to measurement errors is also influenced by the relative signal/noise ratio of the cross spectra. Figures 13 and 14 both indicate that the measurement errors are largest for the recovered cross-spectral ratio when the signal level is small. The accuracy can be improved, however, by using different parameters in different regions. For example, for the attitude command responses shown in Figs. 13 and 14 the δ_e cross spectra are better for the high frequencies, while the θ cross spectra are better for the low frequencies.

---

[*]Since the analog pilot was completely linear and time-invariant, there was no remnant. Thus, analysis of analog pilot data was done under the most ideal conditions.

Note:

1. Symbols indicate the frequencies at which theoretical values were calculated

2. Interpolation was used between frequencies to define curves
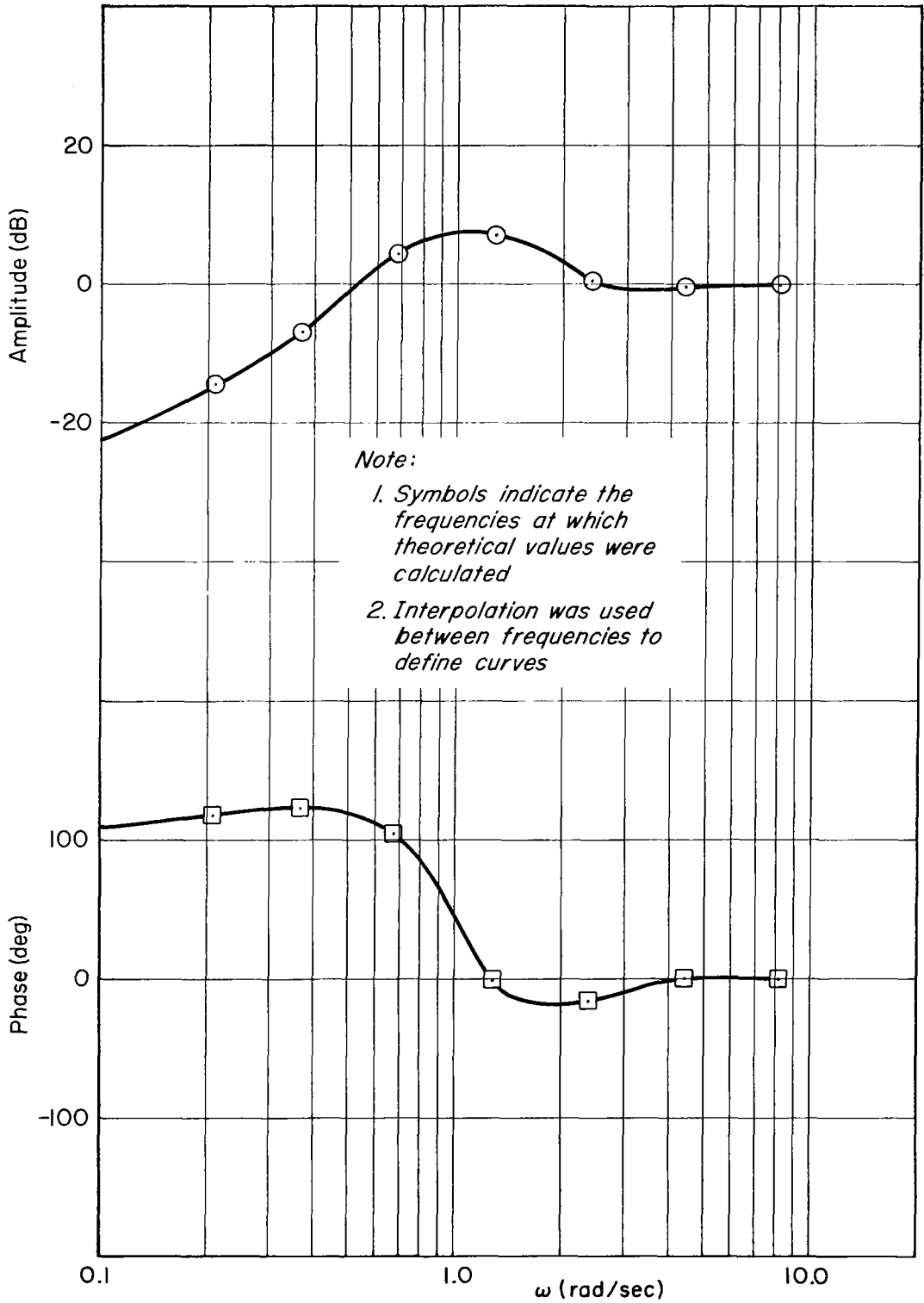
Figure 8. Calculated $\Phi_{h_c h_e}/\Phi_{h_c h_c}$ Cross-Spectral Ratio
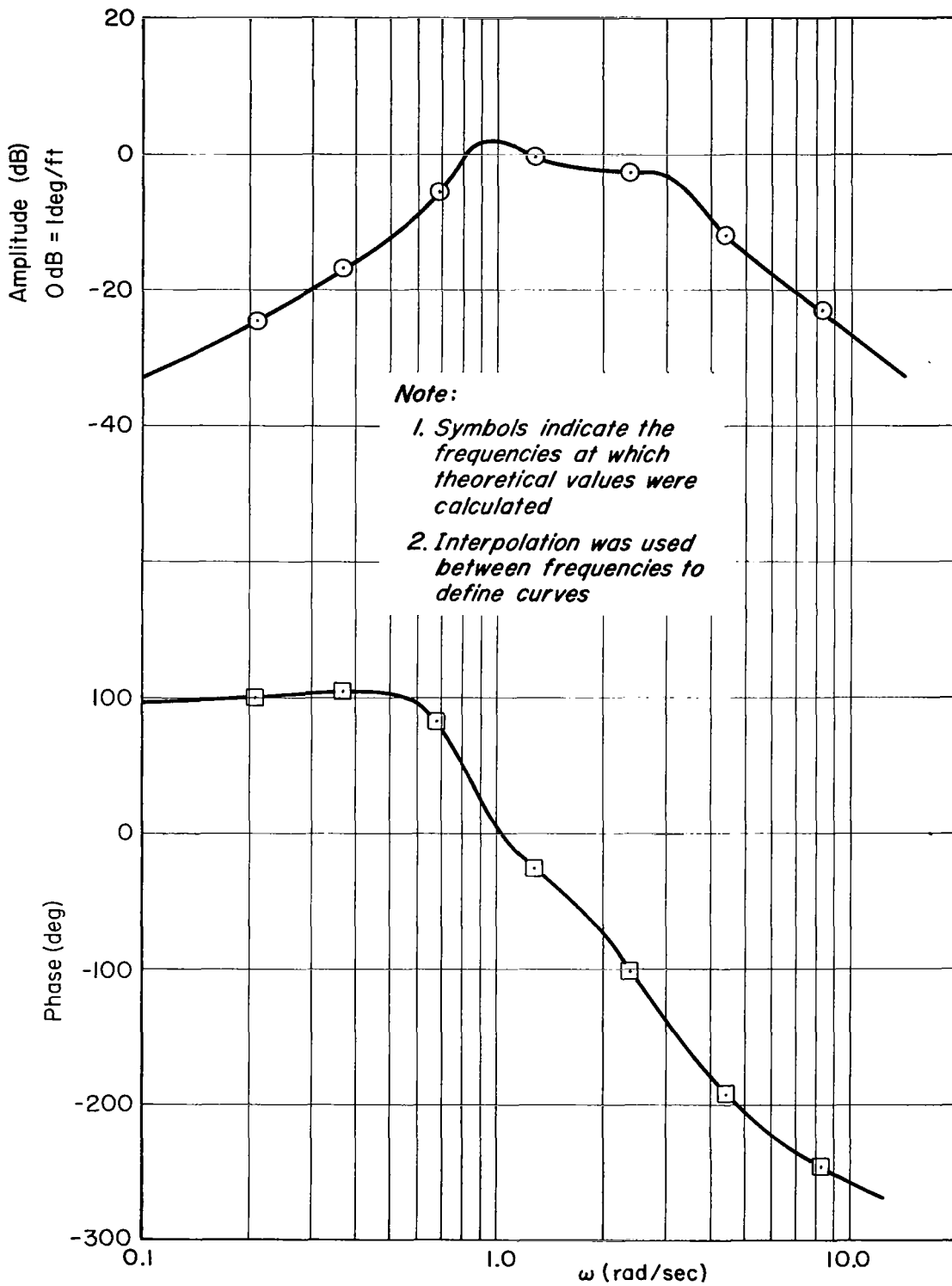
Figure 9. Calculated $\Phi_{h_c\theta}/\Phi_{h_ch_c}$ Cross-Spectral Ratio

35

Note:

1. Symbols indicate the frequencies at which theoretical values were calculated

2. Interpolation was used between frequencies to define curves
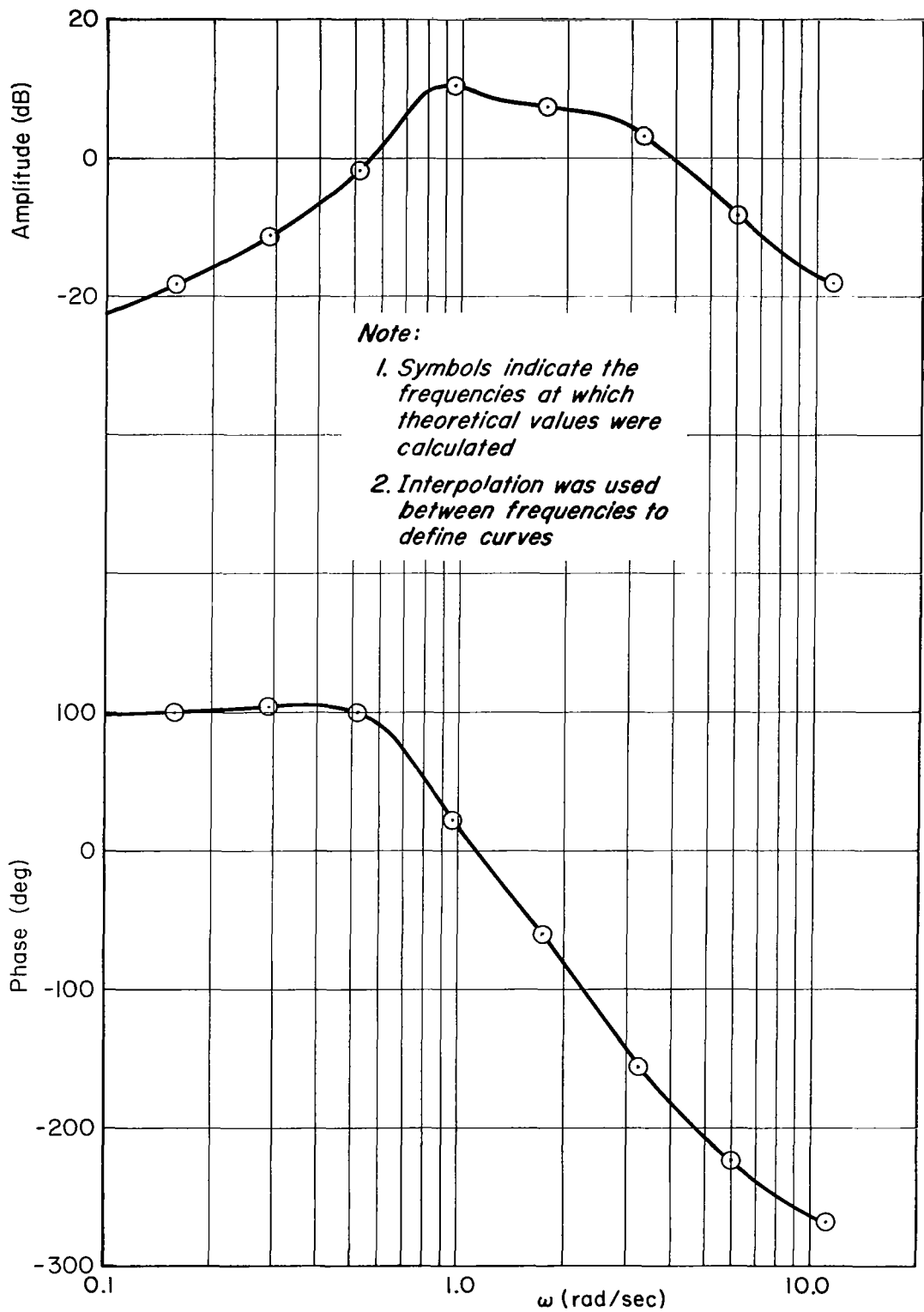
Figure 10. Calculated $\Phi_{\theta_c\theta}/\Phi_{\theta_c\theta_c}$ Cross-Spectral Ratio

Figure 11. Measured $\Phi_{h_c\theta}/\Phi_{h_ch_c}$ Cross-Spectral Ratio, Analog Pilot

37

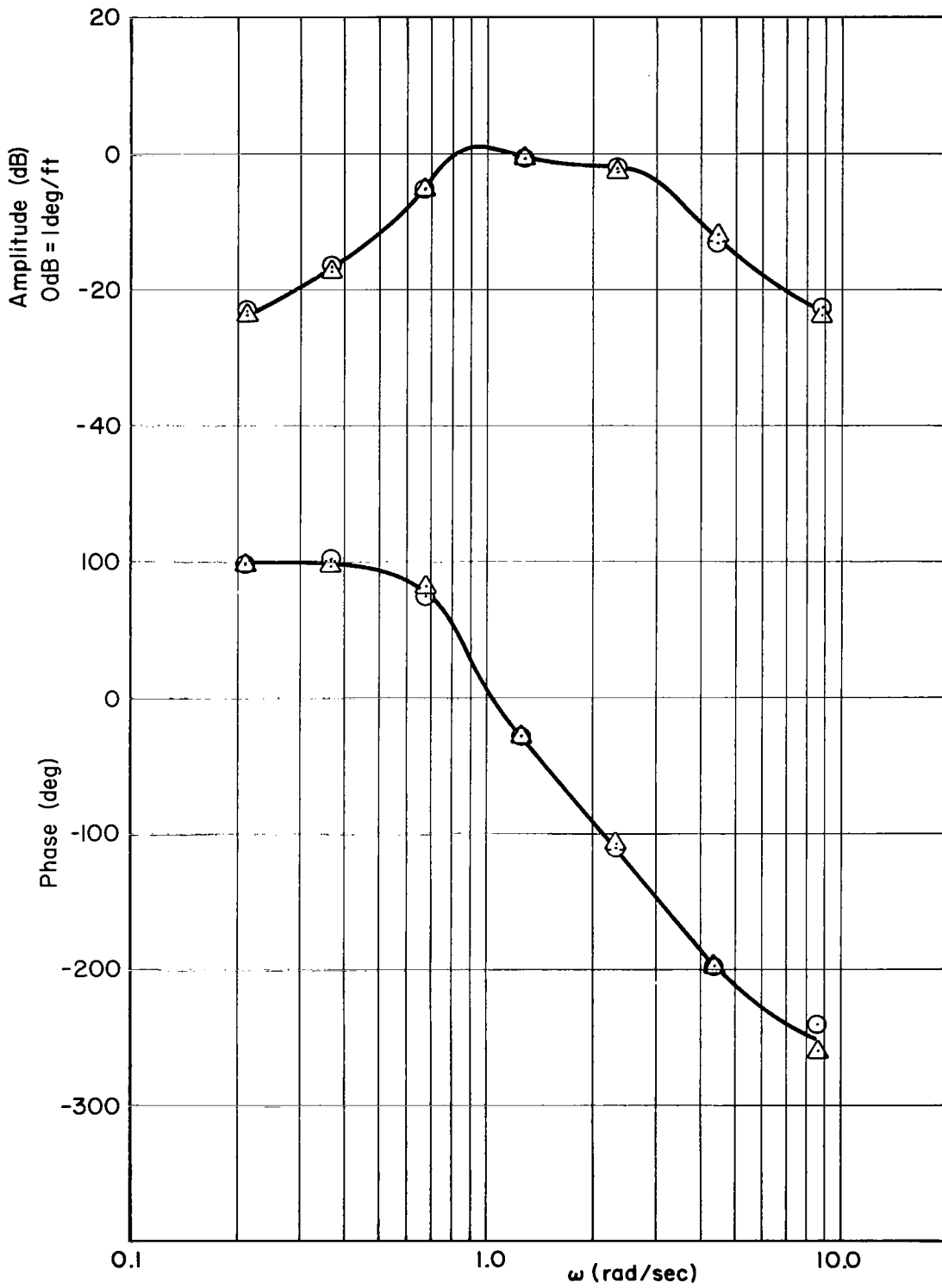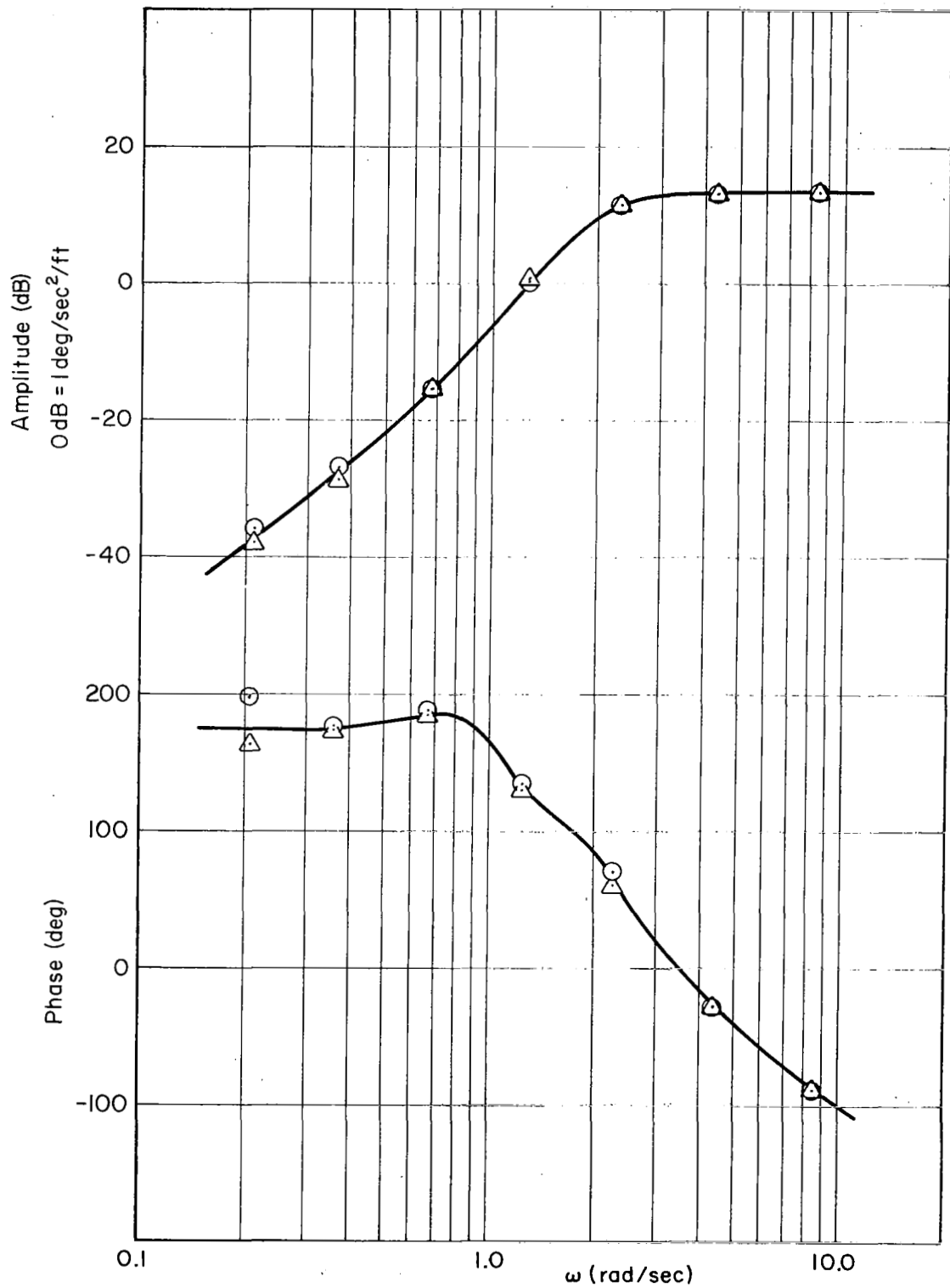Figure 12. Measured $\Phi_{h_c\delta_e}/\Phi_{h_ch_c}$ Cross-Spectral Ratio, Analog Pilot
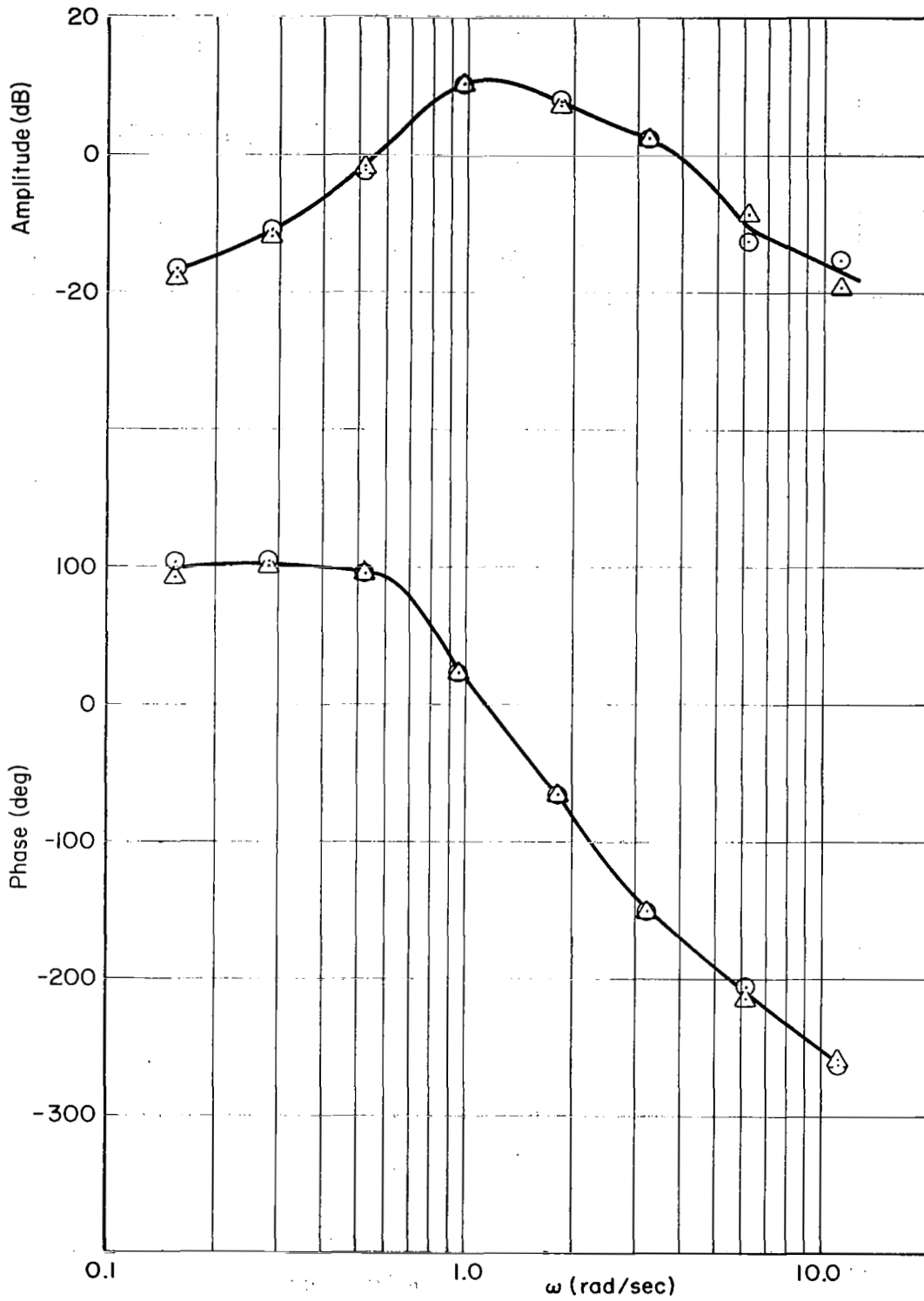
Figure 13. Measured $\Phi_{\theta_c\theta}/\Phi_{\theta_c\theta_c}$ Cross-Spectral Ratio, Analog Pilot

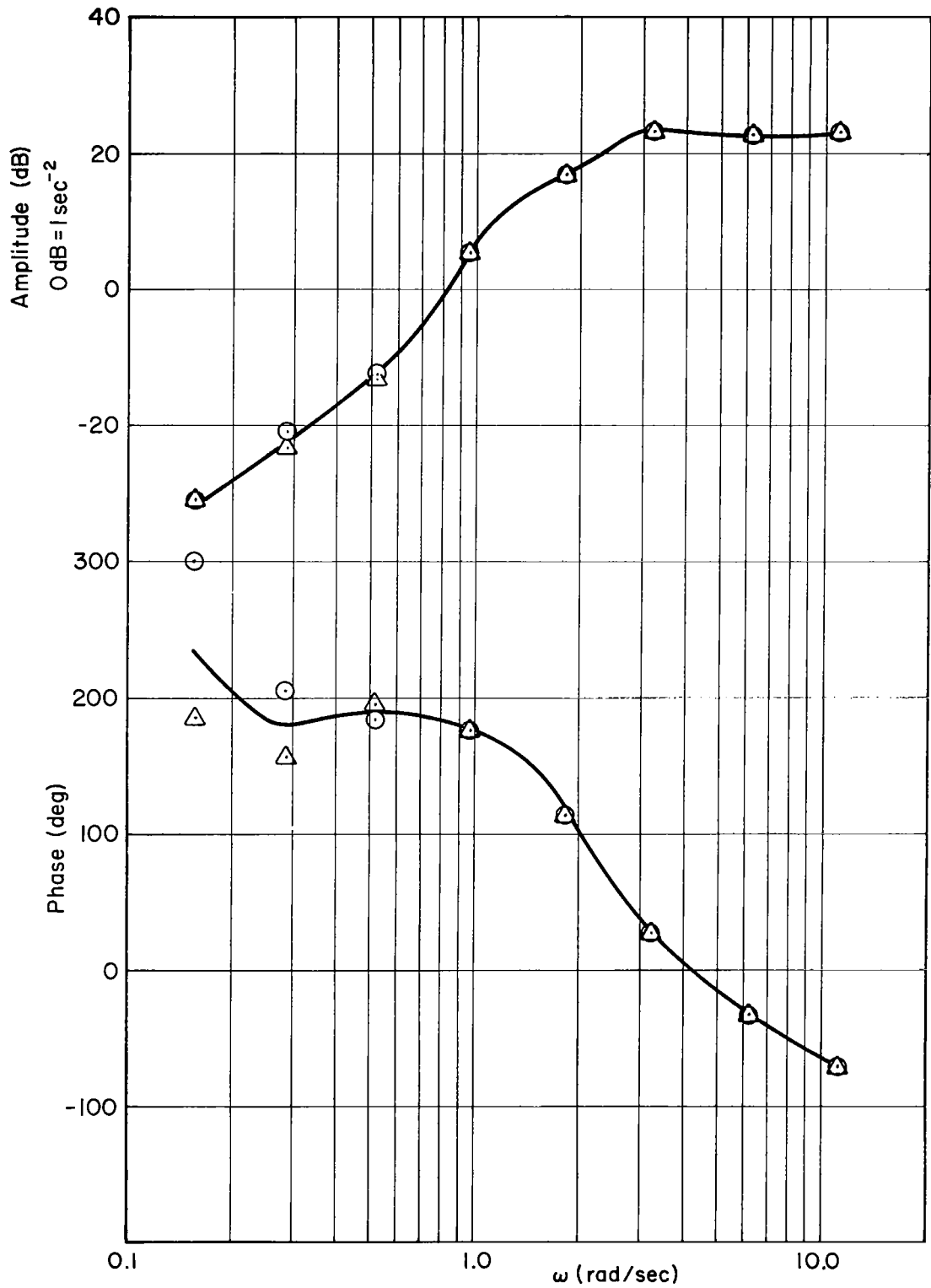Figure 14. Measured $\Phi_{\theta_c \delta_e} / \Phi_{\theta_c \theta_c}$ Cross-Spectral Ratio, Analog Pilot

The Y_h and Y_θ describing functions derived from the measured data are plotted in Figs. 15a and 15b. In the case of the outer-loop describing function the pure gain is clearly indicated. The inner-loop describing function Y_θ is well defined at the higher frequencies, but at the lower frequencies the function is not clearly defined due to the variability. No improvement was obtained by using a different numerator ratio since the problem exists in taking the difference of two nearly equal cross-spectral ratios in the denominator. The $\left(\Phi_{\theta_c\theta_e}/\Phi_{\theta_c\theta_c}\right)-\left(\Phi_{h_ch}/\Phi_{h_ch_c}\right)$ denominator was not computed for the measured data because in the digital conversion process the h data was lost.

A comparison of these measured analog pilot describing functions with the theoretical values shows basically good agreement. The variance in both Y_h and Y_θ is greater for the measured results. The larger variance indicated is due primarily to measurement errors since the errors caused by curve fairing and interpolation of the cross-spectral ratios were essentially the same for either the calculated or measured data. This brief comparison of the errors suggests that the measurement errors are roughly comparable to those due to curve fitting and interpolating.

Several conclusions may be expressed regarding the direct measurement technique based on the preceding results and discussions. The basic or theoretical limitation of the method occurs in computing inner-loop Y_θ describing function at low frequencies, and this aspect has been substantiated by the results. In addition to the above, the following are conclusions which pertain specifically to measurement errors:

1. Measurement accuracy can be improved through increased signal/noise ratios by using different parameters in different regions, e.g., h cross spectra at low frequencies and δ_e cross spectra at high frequencies.

2. Outer-loop describing function can be accurately measured over a wide frequency range.

3. Errors due to curve fairing and interpolation between data points can be significant in the regions where lightly damped poles or zeros occur.

41
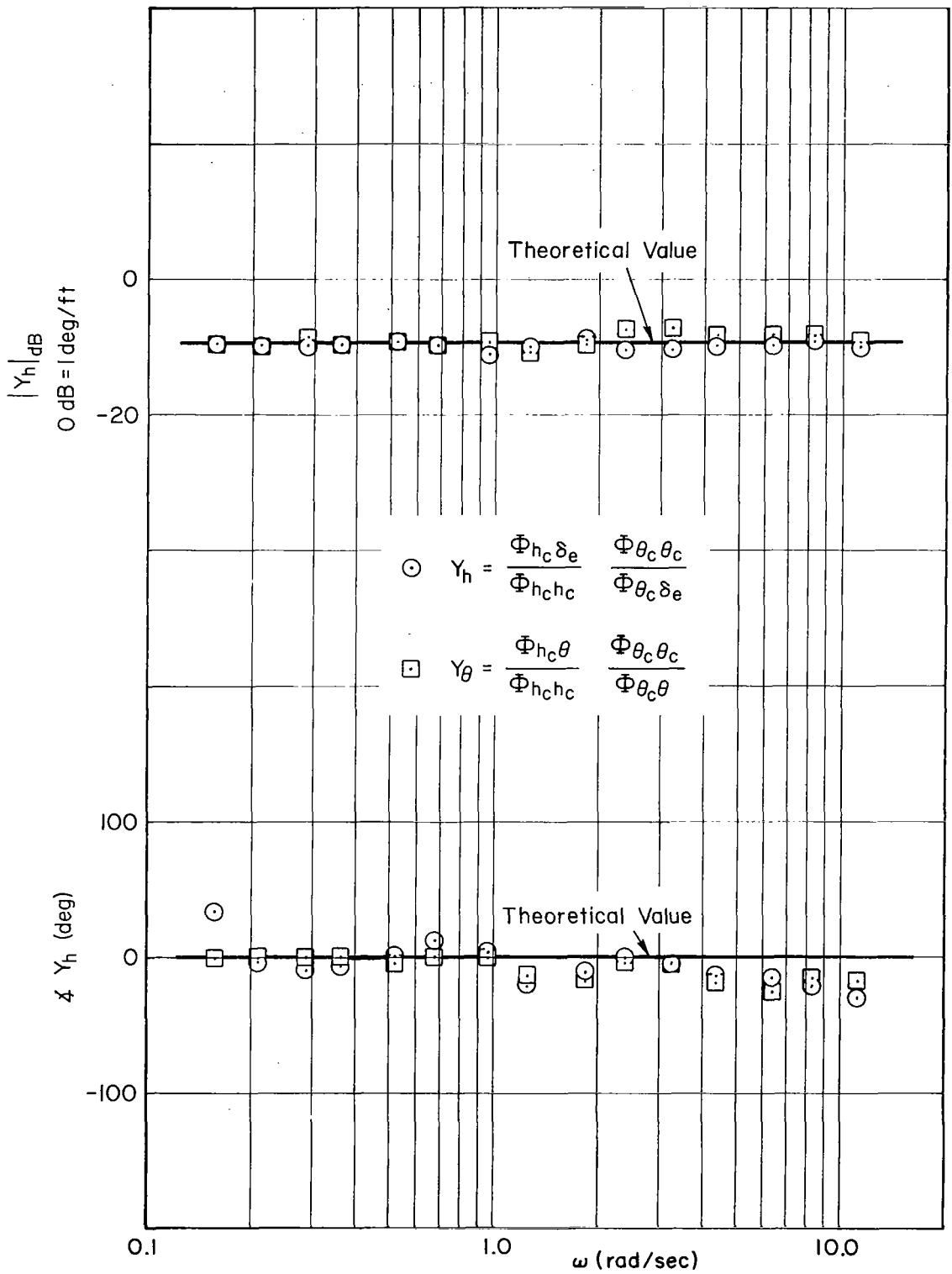
Figure 15. Measured Analog Pilot Describing Function

Theoretical Value

$$Y_\theta = \frac{N_I}{D_I}$$

$$D_I = \frac{\Phi_{h_c h_e}}{\Phi_{h_c h_c}} - \frac{\Phi_{\theta_c \theta}}{\Phi_{\theta_c \theta_c}}$$

$$\odot \quad N_I = \frac{\Phi_{\theta_c \delta_e}}{\Phi_{\theta_c \theta_c}}$$

$$\diamondsuit \quad N_I = \frac{1}{\Theta_\delta} \frac{\Phi_{\theta_c \theta}}{\Phi_{\theta_c \theta_c}}$$

(b) Y_θ
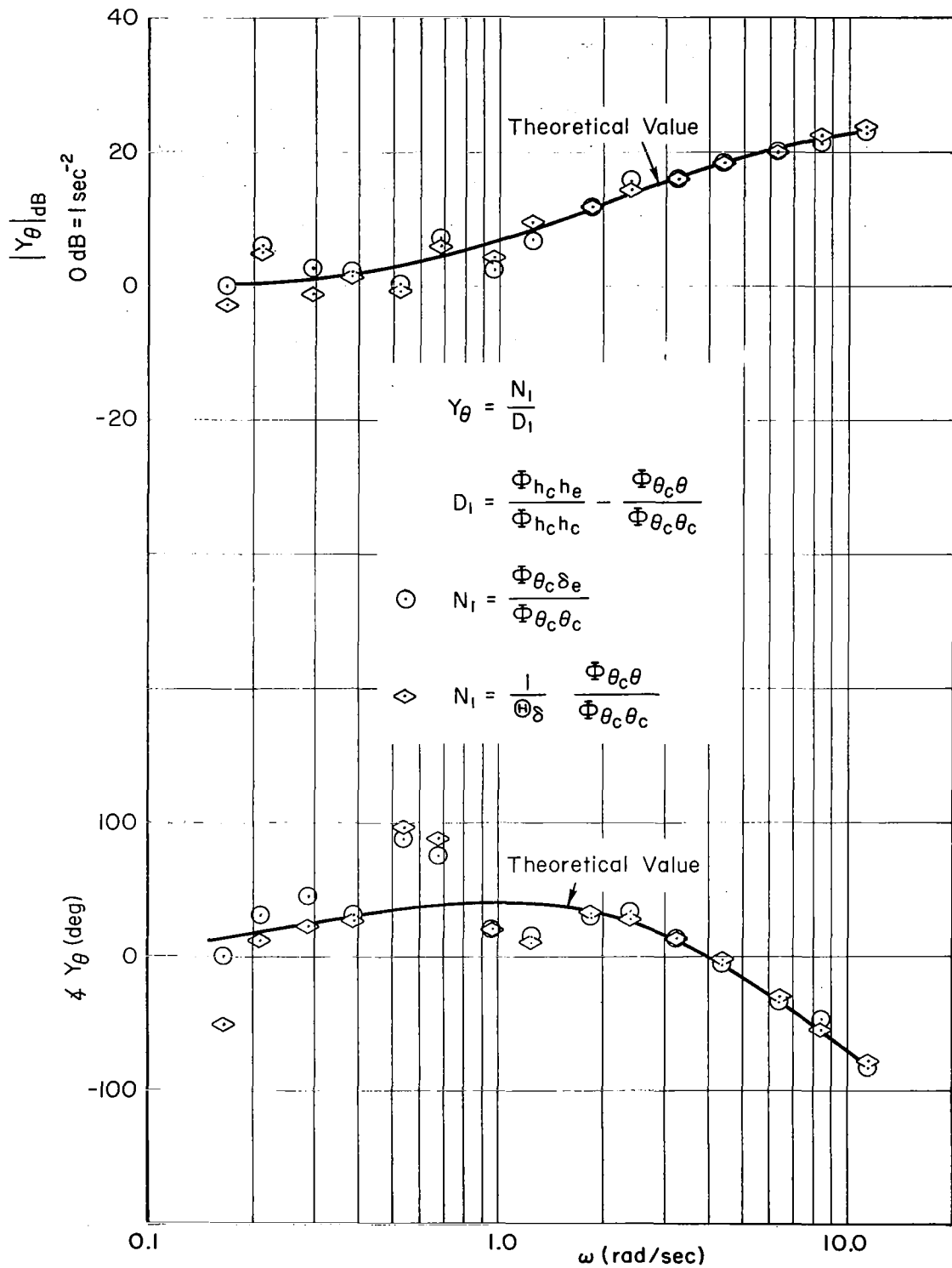
Figure 15. Concluded

43

D. HUMAN PILOT DESCRIBING FUNCTIONS

The following paragraphs discuss the describing functions measured for the two subjects used in the experiments. The emphasis here will be on the implications of these results with regard to the multiloop pilot model. However, some brief comments on the data reduction technique and associated errors will be made.

Let us start by examining the attitude-loop describing function, Y_θ. The results for the single-loop tracking task (attitude alone) are presented in Fig. 16.[*] Several significant features are shown in this figure:

1. The results for the two subjects are nearly identical except for a slightly lower gain, roughly 2 dB, for Subject B.

2. The advantages of using the δ_e instead of the θ cross spectra at the higher frequencies is shown by the lower variability.

3. The data accuracy at the lowest input frequencies is relatively poor; this is due primarily to the low signal level of the attitude error, θ_e.

These single-loop results will now be compared with the multiloop data.

The measured inner-loop describing functions for the multiloop two-input task are shown in Fig. 17. The results shown are the averages[**] over the three repeat runs made for each subject. The main conclusions to be drawn from Fig. 17 are:

1. For frequencies less than 1.5 rad/sec, the data appears to be quite poor.

2. At frequencies above 1.5 rad/sec, the results for the two subjects are nearly identical except for a slightly higher gain, roughly 3 dB, for Subject B.

---

[*]The solid curves are curve fits of the data which will be discussed later.

[**]The various cross-spectral ratios were averaged before the frequency interpolation and subsequent describing function calculations

44

The poor accuracy at the lower frequencies was expected. Section III
discussed the basic problem in trying to make low-frequency measurements
of the inner-loop describing functions. The gain difference between the
two subjects is especially interesting because it is the reverse of the
single-loop difference. In the single-loop task Subject A used a higher
gain than Subject B, but in the multiloop task Subject B had the higher
gain.

Comparison of Figs. 16 and 17 shows how the subjects modified their
attitude control in going from the single-loop task to the multiloop one.
Although there may have been some minor adjustment in the high-frequency
characteristics, the major adjustment appears to be a gain change. Thus
the major differences in Y_θ between subjects or from single-loop to
multiloop are gain changes, which are summarized in Table IV.

TABLE IV

RELATIVE GAINS OF
ATTITUDE LOOP DESCRIBING FUNCTIONS

TASK	SUBJECT	
	A	B
Single-loop	0 dB	—2 dB
Multiloop	—3 dB	0 dB

A difference in piloting technique seems indicated. Subject A had a
higher gain than Subject B for the single-loop task, but reduced his gain
in going to the multiloop task. On the other hand, Subject B used a
higher gain for the multiloop task. However, it is important to note that
the gain differences among all four cases are relatively small, 3 dB or
less.

45

Unflagged Symbols: $Y_\theta = \dfrac{\Phi_{\theta_c \delta_e}}{\Phi_{\theta_c \theta_e}}$

Flagged Symbols: $Y_\theta = \dfrac{\Phi_{\theta_c \theta}}{\Theta_\delta \Phi_{\theta_c \theta_e}}$

Different symbols represent repeat runs
Data displaced only for clarity. Arrows
indicate correct run frequencies
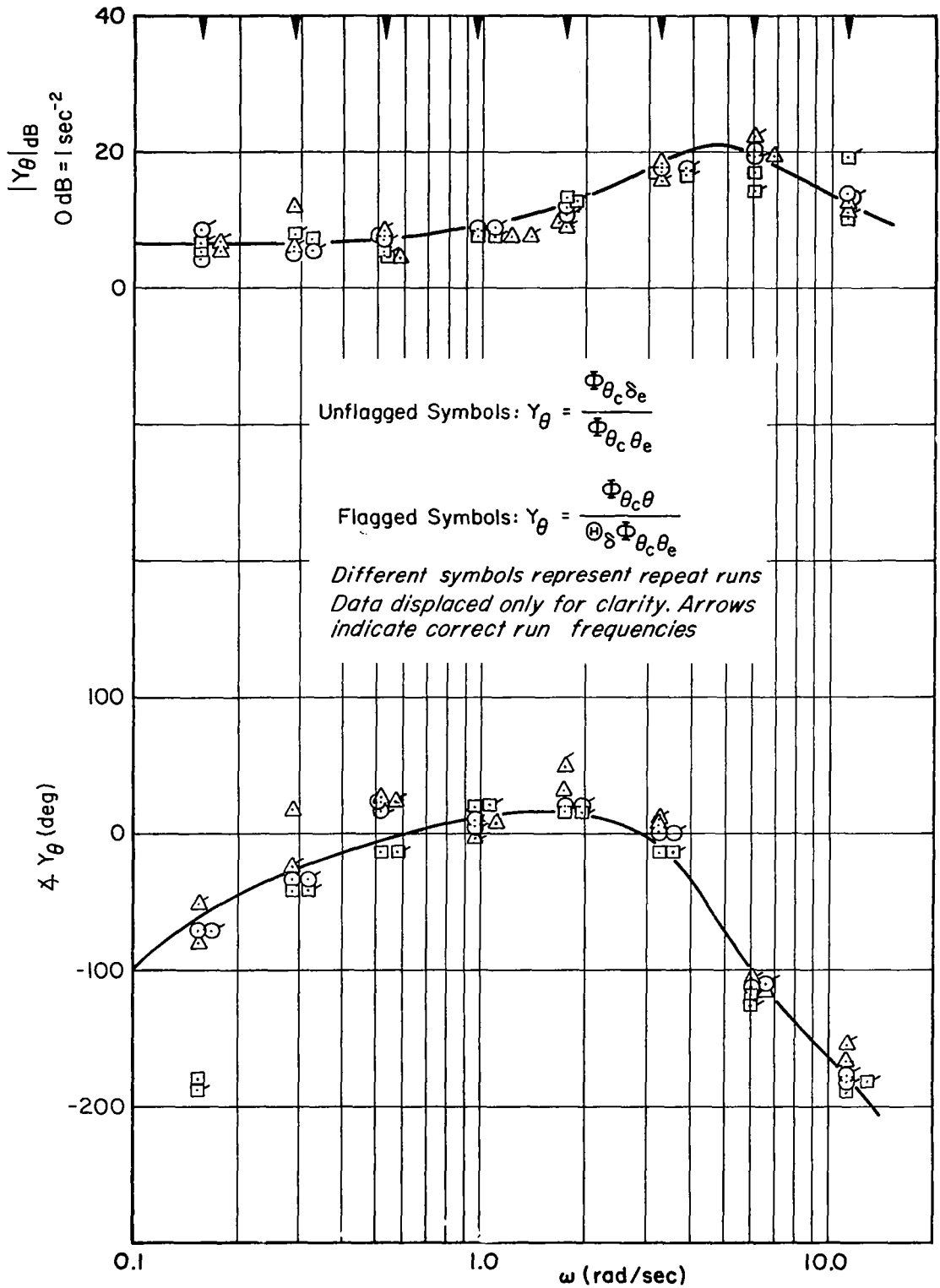
(a) Subject A

Figure 16. Y_θ Measurements, Single Loop

Unflagged Symbols: $Y_\theta = \dfrac{\Phi_{\theta_c \delta_e}}{\Phi_{\theta_c \theta_e}}$

Flagged Symbols: $Y_\theta = \dfrac{\Phi_{\theta_c \theta}}{\Theta_\delta \Phi_{\theta_c \theta_e}}$

Different symbols represent repeat runs
Data displaced only for clarity. Arrows
indicate correct run frequencies
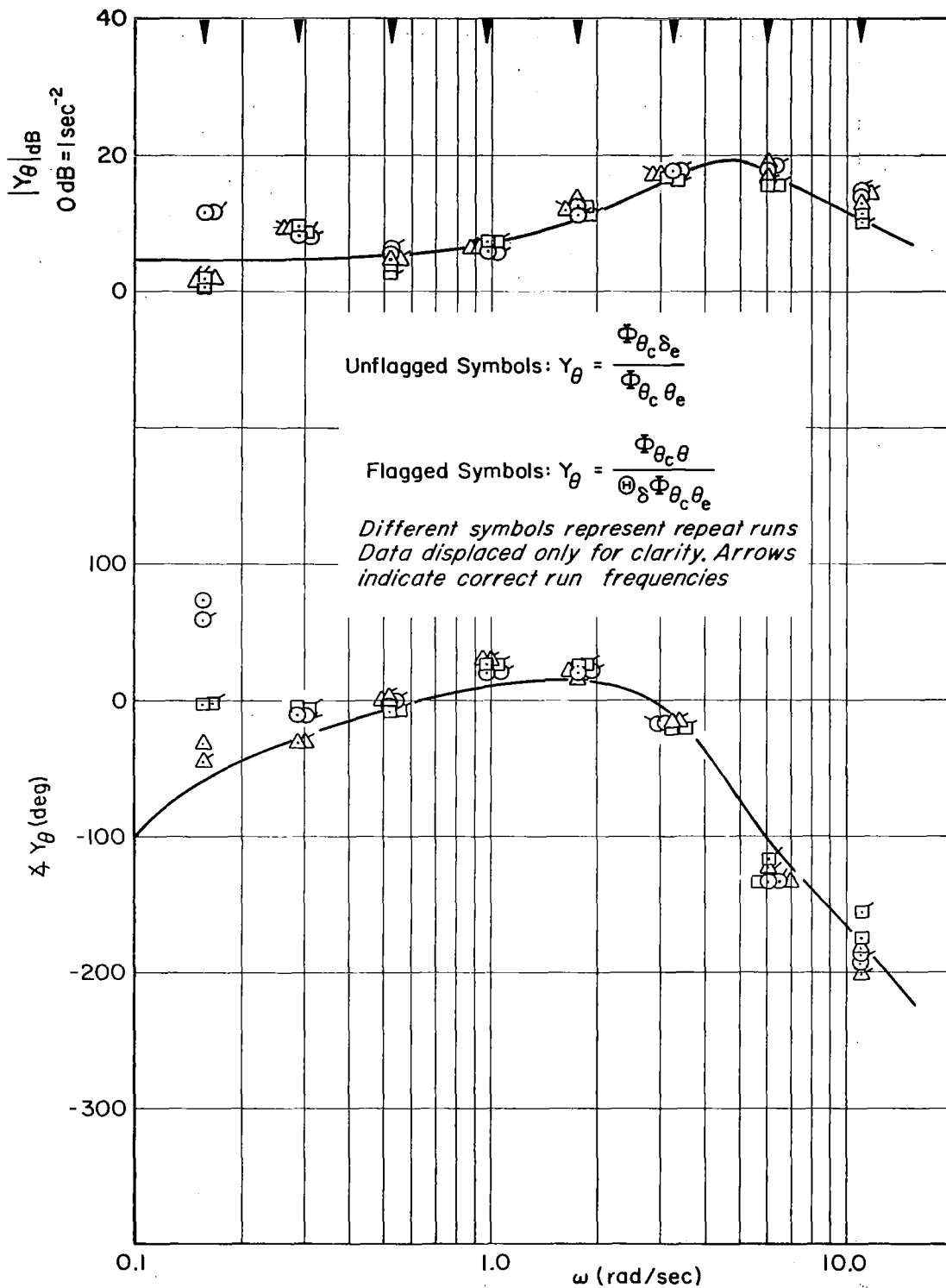
(b) Subject B

Figure 16. Concluded

Figure 17. Y_θ Measurements, Multiloop, θ_c and h_c Inputs

48

Let us now examine the outer-loop (altitude) data. The direct measurements of Y_h from the multiloop two-input task are shown in Fig. 18. For both subjects the magnitude of Y_h is quite constant over the frequency range, and the phase is nearly zero except for some lag at the highest frequencies. The differences between subjects are again quite small, with Subject A showing a slightly higher gain, roughly 2 dB. Subject A's higher gain largely offsets his lower attitude-loop gain so that the magnitudes of $Y_\theta Y_h$ for the two subjects are nearly equal.

The implicit measurement technique was also used to compute Y_h. The averaged data are shown in Fig. 19. The results are poor when compared with the direct measurements; the implicit data show a considerable scatter. The major problem is probably the sensitivit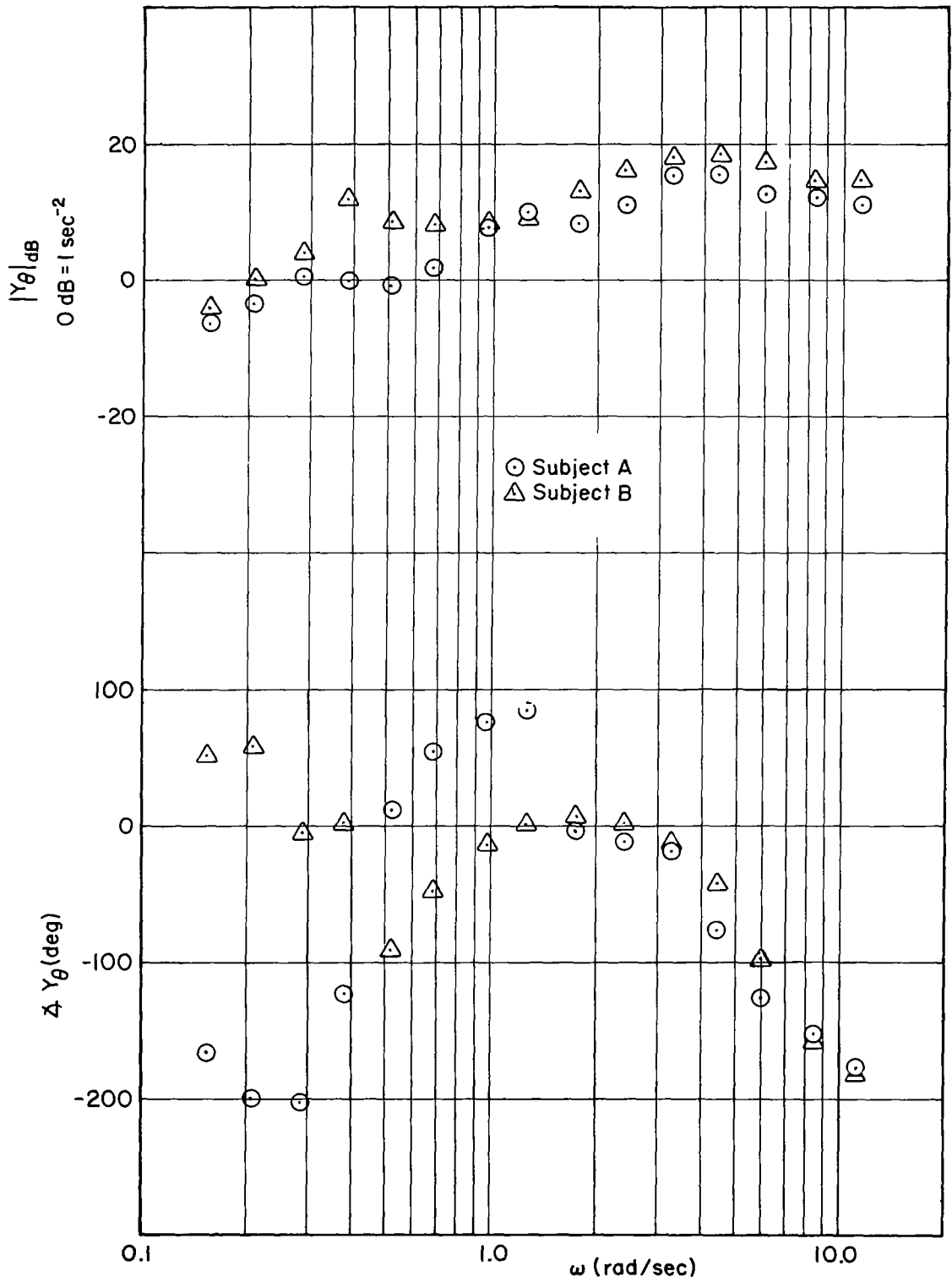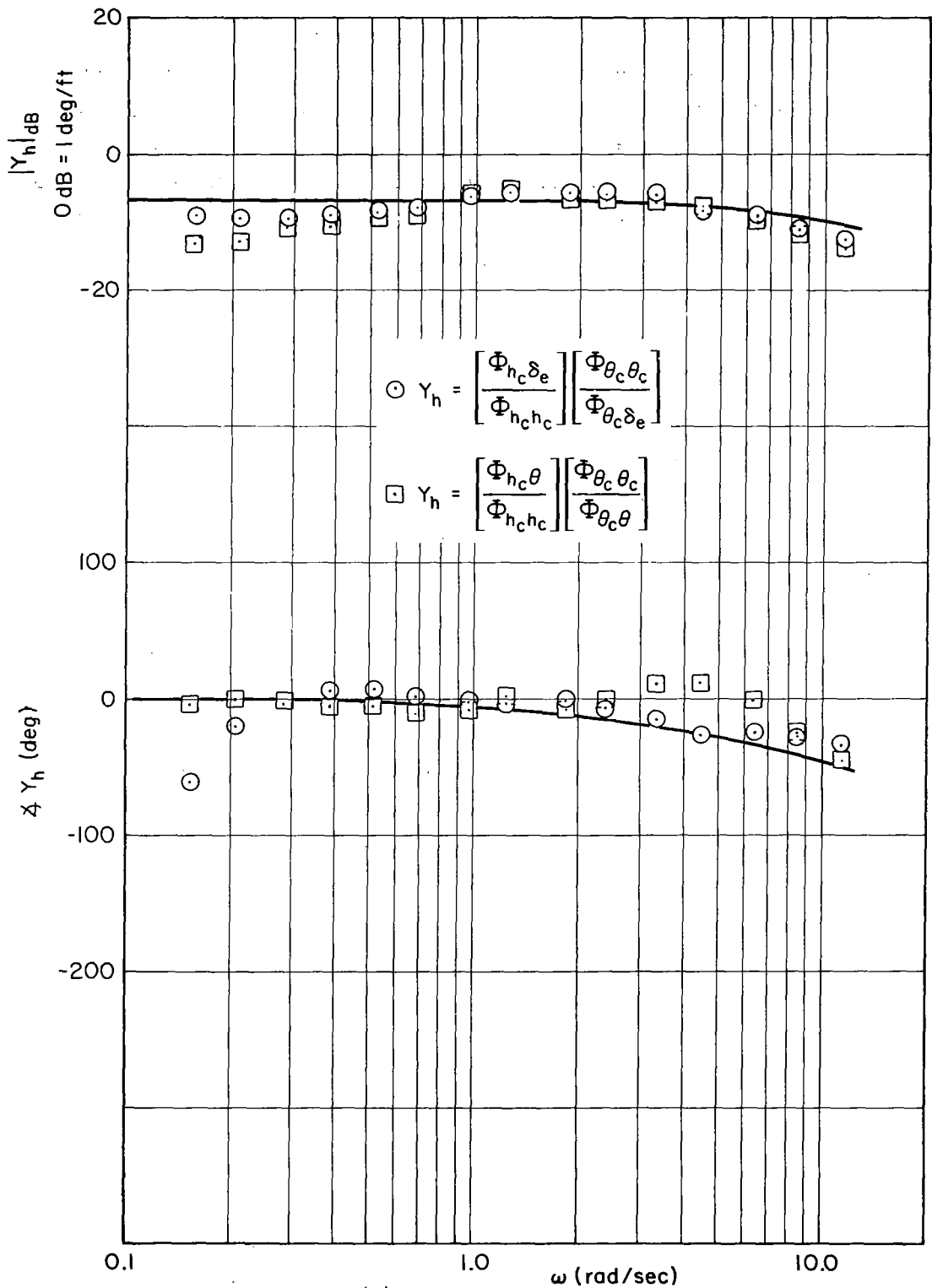y of the implicit results to the attitude-loop describing function. The results of Fig. 19 were computed assuming that Y_θ was the same in the multiloop one-input task as it was in the single-loop task. We have already shown that there is at least a gain difference between Y_θ for the single-loop and multiloop two-input tasks. There is, however, no way of determining what Y_θ was used in the multiloop one-input task. This is a basic limitation of the implicit technique and severely restricts the usefulness of the method for measuring outer-loop describing functions.

The multiloop one-input data did, however, prove useful in one way. The h_c cross-spectral ratios from the multiloop two-input task (used in the direct measurement calculations) had a great deal of scatter at a frequency of 1.28 rad/sec. This scatter made the fairing and interpolation very difficult. On the other hand, the scatter was much less for the one-input task; see Fig. 20. As the data at other frequencies matched quite closely, the one-input data were used as a guide in fairing and interpolating the two-input data.

The reason for the two-input scatter at 1.28 rad/sec is not completely understood. As the scatter is much less with only one input, the θ_c input appears to be the cause. Apparently some of the pilots' response to θ_c is spilling over to the h_c input frequency of 1.28 rad/sec. Since 1.28 rad/sec is the first component on the h_c shelf and θ_c has a large amplitude component at 0.97 rad/sec, such spillover could have significant effects. Time variations in pilot characteristics could produce such a spillover.

$$Y_h = \left[\frac{\Phi_{h_c \delta_e}}{\Phi_{h_c h_c}}\right]\left[\frac{\Phi_{\theta_c \theta_c}}{\Phi_{\theta_c \delta_e}}\right]$$

$$Y_h = \left[\frac{\Phi_{h_c \theta}}{\Phi_{h_c h_c}}\right]\left[\frac{\Phi_{\theta_c \theta_c}}{\Phi_{\theta_c \theta}}\right]$$

(a) Subject A

Figure 18. Y_h Direct Measurements
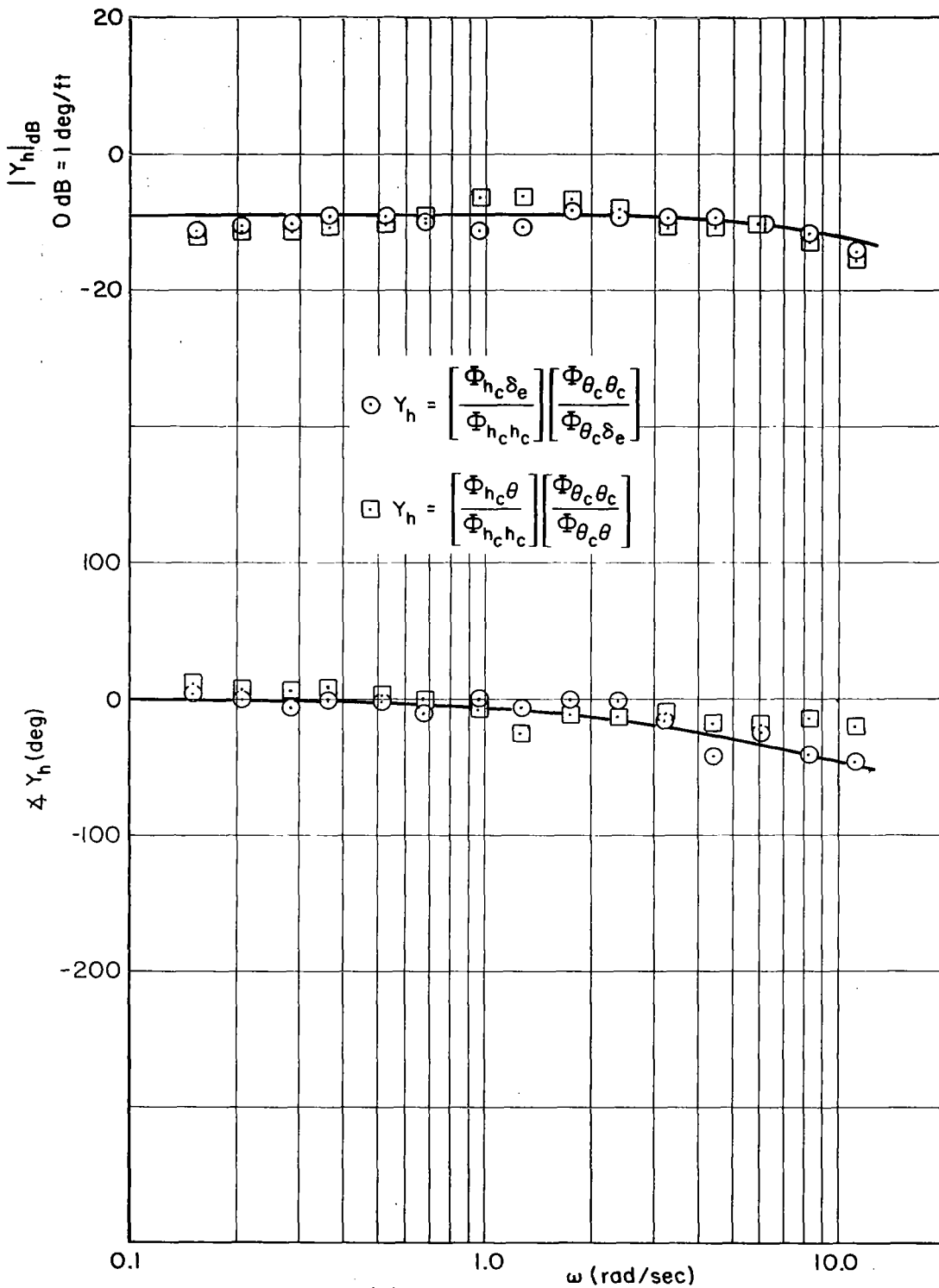
(b) Subject B

Figure 18. Concluded

51

Figure 19. Y_h Implicit Measurements

(a) Two-Input Runs

Figure 20. Typical Scatter in h_c Cross-Spectral Ratios

53
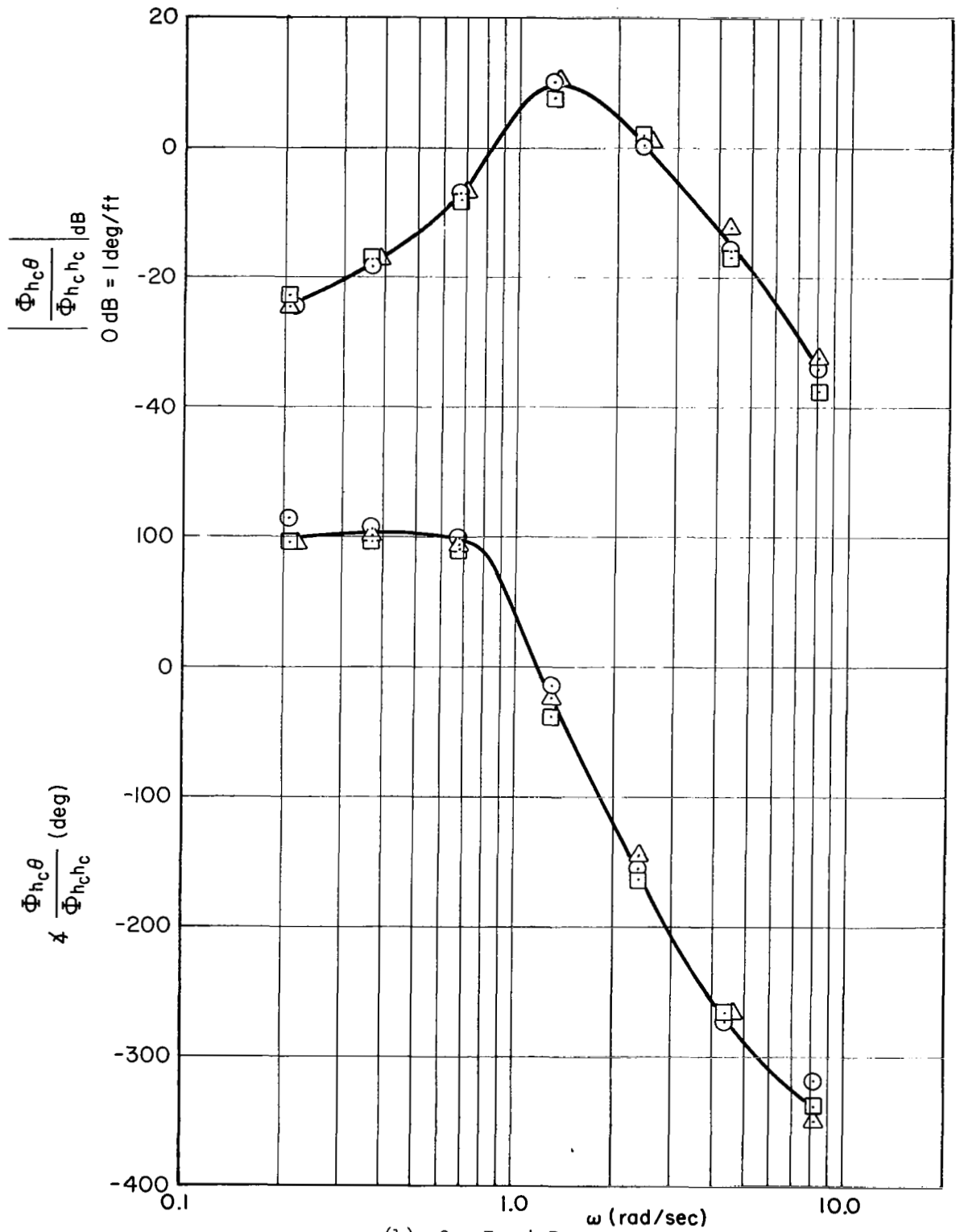
(b) One-Input Runs

Figure 20. Concluded

54

The remainder of this subsection discusses the analytical fits of the describing-function data and ramifications of the data on the multiloop pilot model. The analytical fit for the Y_θ data was of the form
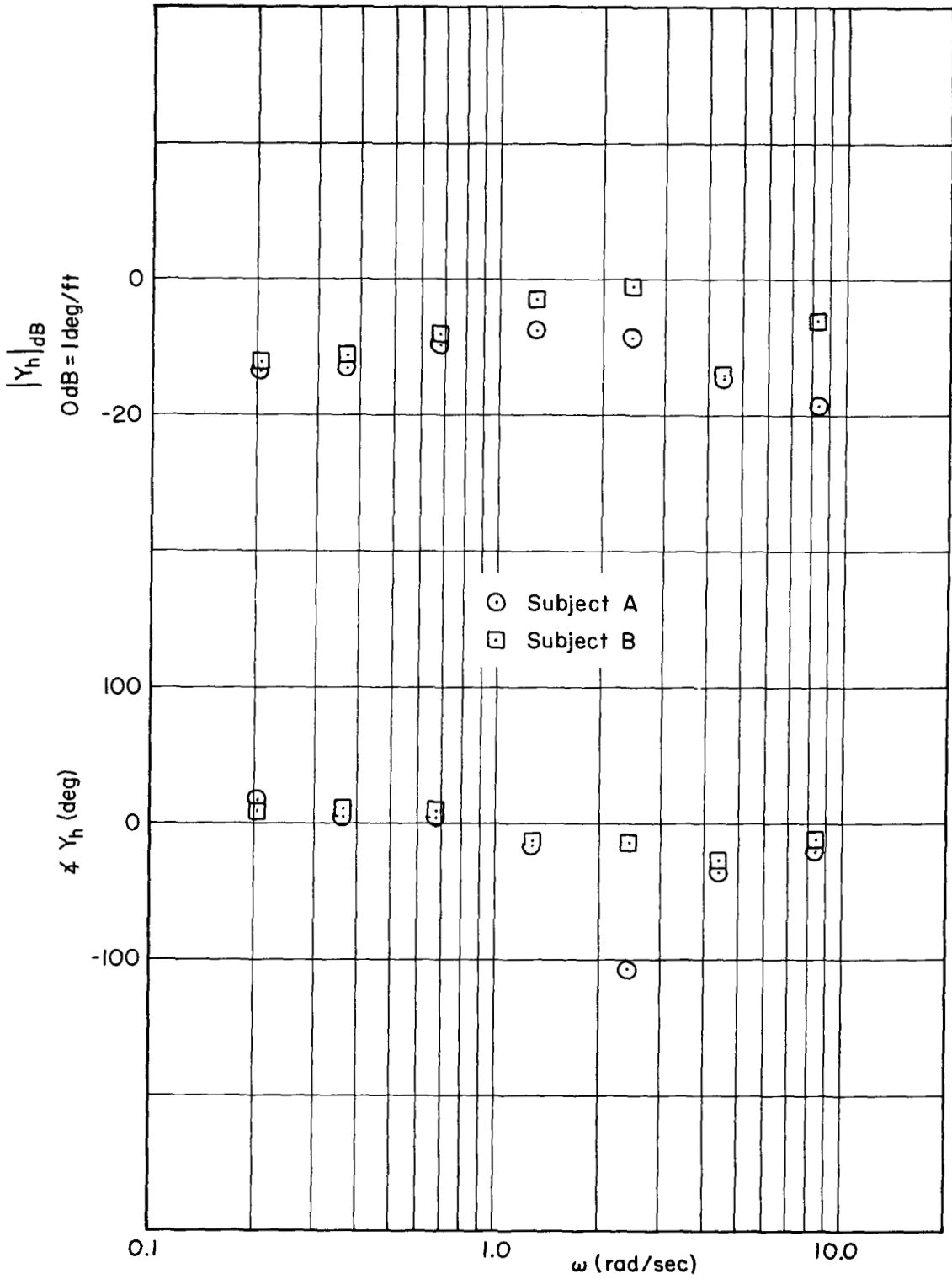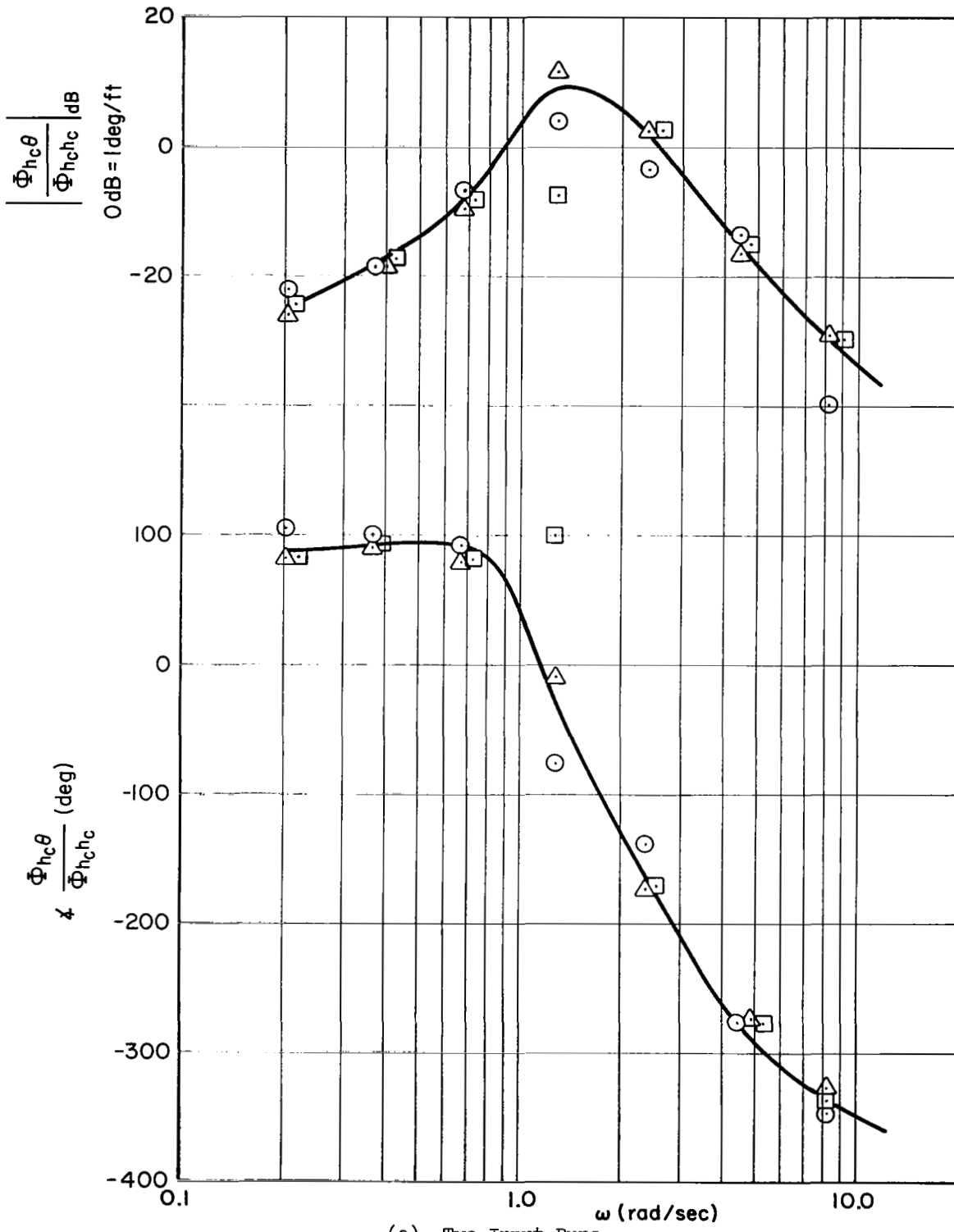
$$Y_\theta = \frac{K_\theta \left(j\omega T_L + 1 \right) e^{-j\left(\frac{\alpha}{\omega} + \omega\tau\right)}}{\left(\frac{j\omega}{\omega_N}\right)^2 + \frac{2\zeta_N}{\omega_N} j\omega + 1} \qquad (12)$$

Numerical values selected for the parameters were

$$K_\theta = \begin{cases} 2.1 \text{ sec}^{-2} \text{ for Subject A, single-loop task} \\ 1.5 \text{ sec}^{-2} \text{ for Subject A, multiloop task} \\ 1.7 \text{ sec}^{-2} \text{ for Subject B, single-loop task} \\ 2.1 \text{ sec}^{-2} \text{ for Subject B, multiloop task} \end{cases}$$

T_L = 0.89 sec

ζ_N = 0.40

ω_N = 4.7 rad/sec

α = 0.18 sec^{-1}

τ = 0.17 sec

These fits for the single-loop task are plotted in Fig. 16.

One unusual feature of this model is the presence of a relatively low-frequency pair of complex poles. Previous single-loop experiments (e.g., Ref. 1) have also indicated complex poles, but at considerably higher frequency. The lower frequency is attributed to manipulator differences. The experiments of Ref. 1 used a low-inertia side stick, whereas the experiments reported here used a conventional center stick with appreciable inertia. These complex poles are the reason the human pilots' response had considerably less high-frequency content than did the analog pilot.

The analytical curve fit used for Y_h was of the form

$$Y_h = \frac{K_h}{j\omega T_h + 1} \qquad (13)$$

55

and the numerical values used were

$$K_h = \begin{cases} 0.45 \text{ deg/ft for Subject A} \\ 0.36 \text{ deg/ft for Subject B} \end{cases}$$

$$T_h = 0.1 \text{ sec}$$

These fits are plotted in Fig. 18.

The closure criteria used by the pilots were studied by closing the attitude and altitude loops with the models of Eqs. 12[*] and 13. Bode and root locus plots of these closures are shown in Fig. 21. The key closure parameters are summarized in Table V. The closure criteria shown in Table V must not be interpreted as the precise values achieved by the pilots because the closures were made with approximate models of the pilots' characteristics. Table V should be considered only as indicative of the actual closure characteristics.

TABLE V

LOOP CLOSURE PARAMETERS FROM ANALYTICAL MODELS

SUBJECT	LOOP	CROSSOVER FREQUENCY (RAD/SEC)	PHASE MARGIN (DEG)	GAIN MARGIN (DB)
A	Attitude	1.95	22	4
B		2.7	8	1
A	Altitude	1.08	4	1
B		0.85	22	4.5

---

[*]In closing the loops the α term in Y_θ was dropped.

□ Closed Loop Poles, Subject A
△ Closed Loop Poles, Subject B

© Systems Technology, Inc.
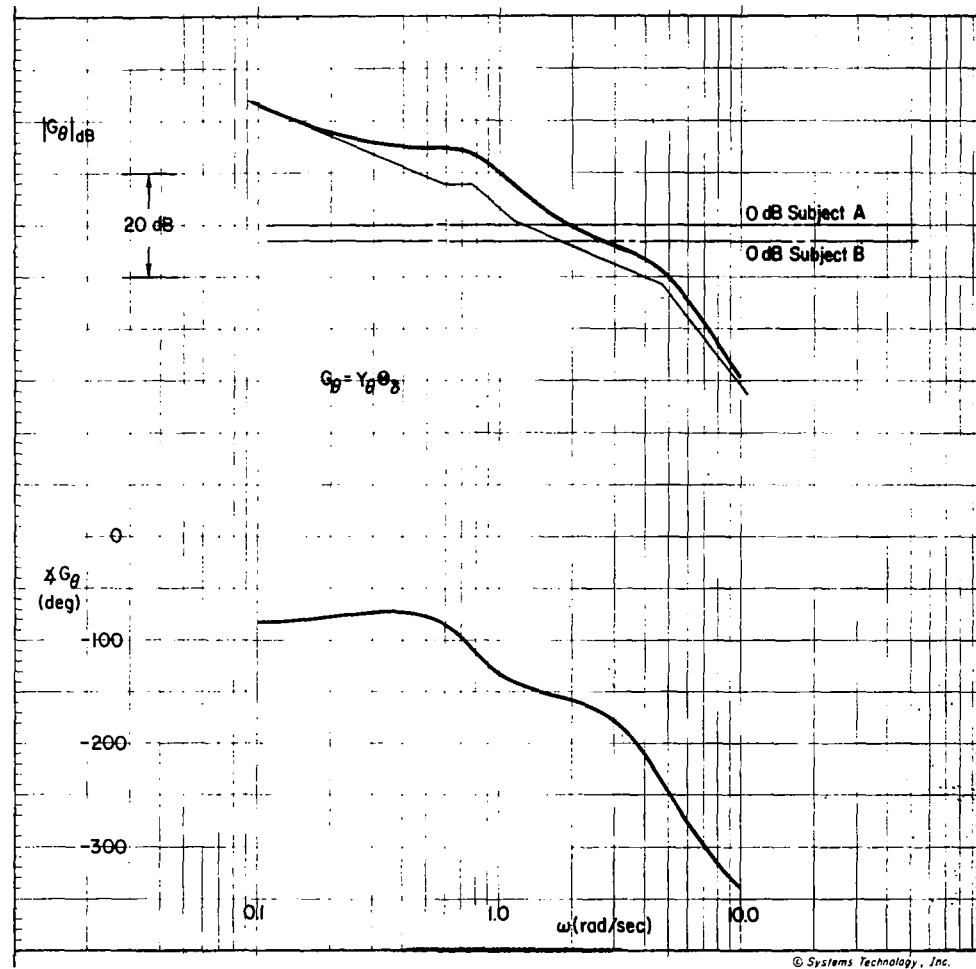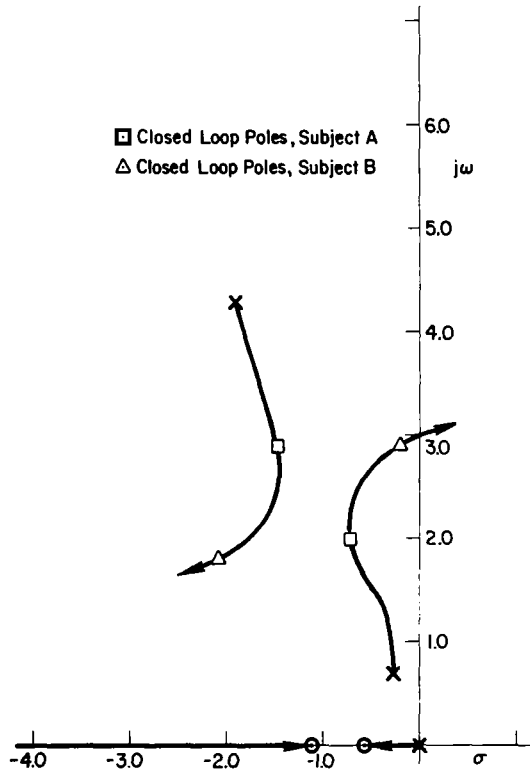
(a) Attitude Loop

Figure 21. Loop Closures with Analytical Models

58

$$G_h = \frac{Y_h Y_\theta H_\delta}{1 + Y_\theta \Theta_\delta}$$

$|G_h|_{dB}$

$\angle G_h$ (deg)

ω(rad/sec)

© Systems Technology, Inc.
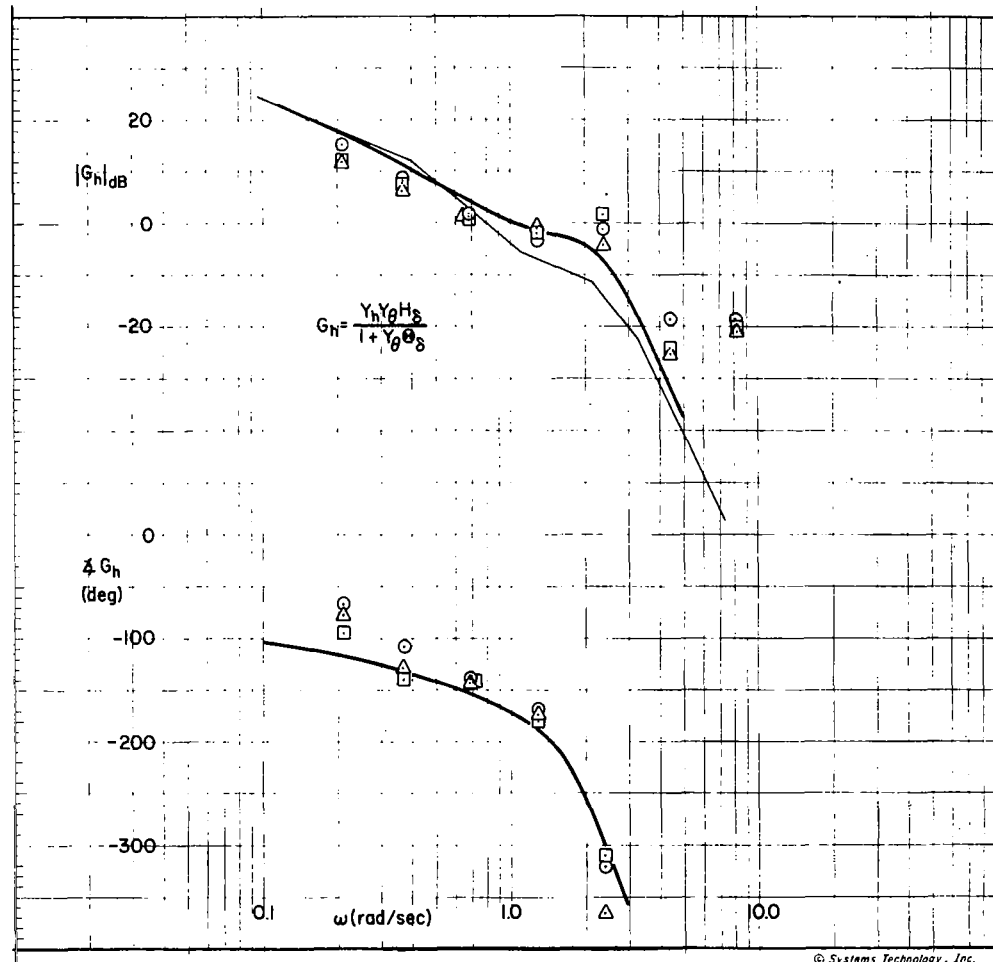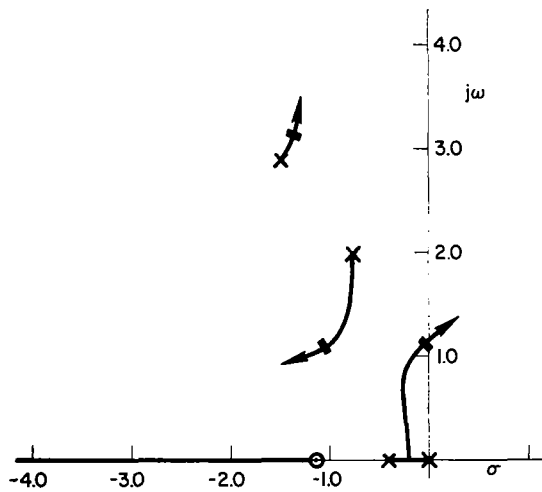
(b)   Altitude Loop, Subject A

Figure 21.   Continued

UNIFIED
SERVO
ANALYSIS
METHOD

$$G_h = \frac{Y_h Y_\theta H_\delta}{1 + Y_\theta \Theta_\delta}$$

© Systems Technology, Inc.
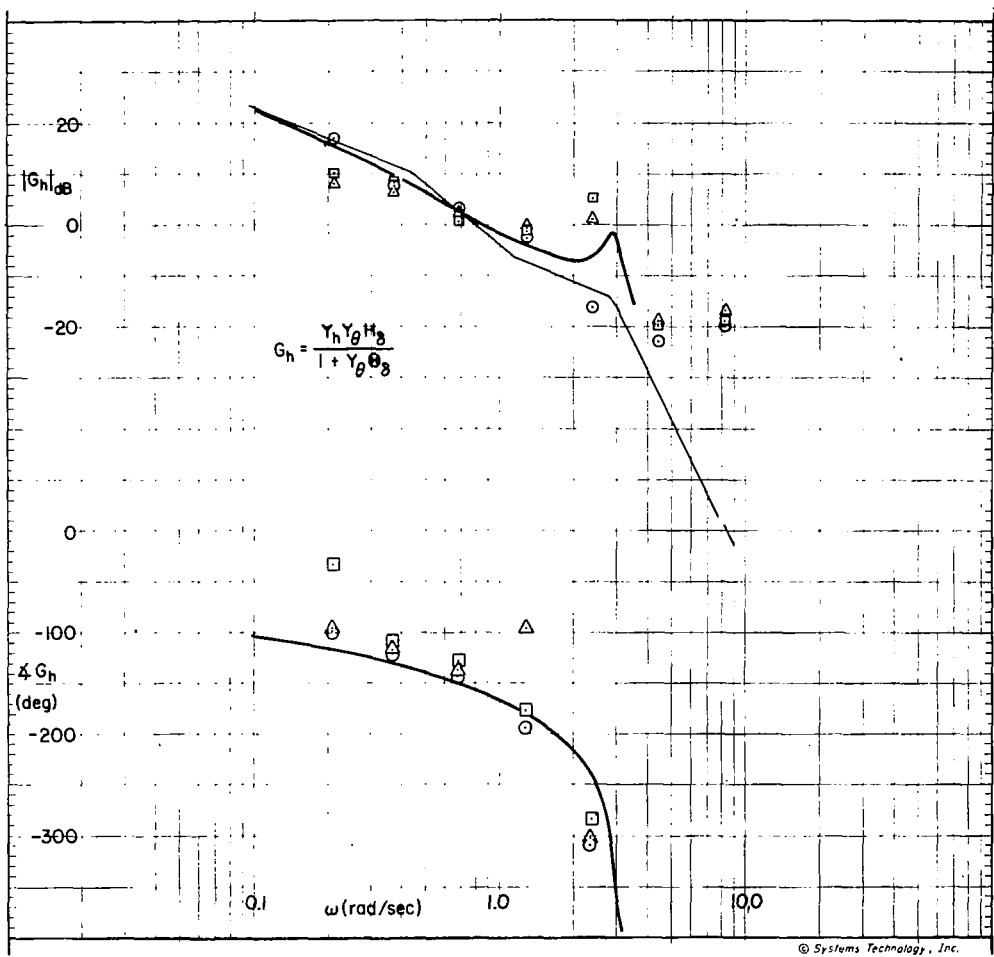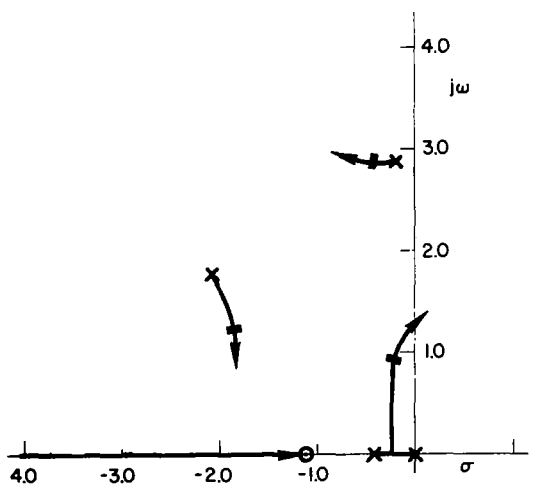
(c) Altitude Loop, Subject B

Figure 21. Concluded

As a cross check on the above, the altitude-loop closure was computed from the ratio $\Phi_{h_c h_e} / \Phi_{h_c h_c}$, which can be written as

$$\frac{\Phi_{h_c h_e}}{\Phi_{h_c h_c}} = \frac{1}{1 + G_h} \tag{14}$$

where

$$G_h = \frac{Y_\theta Y_h H_\delta}{1 + Y_\theta \Theta_\delta} \tag{15}$$

Solving for G_h, we get

$$G_h = \left(\frac{\Phi_{h_c h_e}}{\Phi_{h_c h_c}}\right)^{-1} - 1 \tag{16}$$

The results of these calculations for the individual multiloop, two-input runs are shown in Figs. 21b and 21c. Unfortunately, the results are inaccurate at the very low and very high frequencies. At low frequencies, $\Phi_{h_c h_e} / \Phi_{h_c h_c}$ is inaccurate because the signal level of h_e is too low. At high frequencies, $\Phi_{h_c h_e} / \Phi_{h_c h_c}$ is nearly equal to unity so that the computed G_h is extremely sensitive to small errors in $\Phi_{h_c h_e} / \Phi_{h_c h_c}$. However, in the region of crossover the results should be fairly accurate.

These data suggest some revisions in our estimated closure parameters. In particular, it appears that the crossover frequencies and phase margins for the two subjects are nearly equal, roughly 0.9 rad/sec and 25 deg. These crossover frequency estimates are identical to those obtained from the Crossover Model Parameter Tracker (Table III).

Let us now consider the implications of these results with regard to the multiloop pilot model, Ref. 3. As the two major findings, listed below, are in complete accord with pre-experimental expectations, we believe the results are applicable to a wide variety of similar tasks.

1. Pilot closure of an attitude inner loop is very similar to that used in a single-loop task.

2. When the pilot is controlling both attitude and position through a single manipulator, the series closure model is more appropriate than the parallel one.

60

While it is physically impossible to prove whether the pilots' internal organizations correspond to the series or parallel model, the data presented here are more simply described by the series model. With a parallel model one would have identical lead equalization in both feedbacks. Furthermore, the series model is more in accord with pilots' comments on how they fly an airplane.

The only real surprise in the describing function data was the rather low-frequency pair of complex poles in the attitude loop. As noted earlier, the low frequency is attributed to the relatively high inertia of the manipulator used. Since these poles could significantly restrict the pilot's ability to close a tight attitude loop, additional research on the effects of manipulator characteristics is needed. Some preliminary work in this field was reported in Refs. 6 and 7.

E. REMNANT DATA

Although the primary emphasis in these experiments was on the describing-function measurements, some analysis of pilot remnant was made. The quantities which were examined are relative correlated output (referred to as ρ_a^2 in Ref. 1), the power spectra of the pilots' outputs, and the amplitude distributions of the pilots' outputs. Each of these quantities is described below.

The relative correlated output is the fraction of the pilot's output power which is correlated with the input. In other words, ρ_a^2 is that portion of the output power which exists at input frequencies divided by the total output power. It was computed by summing the squares of the Fourier coefficients of δ_e at input frequencies and dividing by twice the mean square value of δ_e. The results, averaged over repeat runs, are shown in Table VI. There are no consistent effects due to variations in either the task or the subject.

The power spectra of the pilot's output, δ_e, were also digitally computed. The autocorrelations were computed for a maximum of 419 lags (0.05 sec each). The autocorrelations were multiplied by a Hanning lag window and then Fourier transformed. This gave power spectra values every 0.15 rad/sec from zero to 62.8 rad/sec (10 Hz). These data were

61

TABLE VI

RELATIVE CORRELATED OUTPUT (ρ_a^2)

TASK	SUBJECT	
	A	B
Multiloop, θ_c and h_c inputs	0.42	0.28
Multiloop, h_c input	0.35	0.36
Single-loop, θ_c input	0.30	0.36

carefully examined for any spikes which could have been caused by pilot nonlinearities or sampling. None were found. The frequency variations were smooth and the data were quite repeatable. This is in accord with the Ref. 1 conclusion that the major source of remnant is nonstationary pilot behavior.

A complete presentation of the power spectral results is both impractical and unnecessary. However, the results are summarized in Fig. 22. The data points shown in this figure are eyeball averages taken over the three repeat runs and several adjacent frequencies. Peaks at the input frequencies are not shown. Data for frequencies less than 1 rad/sec are not shown because the effective filter bandwidth was not narrow enough to get between the input frequencies. The estimated noise level is based on identical calculations for the analog pilot runs, for which the output should be zero except at input frequencies.

The shape of the spectra are similar to those given in Ref. 1 and have an amplitude attenuation of roughly 30 to 40 dB/decade. As with the ρ_a^2 data, there are no consistent variations due to either the task or the subject.

The amplitude distributions of the pilot's output were computed for all the recorded runs. The distributions for the multiloop runs generally

appeared to have a Gaussian form although in some cases the distributions were much flatter than Gaussian. As the amplitude distributions of the inputs also differed appreciably from Gaussian because of the limited number of components,[*] the observed output distributions are not too surprising.

The amplitude distributions for the single-loop runs (θ_c input) were considerably different and exhibited a bimodal tendency which was especially pronounced for Subject B. Sample output distributions of both subjects are shown in Fig. 23, and portions of the time histories of these same two runs were given in Figs. 5f and 5g. Differences in piloting technique are clearly shown in both the time histories and amplitude distributions. Subject B's output was consistently more like a square wave than Subject A's. Bimodal-like output distributions have frequently been observed for controlled elements which required significant pilot leads, e.g., Ref. 1.

---

[*]The amplitude distribution of θ_c is governed primarily by the four lowest frequency components and that of h_c by the three lowest frequency components. In either input the shelf (components with one-tenth the amplitude) has little effect on the distribution.
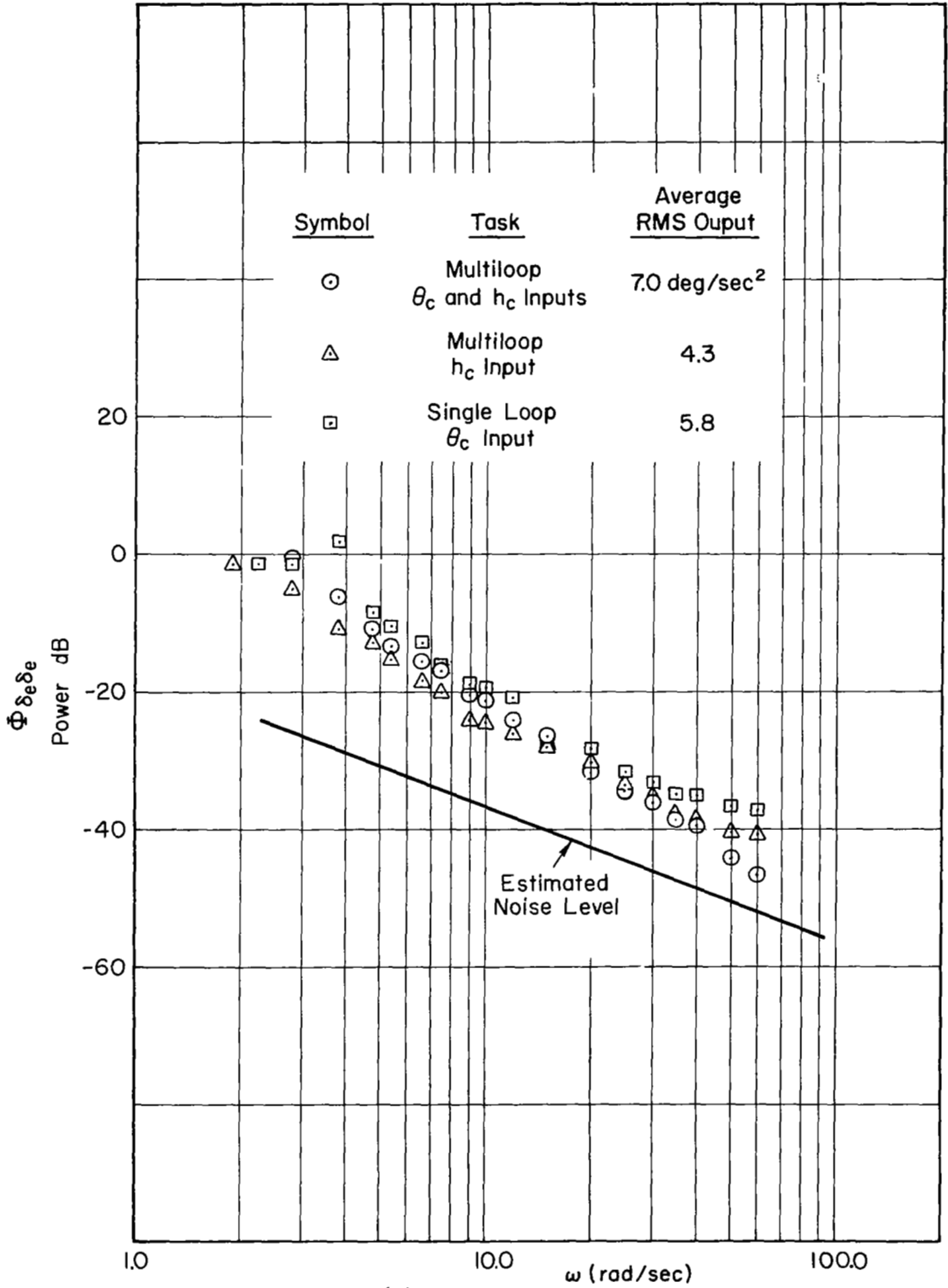
(a)   Subject A

Figure 22.   Output Power Spectrum
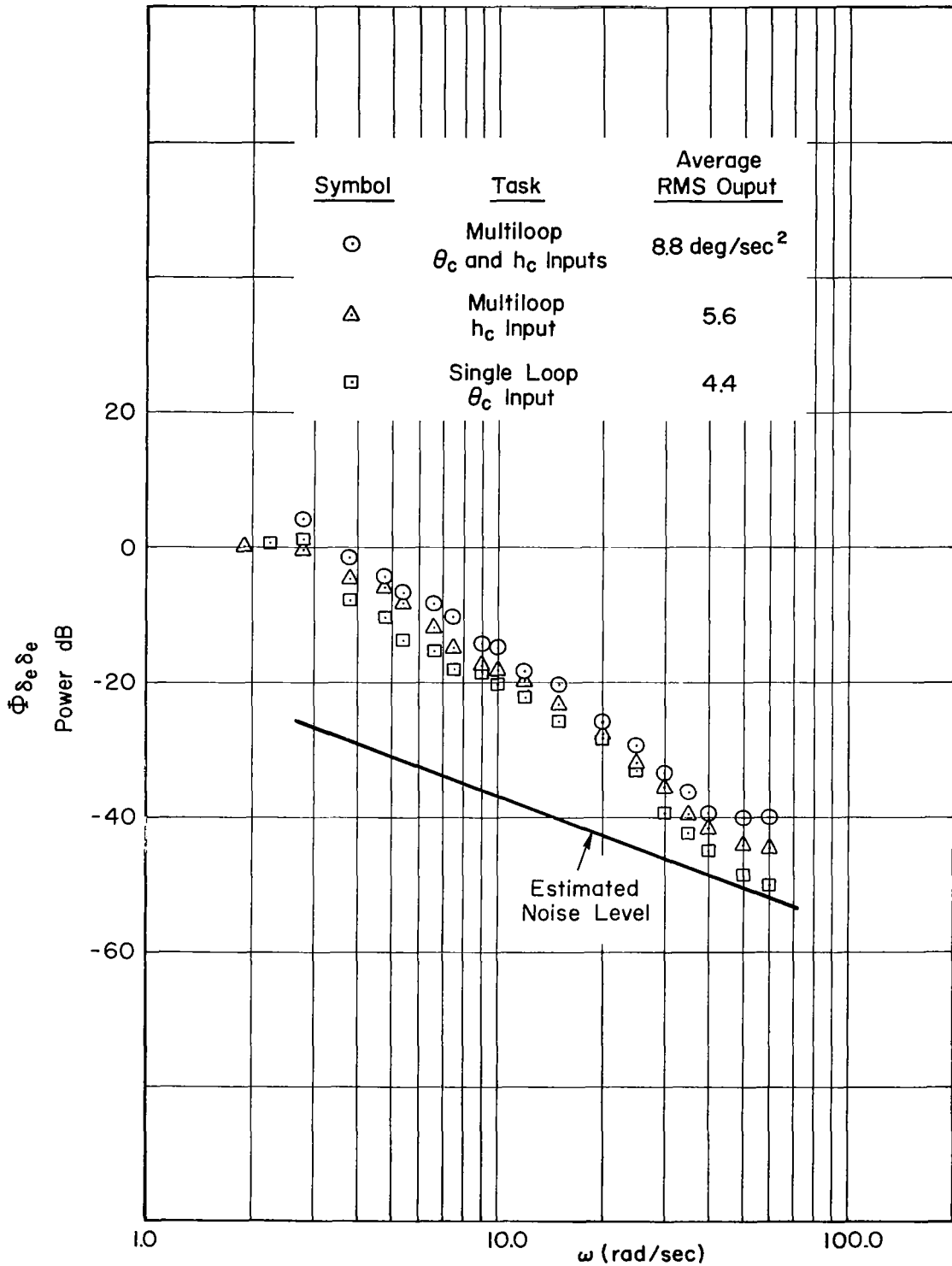
(b) Subject B

Figure 22. Concluded
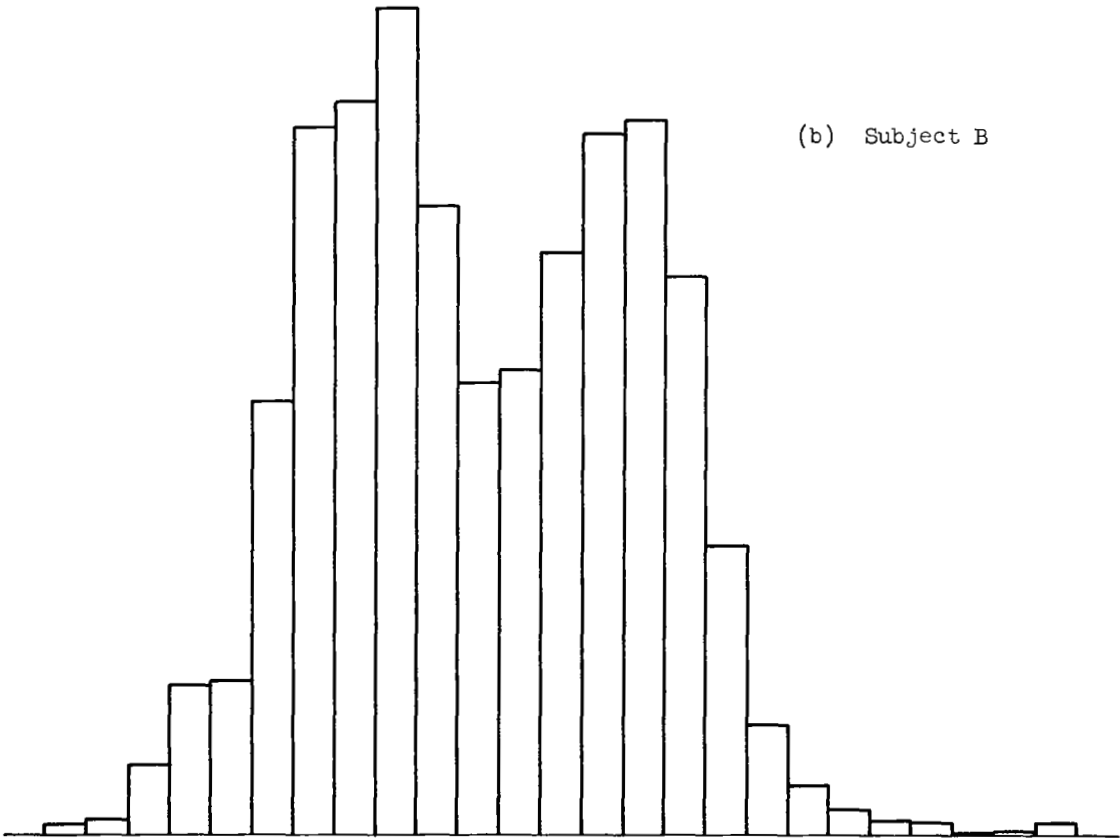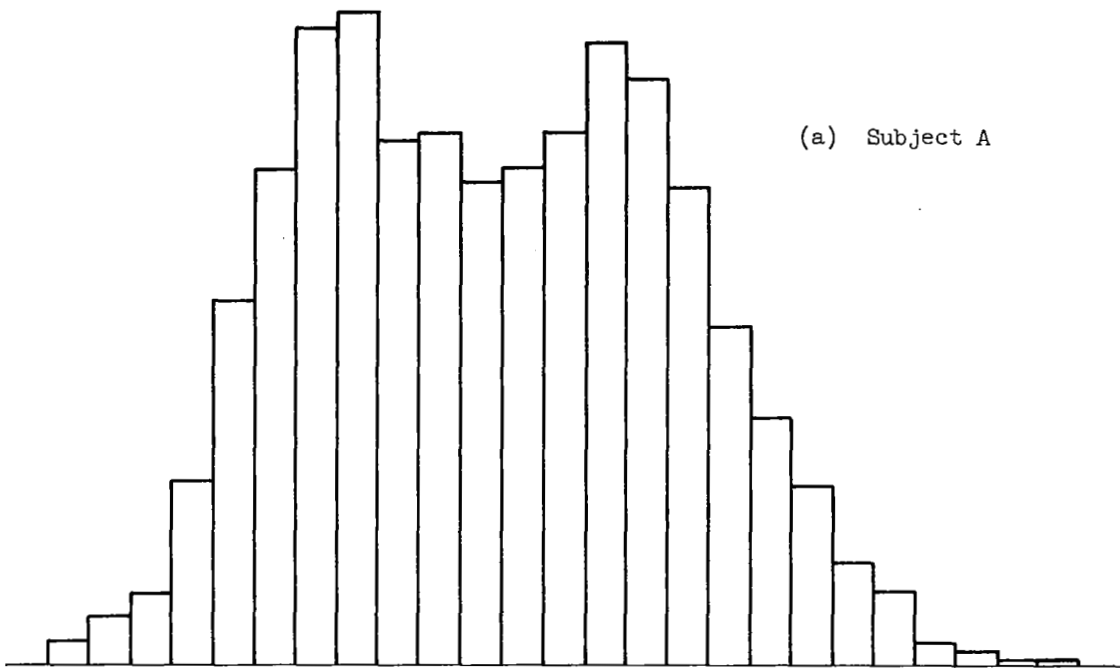
Figure 23. Amplitude Distribution of Pilot's Output,
Single-Loop Task, θ_c Input

66

SECTION VI

CONCLUSIONS

The results of a brief set of multiloop manual tracking experiments have been discussed. The two major objectives of this work were to substantiate the analytical predictions regarding the feasibility of measuring multiloop describing functions, and to provide a spot check of the multiloop pilot model. The key conclusions reached relative to both these objectives are summarized below.

A. MULTILOOP DESCRIBING FUNCTION MEASUREMENT TECHNIQUES

1. Measurement of multiloop describing functions is feasible although the techniques are considerably more complex than those required for single-loop compensatory tasks. However, there are certain fundamental limitations which restrict the accuracy of some of the multiloop results; see items 2-4, below.

2. The direct measurement technique can provide good results for the outer-loop describing function, but for the inner-loop describing function the method is limited to frequencies in the region of the inner-loop crossover and above.

3. Good low-frequency data for the inner-loop describing function can only be obtained via the implicit technique, i.e., from single-loop (inner-loop alone) tests. Comparison of the high-frequency direct and implicit results can be used to determine minor differences between attitude loop alone and as an inner loop.

4. The implicit measurement technique for the outer-loop describing function is inadequate. However, the data from multiloop, single-input tests can be quite useful in the fairing and interpolation of the multiple-input data.

5. In either the direct or implicit technique, it is advisable to use different expressions for the describing functions involving other cross-spectral ratios in the various frequency regions. The use of different parameters at different frequencies takes advantage of the signal conditioning inherent in the controlled element to maintain good signal/noise ratios. It can also reduce interpolation errors.

67

B. MULTILOOP PILOT MODEL

1. The results for the one test configuration support the existing multiloop model. The measured describing functions agree quite well with the pre-experimental predictions.

2. The attitude inner loops were closed very similar to the closures for the attitude-alone task. Consequently, single-loop attitude-tracking results should be directly applicable to inner-loop closures.

3. The series closure model is the more appropriate one for multiloop feedbacks through one controller. A series model to match the data is simpler than a parallel one and is more consistent with pilot comments on how they fly an airplane.

4. The relatively low-frequency pair of complex poles in the altitude describing function was probably due to the relatively high inertia of the manipulator used. Since these poles can significantly affect achievable crossover frequencies and performance, additional research on the effects of manipulator characteristics is highly desirable.

REFERENCES

1. McRuer, Duane T., Dunstan Graham, and Ezra S. Krendel, "Manual Control of Single-Loop Systems: Parts I and II," J. Franklin Institute, Vol. 238, No. 1, Jan. 1967, pp. 1-29; No. 2, Feb. 1967, pp. 145-168.

2. Stapleford, R. L., D. T. McRuer, and R. Magdaleno, Pilot Describing Function Measurements in a Multiloop Task, NASA CR-542, Aug. 1966.

3. McRuer, D. T., and H. R. Jex, "A Review of Quasi-Linear Pilot Models," IEEE Trans., Vol. HFE-8, No. 3, Sept. 1967 (forthcoming).

4. Stapleford, Robert L., and Irving L. Ashkenas, "Effects of Manual Altitude Control and Other Factors on Short-Period Handling Quality Requirements," J. Aircraft, Vol. 5, # 1, Jan.-Feb. 1968.

5. Bullard, E. C., F. E. Oglebay, W. H. Munk, and G. R. Miller, A User's Guide to BOMM, A System of Programs for the Analysis of Time Series, Univ. of Calif.-La Jolla, Apr. 1964.

6. Magdaleno, R. E., and D. T. McRuer, Effects of Manipulator Restraints on Human Operator Performance, AFFDL-TR-66-72, Dec. 1966.

7. McRuer, D. T., and R. E. Magdaleno, Human Pilot Dynamics with Various Manipulators, AFFDL-TR-66-138, Dec. 1966.

8. Pritchard, F. E., C. C. Easterbrook, and G. E. McVehil, Spectral and Exceedance Probability Models of Atmospheric Turbulence for Use in Aircraft Design and Operation, AFFDL-TR-65-122, Nov. 1965.

APPENDIX A

EQUATIONS OF MOTION AND TRANSFER FUNCTIONS

Linearized perturbation equations of motion were used in the experimental simulation. These equations were further simplified by the following assumptions:

1. Constant airspeed (short-period approximation).
2. Operating point conditions are straight and level flight.
3. Stability derivatives $M_{\dot{w}}$ and Z_{δ_e} are negligible.
4. Gust disturbances act only through static derivatives, i.e., gust-gradient effects are negligible.

Under these conditions the equations of motion in stability axes are simply

$$\begin{bmatrix} s - Z_w & -U_o s \\ -M_w & s(s - M_q) \end{bmatrix} \begin{Bmatrix} w \\ \theta \end{Bmatrix} = \begin{bmatrix} 0 & -Z_w \\ M_{\delta_e} & -M_w \end{bmatrix} \begin{Bmatrix} \delta_e \\ w_g \end{Bmatrix} \qquad (A-1)$$

and the kinematic expression for altitude is

$$\dot{h} = U_o \theta - w \qquad (A-2)$$

or

$$h = \frac{1}{s}(U_o \theta - w) \qquad (A-3)$$

The numerical values which were used for the parameters of Eq. A-1 are:

$$U_o = 223 \text{ ft/sec} \qquad\qquad Z_w = -0.585 \text{ sec}^{-1}$$

$$M_w = -0.0026 \text{ (ft-sec)}^{-1} \qquad M_q = -0.0071 \text{ sec}^{-1}$$

$$M_{\delta_e} = 1^*$$

The resulting transfer function elements are shown in both literal and numerical form in Table A-1.

---

[*]The value of M_{δ_e} is completely arbitrary as the subjects were allowed to adjust the control sensitivity to provide whatever angular acceleration per stick deflection they preferred. M_{δ_e} is defined as unity only to simplify bookkeeping; as a result, elevator deflection, δ_e, has the dimensions of angular acceleration.

TABLE A-1

TRANSFER FUNCTION ELEMENTS

ELEMENT	SYMBOL	LITERAL FORM	NUMERICAL FORM
Characteristic Denominator	Δ	$s\left[s^2 - (Z_w + M_q)s + Z_w M_q - U_o M_w\right]$	$s\left[s^2 + 0.592s + 0.584\right]$ or $s\left[s^2 + 2(0.387)(0.764)s + (0.764)^2\right]$
Elevator Numerators Attitude Altitude	$N^{\theta}_{\delta_e}$ $N^{h}_{\delta_e}$	$M_{\delta_e}(s - Z_w)$ $\dfrac{-U_o Z_w M_{\delta_e}}{s}$	$(s + 0.585)$ $\dfrac{130.5}{s}$
Gust Numerators Attitude Altitude	$N^{\theta}_{w_g}$ $N^{h}_{w_g}$	$-M_w s$ $Z_w(s - M_q)$	$(0.0026)s$ $-0.585(s + 0.0071)$
Coupling Numerator	$N^{\theta\ h}_{\delta_e w_g}$ or $-N^{h\ \theta}_{\delta_e w_g}$	$\dfrac{Z_w M_{\delta_e}}{s}$	$\dfrac{-0.585}{s}$

APPENDIX B

DERIVATION OF DIRECT MEASUREMENT EQUATIONS

1. θ_c and h_c Inputs

For the series closures (Fig. 1) the pilot's stick deflection is given by

$$\begin{aligned} \delta_e &= Y_\theta \theta_e + Y_h Y_\theta h_e + n \\ &= Y_\theta(\theta_c - \theta) + Y_h Y_\theta(h_c - h) + n \end{aligned} \tag{B-1}$$

where n is the pilot's remnant. Forming the cross-spectra between stick deflection and each of the two inputs gives

$$\Phi_{\theta_c \delta_e} = Y_\theta \Phi_{\theta_c \theta_e} - Y_h Y_\theta \Phi_{\theta_c h} \tag{B-2}$$

and

$$\Phi_{h_c \delta_e} = -Y_\theta \Phi_{h_c \theta} + Y_h Y_\theta \Phi_{h_c h_e} \tag{B-3}$$

Solving the two simultaneous equations, we get

$$Y_\theta = \frac{\Phi_{\theta_c \delta_e} \Phi_{h_c h_e} + \Phi_{\theta_c h} \Phi_{h_c \delta_e}}{\Phi_{\theta_c \theta_e} \Phi_{h_c h_e} - \Phi_{\theta_c h} \Phi_{h_c \theta}} \tag{B-4}$$

$$Y_h = \frac{\Phi_{\theta_c \theta_e} \Phi_{h_c \delta_e} + \Phi_{\theta_c \delta_e} \Phi_{h_c \theta}}{\Phi_{\theta_c \delta_e} \Phi_{h_c h_e} + \Phi_{\theta_c h} \Phi_{h_c \delta_e}} \tag{B-5}$$

Equations B-4 and B-5 can be simplified by using the identities:

$$\Phi_{\theta_c \theta_e} = \Phi_{\theta_c \theta_c} - \Phi_{\theta_c \theta} \tag{B-6}$$

$$\Phi_{\theta_c \theta} = \Theta_\delta \Phi_{\theta_c \delta_e} \tag{B-7}$$

$$\Phi_{\theta_c h} = H_\delta \Phi_{\theta_c \delta_e} \qquad (B\text{-}8)$$

$$\Phi_{h_c h_e} = \Phi_{h_c h_c} - \Phi_{h_c h} \qquad (B\text{-}9)$$

$$\Phi_{h_c \theta} = \Theta_\delta \Phi_{h_c \delta_e} \qquad (B\text{-}10)$$

$$\Phi_{h_c h} = H_\delta \Phi_{h_c \delta_e} \qquad (B\text{-}11)$$

The resulting expressions can be written as

$$Y_\theta = \frac{N_1}{D_1} \qquad (B\text{-}12)$$

where

$$N_1 = \frac{\Phi_{\theta_c \delta_e}}{\Phi_{\theta_c \theta_c}}$$

$$= \frac{\Phi_{\theta_c \theta}}{\Theta_\delta \Phi_{\theta_c \theta_c}} \qquad (B\text{-}13)$$

$$= \frac{\Phi_{\theta_c h}}{H_\delta \Phi_{\theta_c \theta_c}}$$

$$D_1 = \frac{\Phi_{\theta_c \theta_e}}{\Phi_{\theta_c \theta_c}} - \frac{\Phi_{h_c h}}{\Phi_{h_c h_c}}$$

$$= \frac{\Phi_{h_c h_e}}{\Phi_{h_c h_c}} - \frac{\Phi_{\theta_c \theta}}{\Phi_{\theta_c \theta_c}} \qquad (B\text{-}14)$$

and

$$Y_h = \frac{\Phi_{h_c \delta_e} / \Phi_{h_c h_c}}{\Phi_{\theta_c \delta_e} / \Phi_{\theta_c \theta_c}}$$

$$= \frac{\Phi_{h_c \theta} / \Phi_{h_c h_c}}{\Phi_{\theta_c \theta} / \Phi_{\theta_c \theta_c}} \qquad (B\text{-}15)$$

$$= \frac{\Phi_{h_c h} / \Phi_{h_c h_c}}{\Phi_{\theta_c h} / \Phi_{\theta_c \theta_c}}$$

2. h_c and w_g Inputs

The simultaneous equations for this input combination are Eq. B-3 plus

$$\Phi_{w_g\delta_e} = -Y_\theta\Phi_{w_g\theta} - Y_hY_\theta\Phi_{w_gh} \qquad (B-16)$$

The resulting expressions for Y_θ and Y_h are

$$Y_\theta = \frac{-(\Phi_{w_gh}\Phi_{h_c\delta_e} + \Phi_{w_g\delta_e}\Phi_{h_ch_e})}{\Phi_{w_gh}\Phi_{h_c\theta} + \Phi_{w_g\theta}\Phi_{h_ch_e}} \qquad (B-17)$$

$$Y_h = \frac{\Phi_{w_g\delta_e}\Phi_{h_c\theta} - \Phi_{w_g\theta}\Phi_{h_c\delta_e}}{\Phi_{w_gh}\Phi_{h_c\delta_e} + \Phi_{w_g\delta_e}\Phi_{h_ch_e}} \qquad (B-18)$$

These expressions can be rewritten by using the identities of Eq. B-9 through B-11 and the following

$$\Phi_{w_g\theta} = \Theta_\delta\Phi_{w_g\delta_e} + \Theta_g\Phi_{w_gw_g} \qquad (B-19)$$

$$\Phi_{w_gh} = H_\delta\Phi_{w_g\delta_e} + H_g\Phi_{w_gw_g} \qquad (B-20)$$

$$\Theta_\delta H_g - \Theta_g H_\delta = \frac{N_{\delta_e w_g}^{\theta\,h}}{\Delta} \qquad (B-21)$$

With these identities Y_θ can be written as

$$Y_\theta = \frac{N_2}{D_2} \qquad (B-22)$$

74

where

$$N_2 = -\left[\frac{\Phi_{w_g\delta_e}}{\Phi_{w_gw_g}} + H_g\frac{\Phi_{h_c\delta_e}}{\Phi_{h_ch_c}}\right]$$

$$= \frac{1}{\Theta_\delta}\left[\Theta_g - \frac{\Phi_{w_g\theta}}{\Phi_{w_gw_g}} - H_g\frac{\Phi_{h_c\theta}}{\Phi_{h_ch_c}}\right] \qquad (B\text{-}23)$$

$$= \frac{1}{H_\delta}\left[H_g\frac{\Phi_{h_ch_e}}{\Phi_{h_ch_c}} - \frac{\Phi_{w_gh}}{\Phi_{w_gw_g}}\right]$$

and

$$D_2 = \Theta_g + \Theta_\delta\frac{\Phi_{w_g\delta_e}}{\Phi_{w_gw_g}} + \frac{N_{\delta_ew_g}^{\theta\ h}}{\triangle}\frac{\Phi_{h_c\delta_e}}{\Phi_{h_ch_c}}$$

$$= \frac{\Phi_{w_g\theta}}{\Phi_{w_gw_g}} + \frac{1}{\Theta_\delta}\frac{N_{\delta_ew_g}^{\theta\ h}}{\triangle}\frac{\Phi_{h_c\theta}}{\Phi_{h_ch_c}} \qquad (B\text{-}24)$$

$$= \frac{1}{H_\delta}\left[\Theta_\delta\frac{\Phi_{w_gh}}{\Phi_{w_gw_g}} - \frac{N_{\delta_ew_g}^{\theta\ h}}{\triangle}\frac{\Phi_{h_ch_e}}{\Phi_{h_ch_c}}\right]$$

Y_h can be written as

$$Y_h = \frac{\Theta_g}{N_2}\frac{\Phi_{h_c\delta_e}}{\Phi_{h_ch_c}}$$

$$= \frac{\Theta_g}{\Theta_\delta N_2}\frac{\Phi_{h_c\theta}}{\Phi_{h_ch_c}} \qquad (B\text{-}25)$$

$$= \frac{\Theta_g}{H_\delta N_2}\frac{\Phi_{h_ch}}{\Phi_{h_ch_c}}$$

3. θ_c and w_g Inputs

The simultaneous equations for this input pair are Eqs. B-2 and B-16. The following expressions for Y_θ and Y_h result from those equations:

$$Y_\theta = \frac{\Phi_{\theta_c \delta_e} \Phi_{w_g h} - \Phi_{\theta_c h} \Phi_{w_g \delta_e}}{\Phi_{\theta_c \theta_e} \Phi_{w_g h} + \Phi_{\theta_c h} \Phi_{w_g \theta}} \qquad (B-26)$$

$$Y_h = \frac{\Phi_{\theta_c \theta_e} \Phi_{w_g \delta_e} + \Phi_{\theta_c \delta_e} \Phi_{w_g \theta}}{\Phi_{\theta_c h} \Phi_{w_g \delta_e} - \Phi_{\theta_c \delta_e} \Phi_{w_g h}} \qquad (B-27)$$

By using Eqs. B-6 through B-8 and B-19 through B-21, Y_θ can be rewritten as

$$Y_\theta = \frac{N_3}{D_3} \qquad (B-28)$$

where

$$
\begin{aligned}
N_3 &= H_g \frac{\Phi_{\theta_c \delta_e}}{\Phi_{\theta_c \theta_c}} \\[2mm]
&= \frac{H_g}{\Theta_\delta} \frac{\Phi_{\theta_c \theta}}{\Phi_{\theta_c \theta_c}} \qquad (B-29) \\[2mm]
&= \frac{H_g}{H_\delta} \frac{\Phi_{\theta_c h}}{\Phi_{\theta_c \theta_c}}
\end{aligned}
$$

and

$$
\begin{aligned}
D_3 &= H_g + H_\delta \frac{\Phi_{w_g \delta_e}}{\Phi_{w_g w_g}} - \frac{N_{\delta_e w_g}^{\theta\ h}}{\Delta} \frac{\Phi_{\theta_c \delta_e}}{\Phi_{\theta_c \theta_c}} \\[2mm]
&= \frac{1}{\Theta_\delta} \left[\frac{N_{\delta_e w_g}^{\theta\ h}}{\Delta} \frac{\Phi_{\theta_c \theta_e}}{\Phi_{\theta_c \theta_c}} + H_\delta \frac{\Phi_{w_g \theta}}{\Phi_{w_g w_g}} \right] \qquad (B-30) \\[2mm]
&= \frac{\Phi_{w_g h}}{\Phi_{w_g w_g}} - \frac{1}{H_\delta} \frac{N_{\delta_e w_g}^{\theta\ h}}{\Delta} \frac{\Phi_{\theta_c h}}{\Phi_{\theta_c \theta_c}}
\end{aligned}
$$

76

Y_h can be written as

$$Y_h = \frac{-1}{N_3}\left(\frac{\Phi_{w_g\delta_e}}{\Phi_{w_g w_g}} + \Theta_g \frac{\Phi_{\theta_c\delta_e}}{\Phi_{\theta_c\theta_c}}\right)$$

$$= \frac{1}{\Theta_\delta N_3}\left(\Theta_g \frac{\Phi_{\theta_c\theta_e}}{\Phi_{\theta_c\theta_c}} - \frac{\Phi_{w_g\theta}}{\Phi_{w_g w_g}}\right) \qquad (B\text{-}31)$$

$$= \frac{1}{H_\delta N_3}\left(H_g - \frac{\Phi_{w_g h}}{\Phi_{w_g w_g}} - \Theta_g \frac{\Phi_{\theta_c h}}{\Phi_{\theta_c\theta_c}}\right)$$

77

APPENDIX C

PREDICTED CLOSED-LOOP DYNAMICS

During the pre-experimental analyses, a predicted set of pilot loop closures were computed. The primary objective was to provide estimates of the closed-loop dynamics which could be used in preliminary evaluations of potential data reduction techniques.

The inner-loop (attitude to elevator) closure was based on the quasi-linear pilot model of Ref. 1. Because of low short-period frequency ($\omega_{sp} = 0.764$ rad/sec) the controlled element appears as K/s^2 in the region of crossover (roughly 2-3 rad/sec); consequently, the pilot should use a low-frequency lead so the net open-loop transfer function looks like K/s in the region of crossover. An appropriate pilot model is therefore

$$Y_\theta = \frac{\delta_e}{\theta_e} = K_\theta (T_L s + 1) e^{-\tau s} \tag{C-1}$$

In calculating the closed-loop characteristics, it was convenient to replace the time delay term with a suitable approximation. The model actually used was of the form

$$Y_\theta = K_\theta (T_L s + 1) \left(\frac{s - \frac{4}{\tau}}{s + \frac{4}{\tau}} \right)^2 \tag{C-2}$$

The numerical values used for the various parameters were

$$K_\theta = 1 \ \text{sec}^{-2}$$

$$T_L = 2 \ \text{sec}$$

$$\tau = 0.4 \ \text{sec}$$

This results in a crossover frequency of 2.3 rad/sec with a gain margin of 5 dB and a phase margin of 30 deg; see Fig. C-1.

$$G(s) = \frac{Y_\theta N_{\delta_e}^{\theta}}{\Delta} = \frac{2(s+0.5)(s+0.585)(s-10)^2}{s[s^2+2(0.387)(0.764)s+(0.764)^2](s+10)^2}$$
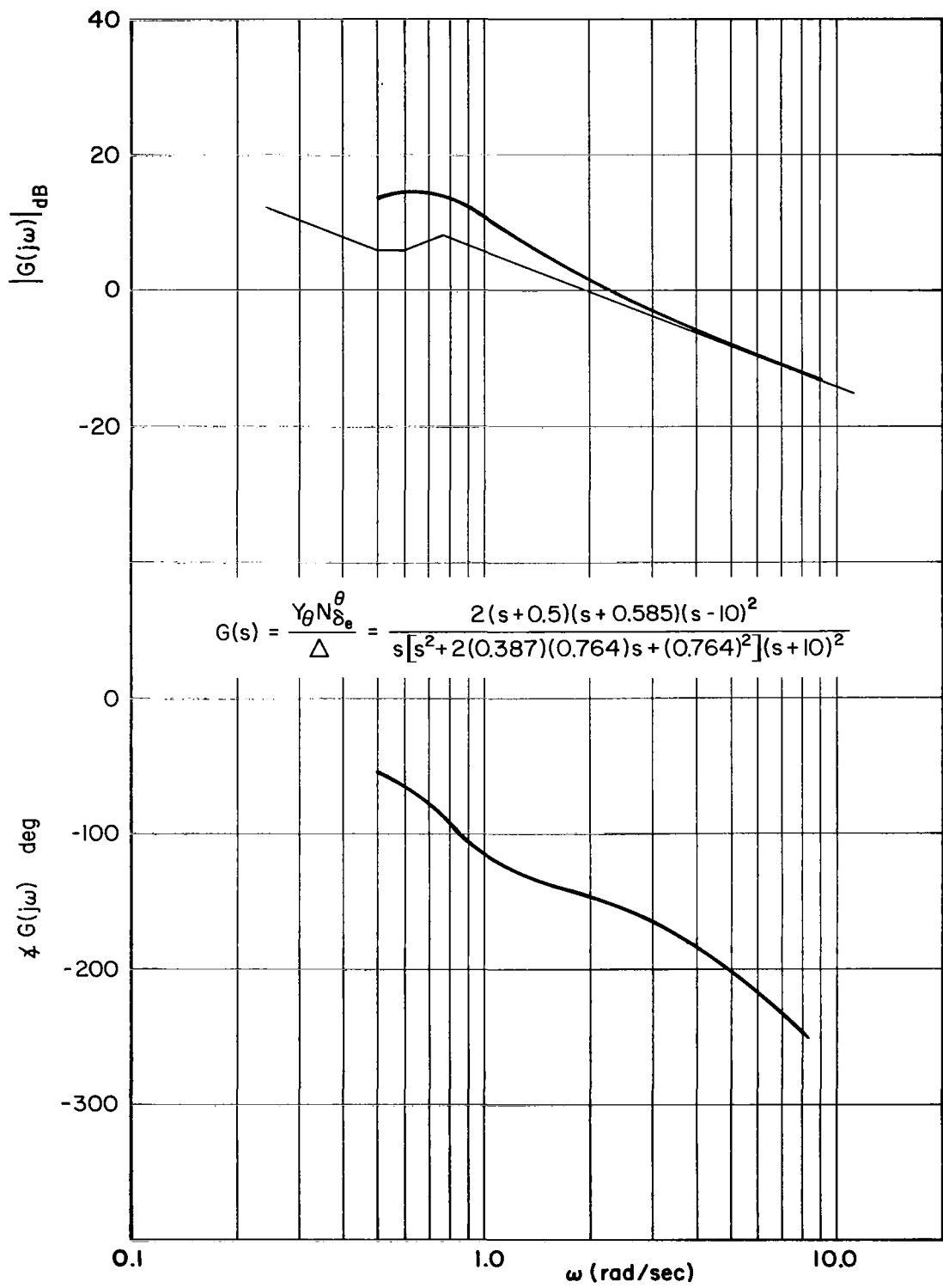
Figure C-1. Predicted Inner-Loop Closure

For the outer, or altitude, loop a series loop structure was assumed; see Fig. C-2. The total loop transfer function is then given by (outer loop open, inner loop closed)

$$\left(\frac{h}{h_e}\right)' = \frac{Y_h Y_\theta N_{\delta_e}^h}{\Delta'} \tag{C-3}$$

where $\Delta' = \Delta + Y_\theta N_{\delta_e}^\theta$

$$\tag{C-4}$$

$$= \frac{(s + 0.288)(s + 1.31)(s + 19.3)\left[s^2 + 2(0.298)(2.83)s + (2.83)^2\right]}{(s + 10)^2}$$

A pure-gain element was assumed for the outer loop, i.e., $Y_h = K_h$ because relatively little is known about pilot dynamics and adjustment rules for outer loops. Furthermore, performance with a pure-gain outer loop appeared adequate. For

$$K_h = 0.006 \text{ rad/ft} = 0.344 \text{ deg/ft}$$

a crossover frequency of 0.8 rad/sec was obtained with a gain margin of 6 dB and a phase margin of 25 deg; see Fig. C-2.

For the pilot model described above, the closed-loop responses to θ_c, h_c, and w_g inputs were computed. These results are shown in Figs. C-3 through C-13. In these figures

$$\Delta'' = \Delta + Y_\theta N_{\delta_e}^\theta + Y_h Y_\theta N_{\delta_e}^h \tag{C-5}$$

$$G(s) = \frac{Y_\theta Y_h N_{\delta_e}^h}{\Delta + Y_\theta N_{\delta_e}^\theta}$$

$$= \frac{1.57(s+0.5)(s-10)^2}{s(s+0.288)(s+1.31)(s+19.3)\left[s^2+2(0.298)(2.83)s+(2.83)^2\right]}$$
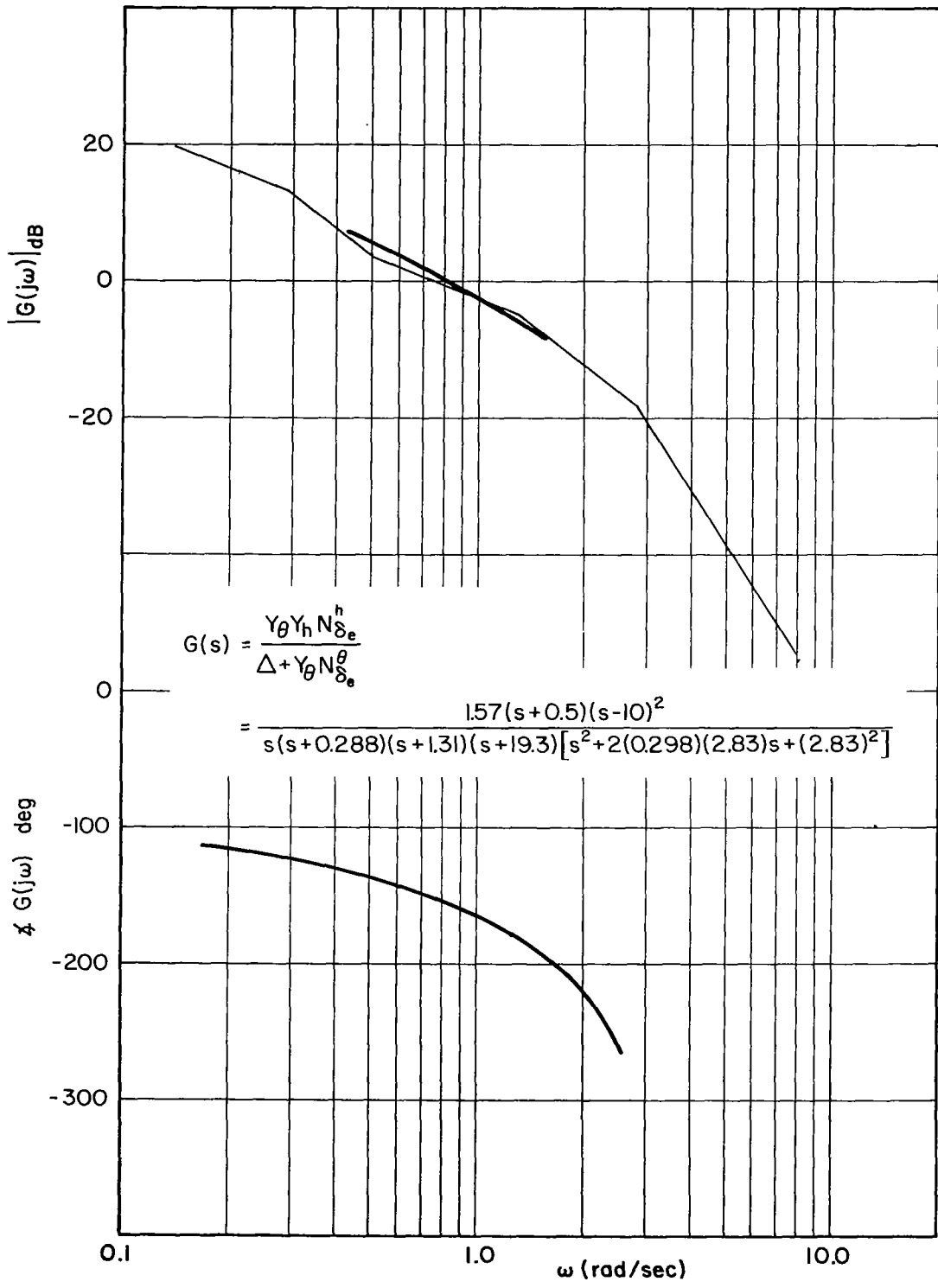
Figure C-2. Predicted Outer-Loop Closure

81

$$\frac{\theta}{\theta_c} = \frac{Y_\theta N_{\delta_e}^\theta}{\Delta''}$$

$$= \frac{2s(s+0.5)(s+0.585)(s-10)^2}{(s+0.61)(s+19.3)\left[s^2+2(.39)(2.78)s+(2.78)^2\right]\left[s^2+2(.26)(.93)s+(.93)^2\right]}$$
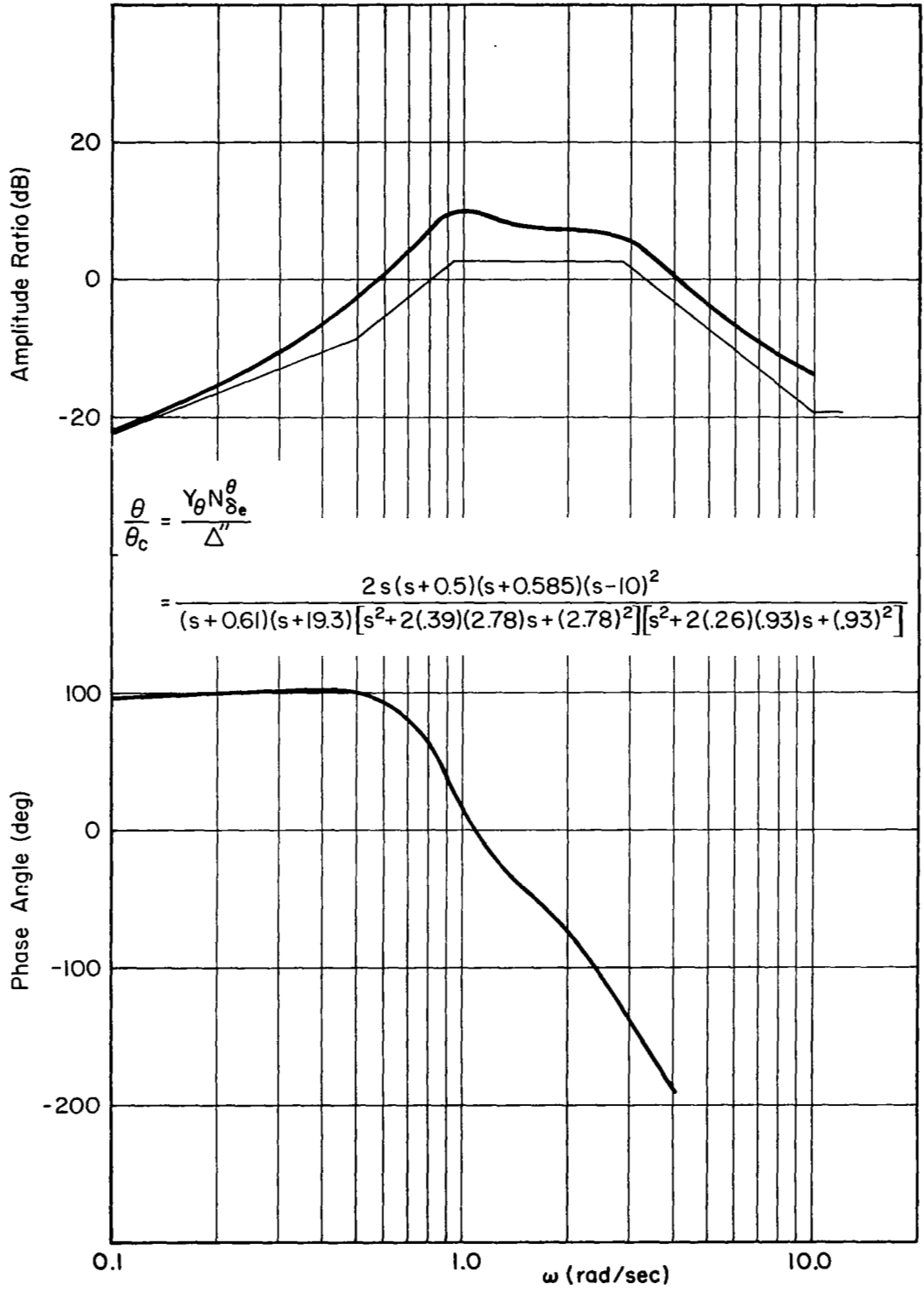
Figure C-3. Predicted Closed-Loop Response, θ/θ_c

The figure contains the following equation:

$$\frac{\theta_e}{\theta_c} = \frac{\Delta + Y_h Y_\theta N_{\delta_e}^h}{\Delta''}$$

$$= \frac{(s+0.61)(s+1.16)(s+7.99)(s+12.2)\left[s^2 - 2(.48)(1.06)s + (1.06)^2\right]}{(s+0.61)(s+19.3)\left[s^2 + 2(.39)(2.78)s + (2.78)^2\right]\left[s^2 + 2(.26)(.93)s + (.93)^2\right]}$$
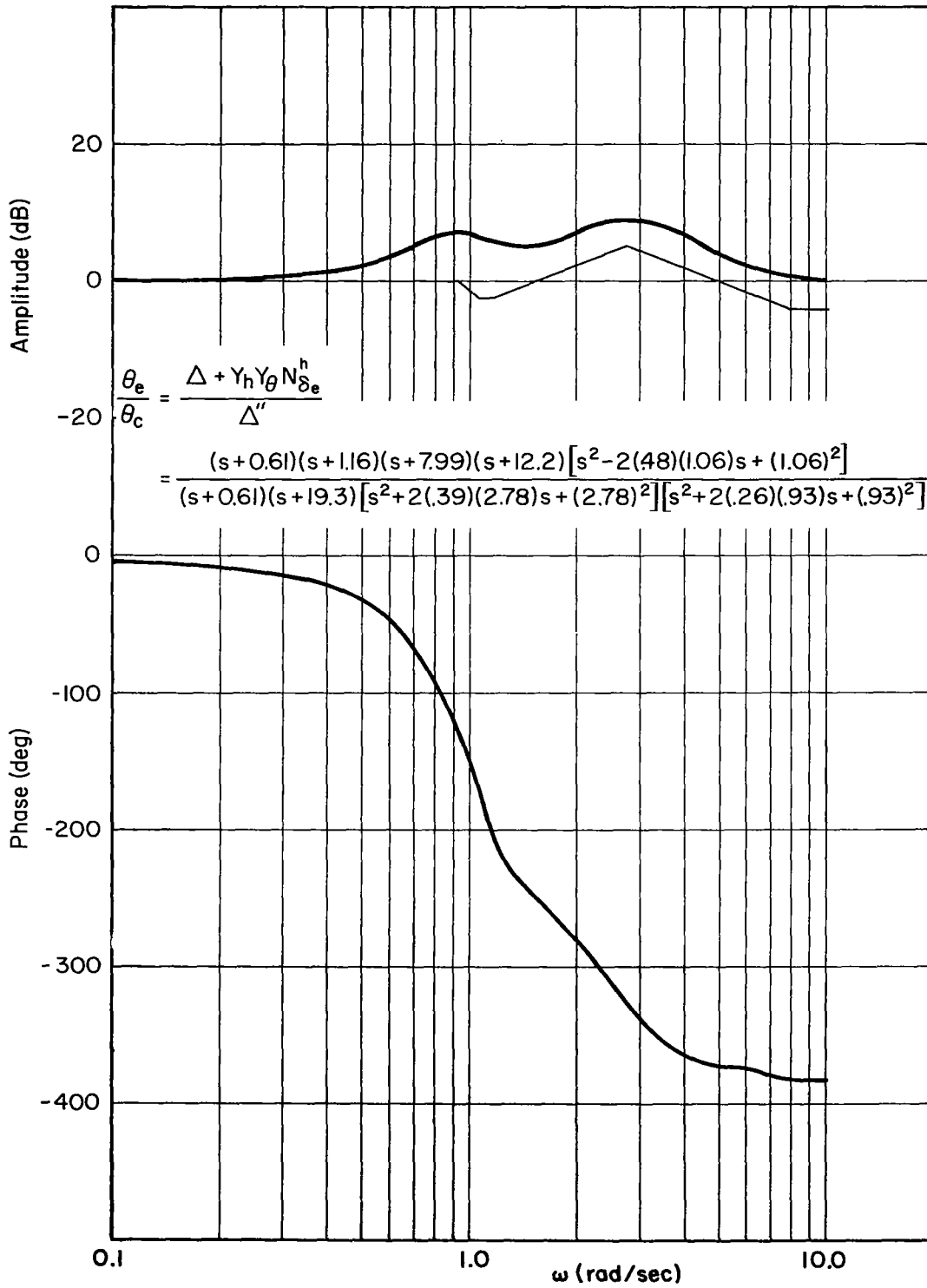
Figure C-4. Predicted Closed-Loop Response, θ_e/θ_c

83

The figure contains the following equation:

$$\frac{h}{\theta_c} = \frac{Y_\theta N^h_{\delta_e}}{\Delta''}$$

$$= \frac{261(s+.5)(s-10)^2}{(s+0.61)(s+19.3)\left[s^2+2(.39)(2.78)s+(2.78)^2\right]\left[s^2+2(.26)(.93)s+(.93)^2\right]}$$
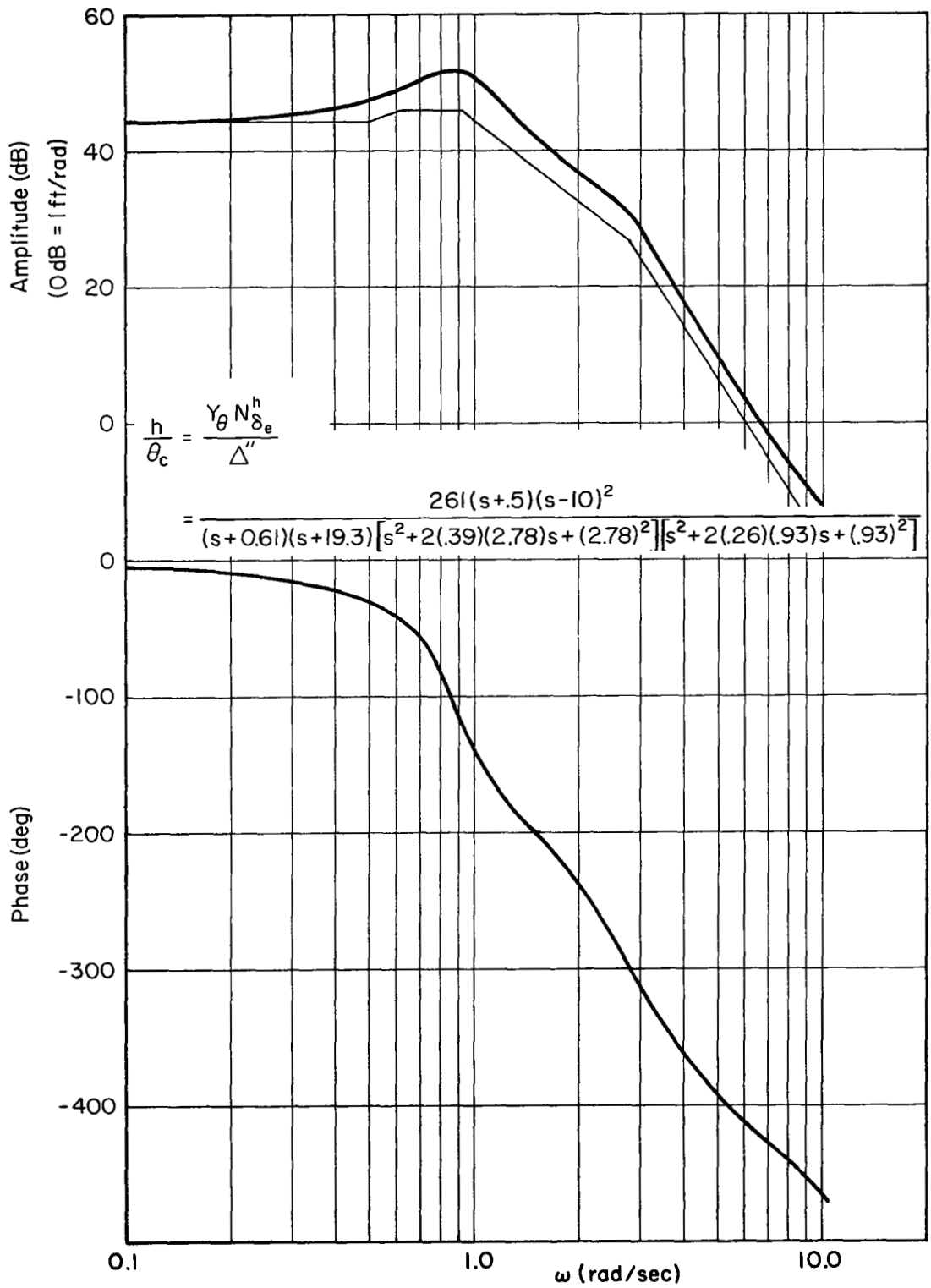
Figure C-5. Predicted Closed-Loop Response, h/θ_c

84
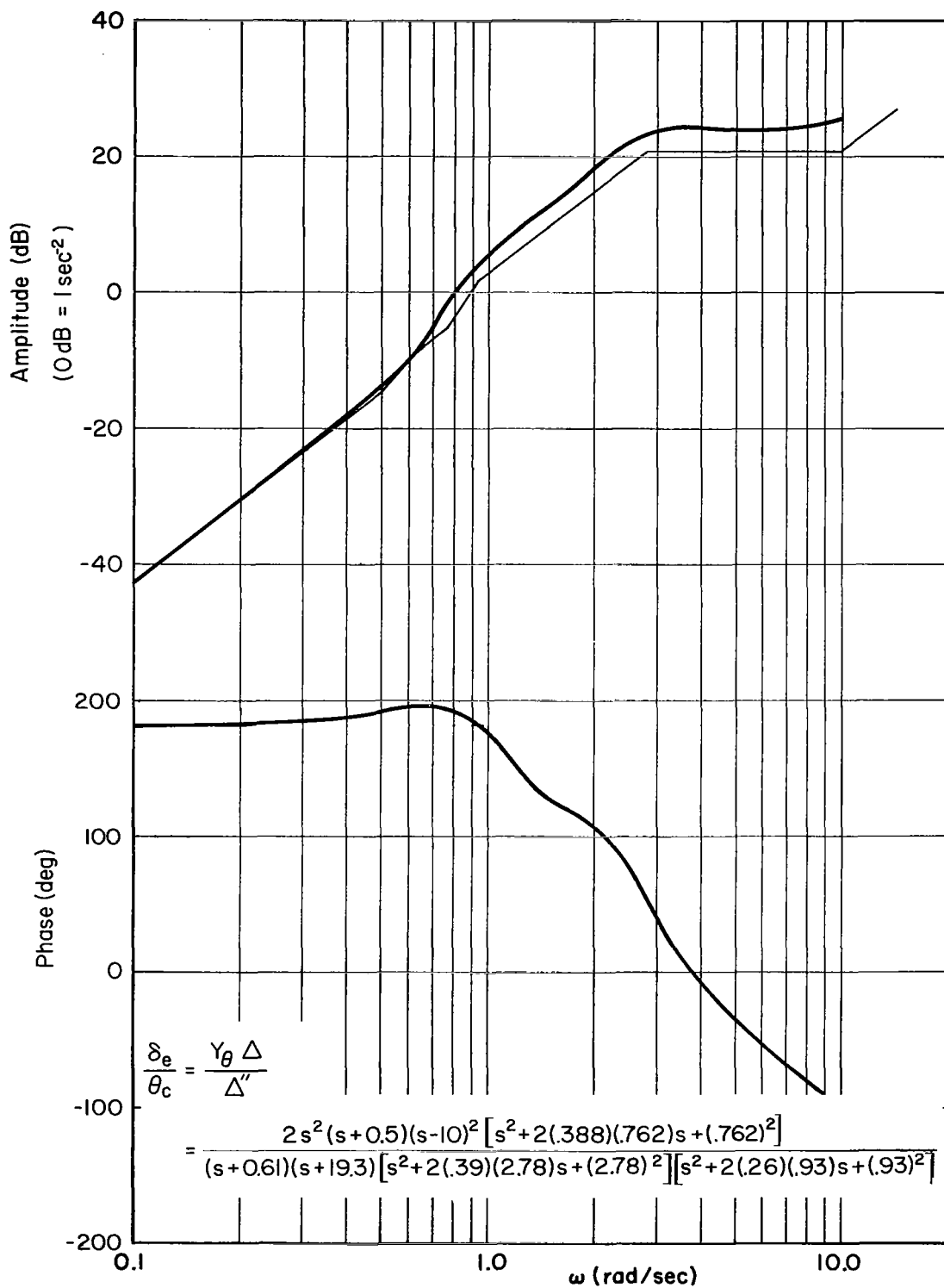
Figure C-6. Predicted Closed-Loop Response, δ_e/θ_c

The equation shown within the figure:

$$\frac{\delta_e}{\theta_c} = \frac{Y_\theta \, \Delta}{\Delta''}$$

$$= \frac{2s^2(s+0.5)(s-10)^2\left[s^2+2(.388)(.762)s+(.762)^2\right]}{(s+0.61)(s+19.3)\left[s^2+2(.39)(2.78)s+(2.78)^2\right]\left[s^2+2(.26)(.93)s+(.93)^2\right]}$$

The plotted equation:

$$\frac{\theta}{h_c} = \frac{Y_h Y_\theta N_{\delta_e}^{\theta}}{\Delta''}$$

$$= \frac{0.012\,s(s+0.5)(s+0.585)(s-10)^2}{(s+0.61)(s+19.3)\left[s^2+2(.39)(2.78)s+(2.78)^2\right]\left[s^2+2(.26)(.93)s+(.93)^2\right]}$$
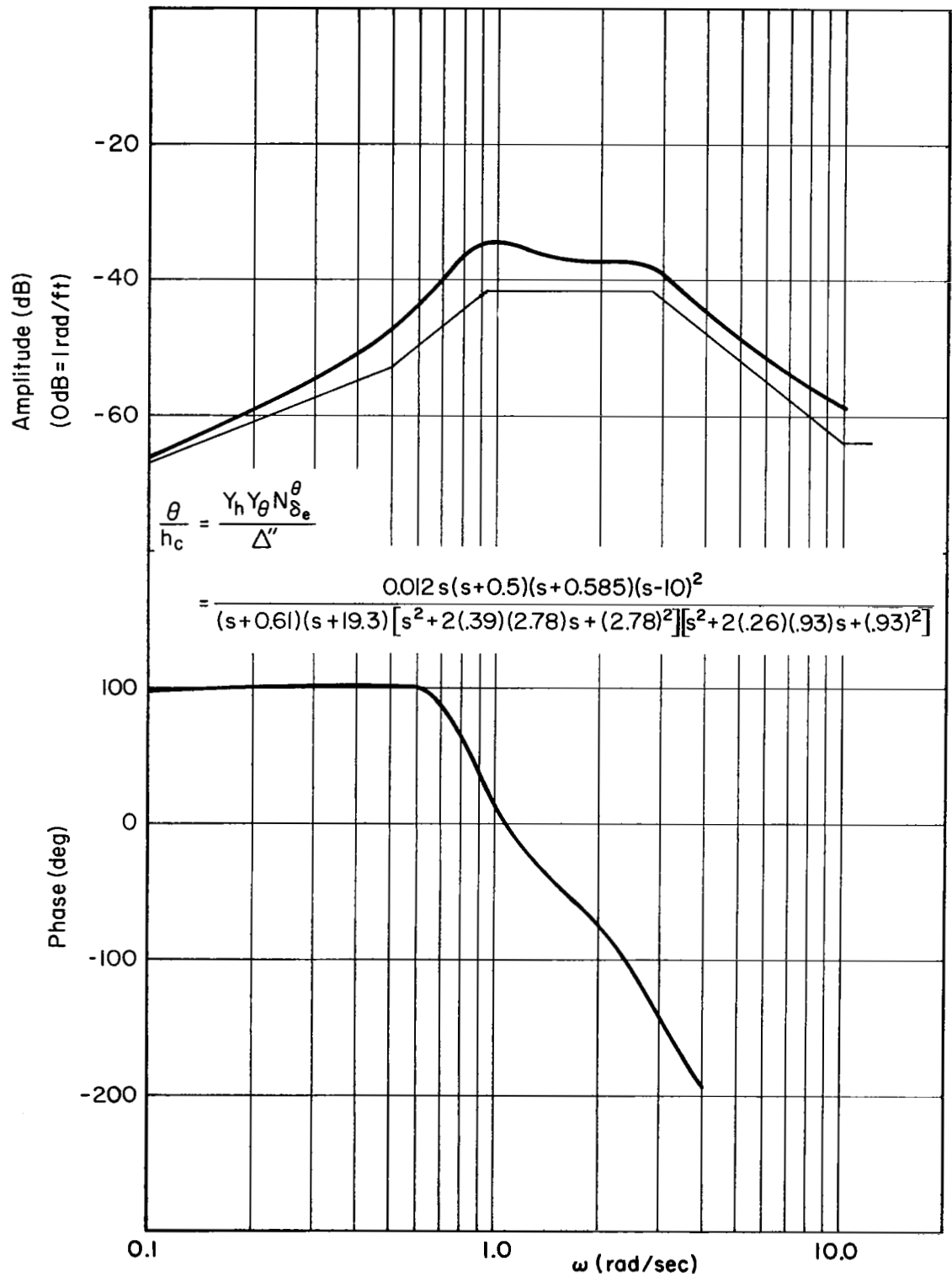
Figure C-7. Predicted Closed-Loop Response, θ/h_c

The figure contains the equation:

$$\frac{h}{h_c} = \frac{Y_h\, Y_\theta\, N_{\delta_e}^h}{\Delta''}$$

$$= \frac{1.57(s+0.5)(s-10)^2}{(s+0.61)(s+19.3)\left[(s^2+2(.39)(2.78)s+(2.78)^2\right]\left[s^2+2(.26)(.93)s+(.93)^2\right]}$$
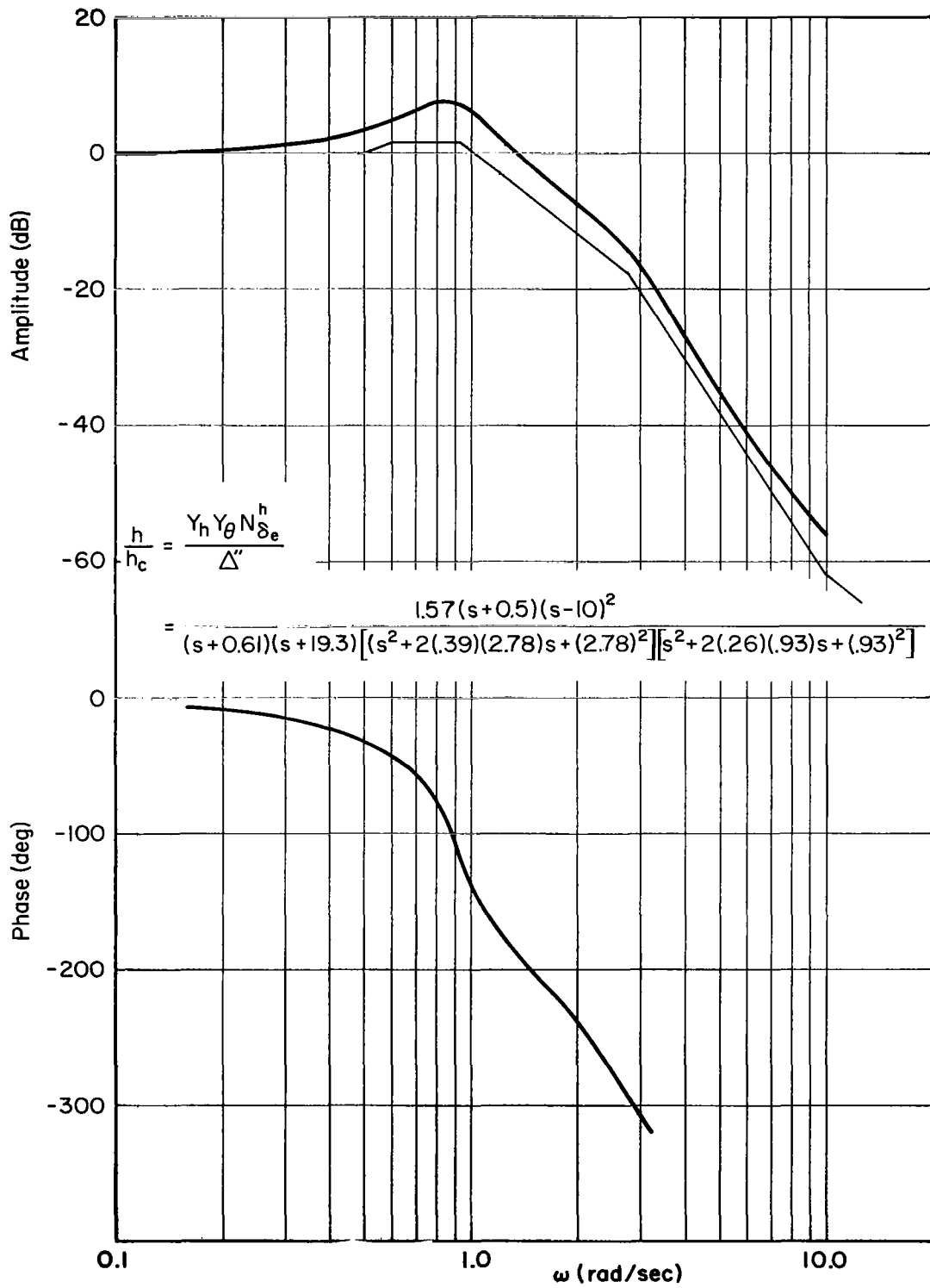
Figure C-8. Predicted Closed-Loop Response, h/h_c

The equation shown within the figure:

$$\frac{h_e}{h_c} = \frac{\Delta + Y_\theta N_{\delta_e}^\theta}{\Delta''}$$

$$= \frac{s(s+0.29)(s+1.31)\left[s^2+2(.30)(2.83)s+(2.83)^2\right](s+19.3)}{(s+0.61)(s+19.3)\left[s^2+2(.39)(2.78)s+(2.78)^2\right]\left[s^2+2(.26)(.93)s+(.93)^2\right]}$$
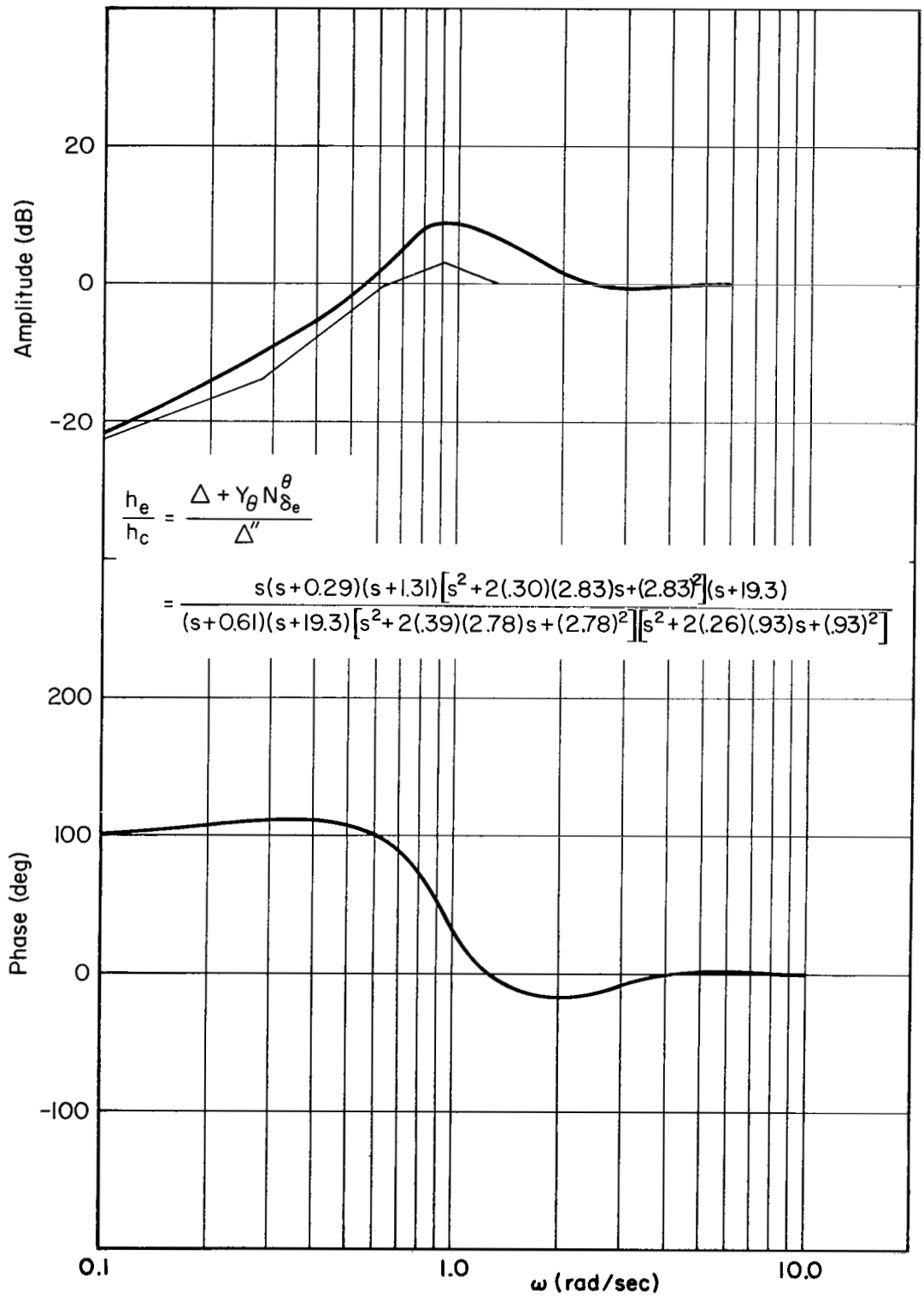
Figure C-9. Predicted Closed-Loop Response, h_e/h_c
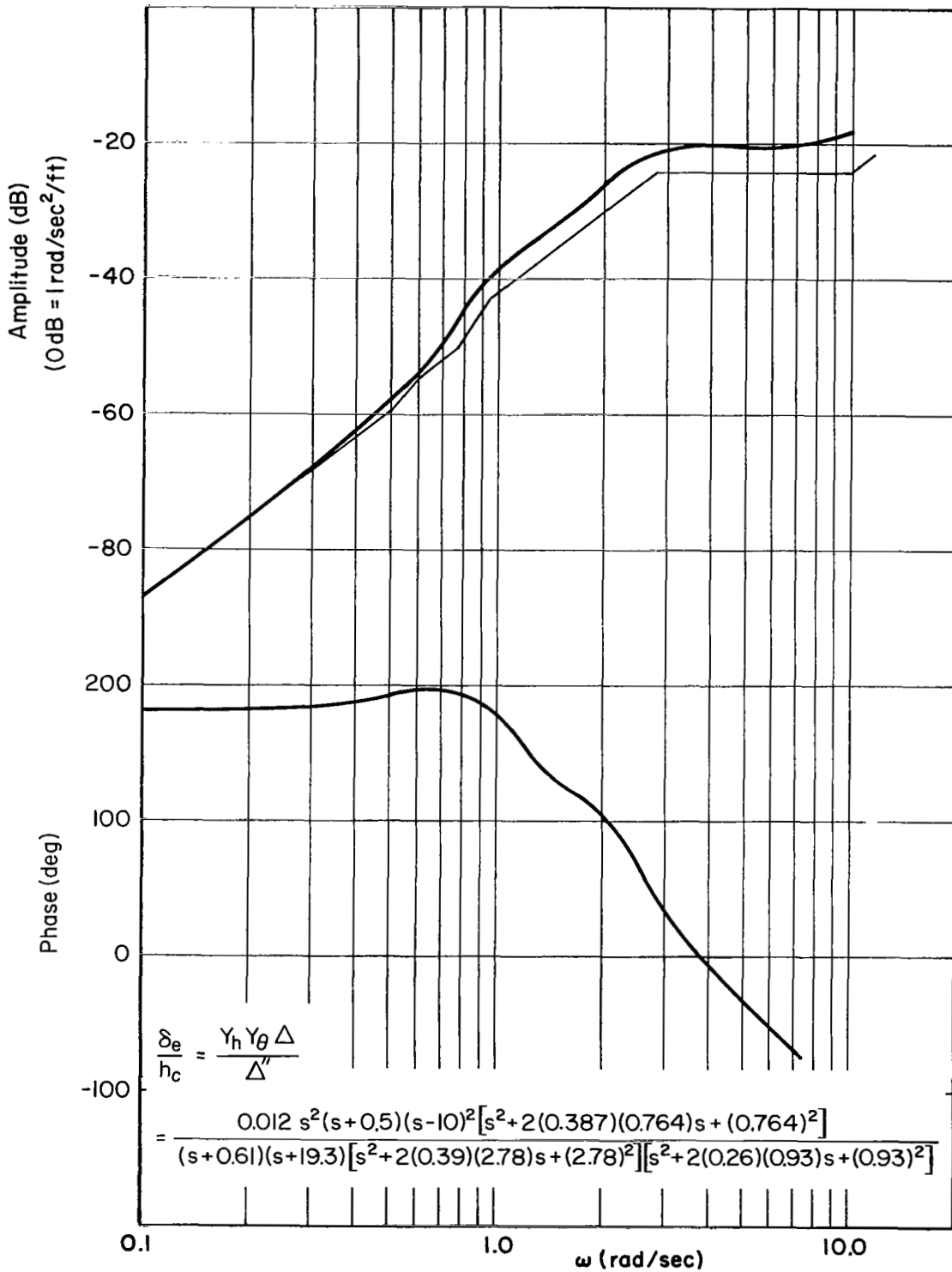
Figure C-10. Predicted Closed-Loop Response, δ_e/h_c

$$\frac{\delta_e}{h_c} = \frac{Y_h Y_\theta \Delta}{\Delta''}$$

$$= \frac{0.012\ s^2(s+0.5)(s-10)^2[s^2+2(0.387)(0.764)s+(0.764)^2]}{(s+0.61)(s+19.3)[s^2+2(0.39)(2.78)s+(2.78)^2][s^2+2(0.26)(0.93)s+(0.93)^2]}$$

89
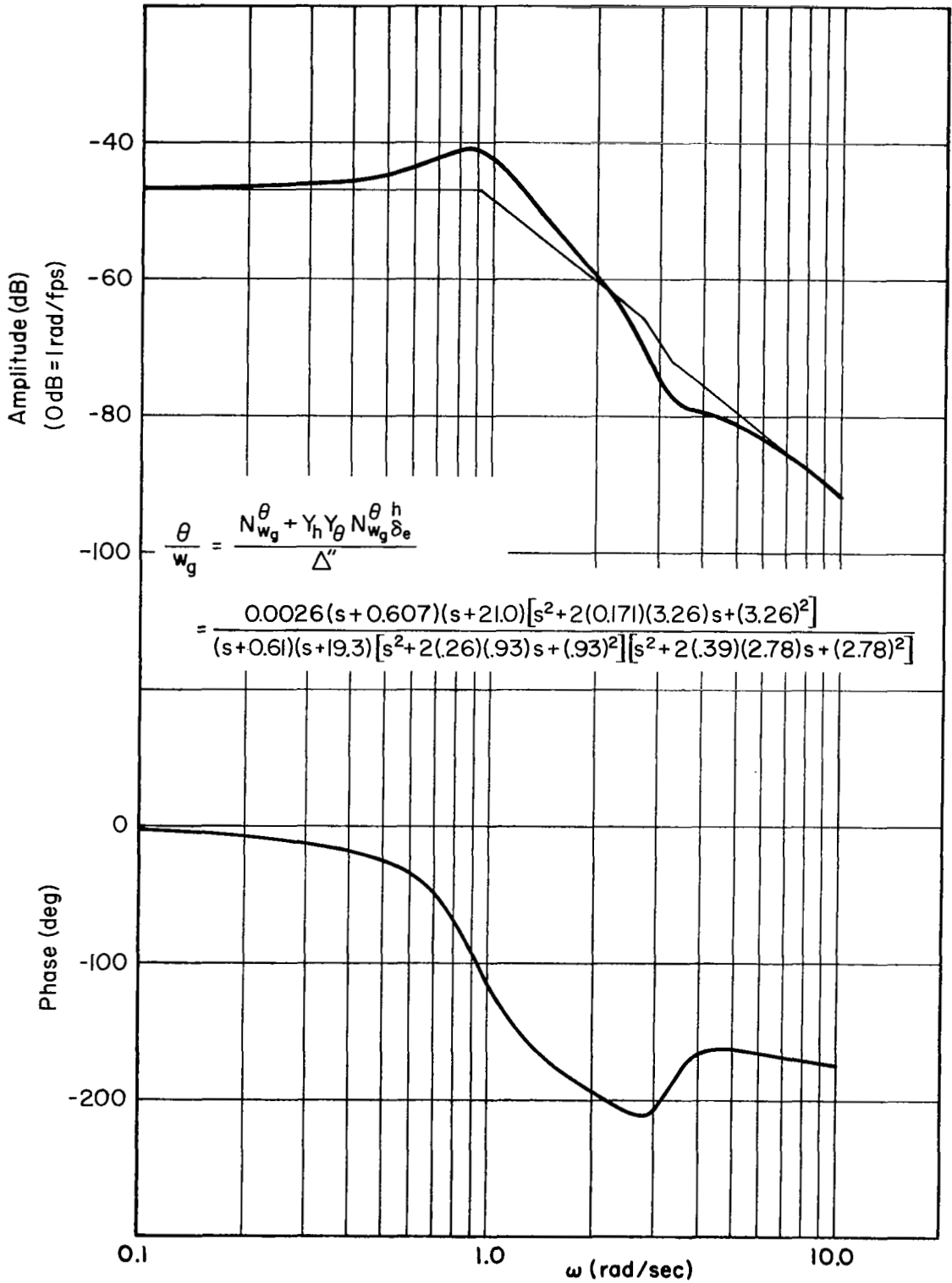
Figure C-11. Predicted Closed-Loop Response, θ/w_g

$$\frac{\theta}{w_g} = \frac{N_{w_g}^{\theta} + Y_h Y_\theta N_{w_g}^{\theta} {}_{\delta_e}^{h}}{\Delta''}$$

$$= \frac{0.0026(s+0.607)(s+21.0)\left[s^2+2(0.171)(3.26)s+(3.26)^2\right]}{(s+0.61)(s+19.3)\left[s^2+2(.26)(.93)s+(.93)^2\right]\left[s^2+2(.39)(2.78)s+(2.78)^2\right]}$$
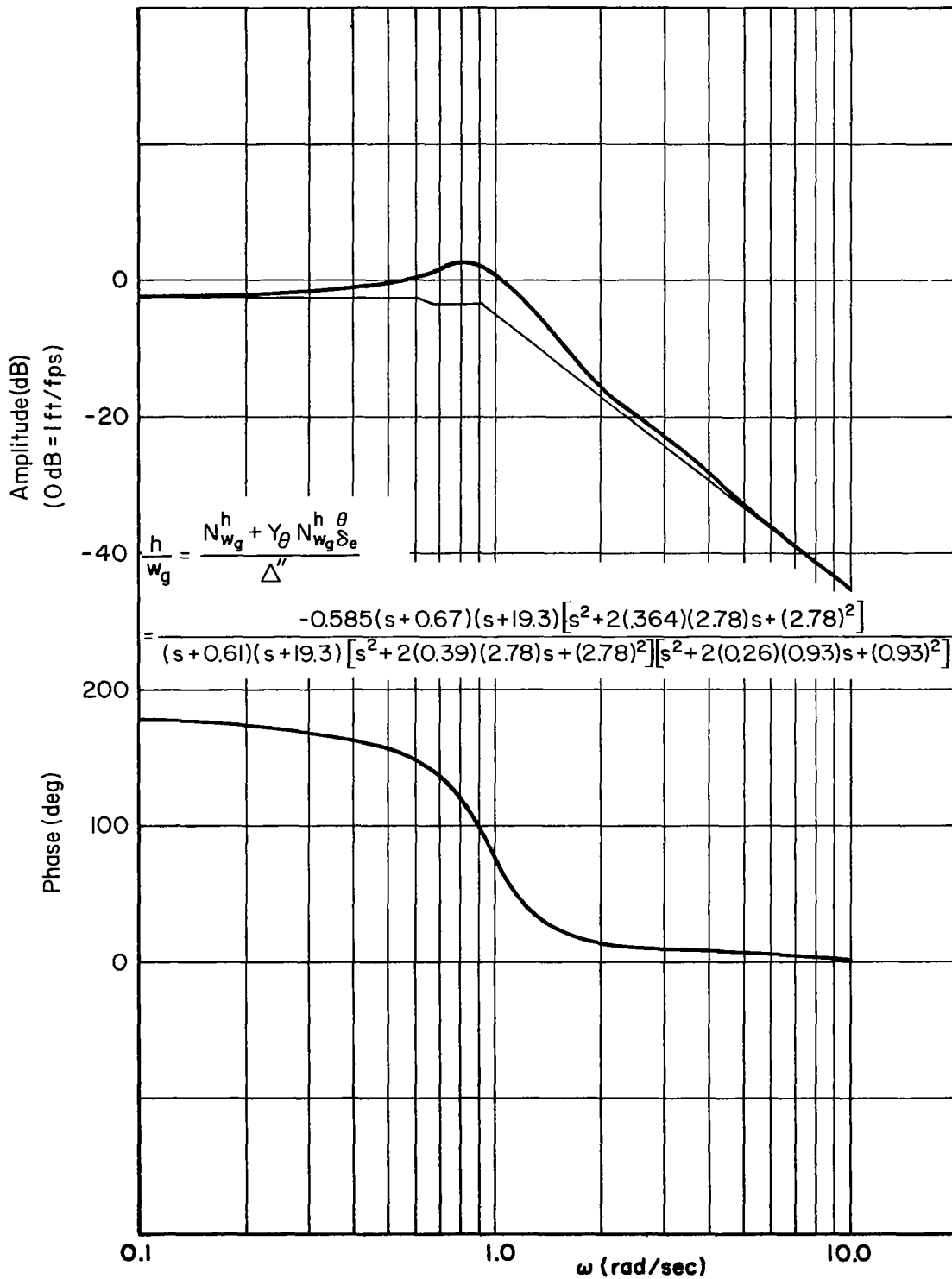
Figure C-12. Predicted Closed-Loop Response, h/w_g

The equation shown in the figure:

$$\frac{h}{w_g} = \frac{N_{w_g}^h + Y_\theta N_{w_g \delta_e}^{h \, \theta}}{\Delta''}$$

$$= \frac{-0.585(s+0.67)(s+19.3)\left[s^2+2(.364)(2.78)s+(2.78)^2\right]}{(s+0.61)(s+19.3)\left[s^2+2(0.39)(2.78)s+(2.78)^2\right]\left[s^2+2(0.26)(0.93)s+(0.93)^2\right]}$$

91

The figure contains the following equations:

$$\frac{\delta_e}{w_g} = \frac{-Y_\theta}{\Delta''}\left[N_{w_g}^\theta + Y_h N_{w_g}^h\right]$$

$$= \frac{0.00182\,s\,(s+0.0274)(s+0.5)(s-10)^2}{(s+0.61)(s+19.3)\left[s^2+2(.26)(.93)s+(.93)^2\right]\left[s^2+2(.39)(2.78)s+(2.78)^2\right]}$$

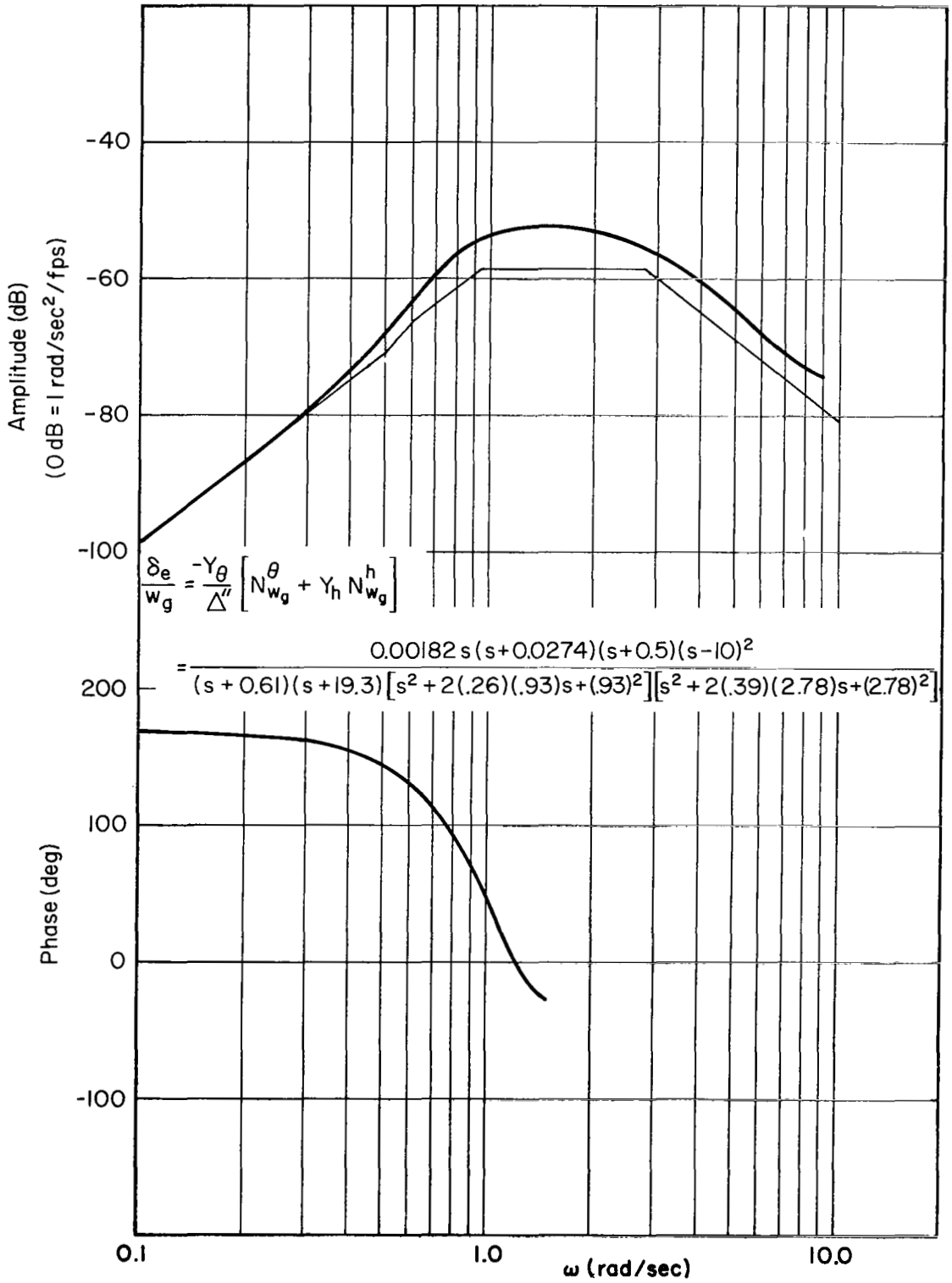Figure C-13. Predicted Closed-Loop Response, δ_e/w_g

92

APPENDIX D

CROSSOVER MODEL PARAMETER TRACKER

The purpose of the Crossover Model Parameter Tracker[*] (COMPT) is to provide a simple on-line approximation to the crossover frequency of a pilot in a tracking task. It can be used either in a single-loop task or the outer-loop of a multiloop task. The operation of COMPT is based on the fact that a pilot generally adjusts his characteristics so that in the region of crossover the total (pilot plus controlled element) open-loop transfer function is approximately $(\omega_c/s)e^{-\tau s}$ (Ref. 1).

In COMPT the tracking experiment error (input, i, minus controlled element output), e, is compared to the model error, e^*, which is given by

$$e^* = \cfrac{i}{1 + \cfrac{\omega_c}{s}\, e^{-\tau s}} \qquad (D-1)$$

The model matching error, $\epsilon = e - e^*$, is then used to vary ω_c to minimize ϵ^2. The adjustment equation is

$$\dot{\omega}_c = -A\epsilon \frac{\partial \epsilon}{\partial \omega_c} = A\epsilon \frac{\partial e^*}{\partial \omega_c} \qquad (D-2)$$

The key feature of COMPT is the use of the first derivative to approximate the effects of variations in ω_c. A nominal value or pre-experimental estimate of ω_c (ω_{c_0}) is set into the model and the model matching error is approximated by

$$\epsilon = e - e^* = e - (e_o{}^* + \Delta e^*)$$

$$\dot{=} e - e_o{}^* - \Delta\omega_c \frac{\partial e^*}{\partial \omega_c} \qquad (D-3)$$

---

[*]This device was developed by L. Gregor Hofmann and John J. Best, Systems Technology, Inc.

where e_o^* is the model error for $\omega_c = \omega_{c_o}$ and $\partial e^*/\partial \omega_c$ is evaluated at $\omega_c = \omega_{c_o}$, i.e.,

$$\frac{\partial e^*}{\partial \omega_c} = \frac{-\dfrac{i}{s} e^{-\tau s}}{\left(1 + \dfrac{\omega_{c_o}}{s} e^{-\tau s}\right)^2}$$

$$= \frac{-\dfrac{e_o^*}{s} e^{-\tau s}}{1 + \dfrac{\omega_{c_o}}{s} e^{-\tau s}}$$

$$(D-4)$$

A complete schematic of COMPT is shown in Fig. D-1.

In the actual mechanization of COMPT the time delay, $e^{-\tau s}$, is represented by a suitable Pade approximation. It is also desirable to first pass the input, i, and tracking error, e, through identical high-pass filters. The filters reduce the low-frequency portions of the signals so that the crossover region is emphasized.

All the elements of COMPT, except for the two multiplications by $\partial e^*/\partial \omega_c$, are linear constant-coefficient filters, and it can be shown that the tracking loop is globally asymptotically stable. Including the high-pass filters, the device can be mechanized on an analog computer with only 13 amplifiers and 1 multiplier (if the multiplier can form the two products xy and xz). The primary disadvantage of COMPT is that the estimated crossover frequency ($\omega_{c_o} + \Delta\omega_c$) can have appreciable errors if the nominal value (ω_{c_o}) differs widely from the true value.
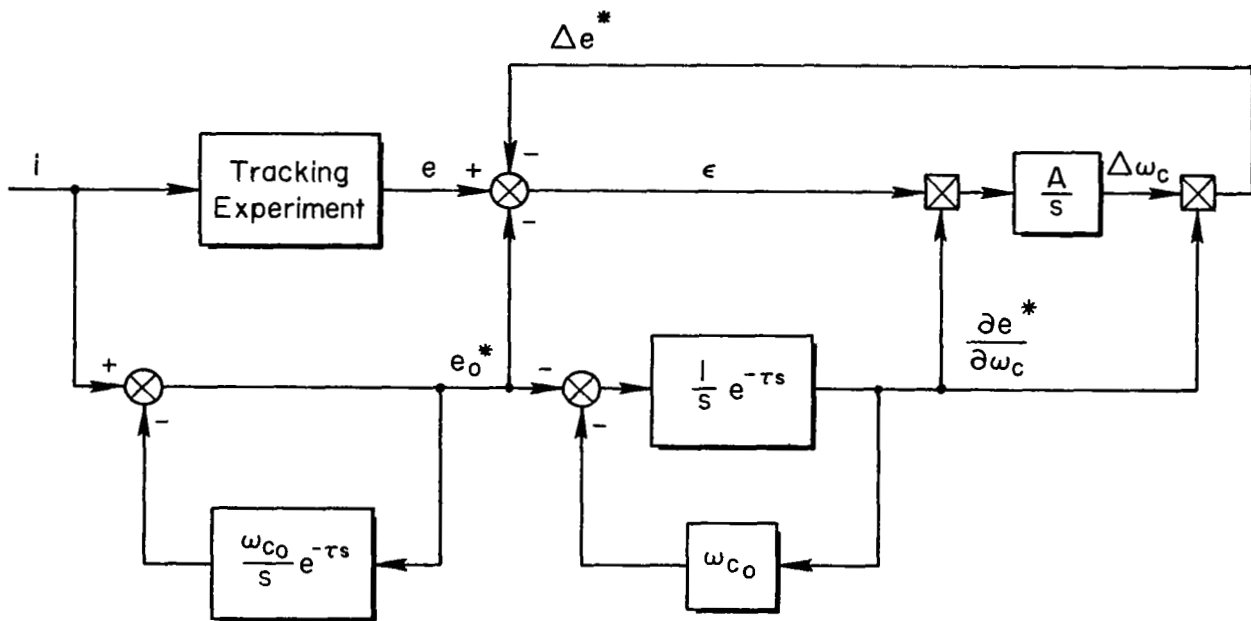
Figure D-1. COMPT Schematic

POSTMASTER: If Undeliverable (Section Postal Manual) Do Not R

---

*"The aeronautical and space activities of the United States shall be
conducted so as to contribute . . . to the expansion of human knowl-
edge of phenomena in the atmosphere and space. The Administration
shall provide for the widest practicable and appropriate dissemination
of information concerning its activities and the results thereof."*

— NATIONAL AERONAUTICS AND SPACE ACT OF 1958

NASA SCIENTIFIC AND TECHNICAL PUBLICATIONS

TECHNICAL REPORTS: Scientific and
technical information considered important,
complete, and a lasting contribution to existing
knowledge.

TECHNICAL NOTES: Information less broad
in scope but nevertheless of importance as a
contribution to existing knowledge.

TECHNICAL MEMORANDUMS:
Information receiving limited distribution
because of preliminary data, security classifica-
tion, or other reasons.

CONTRACTOR REPORTS: Scientific and
technical information generated under a NASA
contract or grant and considered an important
contribution to existing knowledge.

TECHNICAL TRANSLATIONS: Information
published in a foreign language considered
to merit NASA distribution in English.

SPECIAL PUBLICATIONS: Information
derived from or of value to NASA activities.
Publications include conference proceedings,
monographs, data compilations, handbooks,
sourcebooks, and special bibliographies.

TECHNOLOGY UTILIZATION
PUBLICATIONS: Information on technology
used by NASA that may be of particular
interest in commercial and other non-aerospace
applications. Publications include Tech Briefs,
Technology Utilization Reports and Notes,
and Technology Surveys.

Details on the availability of these publications may be obtained from:

SCIENTIFIC AND TECHNICAL INFORMATION DIVISION

NATIONAL AERONAUTICS AND SPACE ADMINISTRATION
Washington, D.C. 20546